2019-06-01

Computational Design and Analysis of Molecular Ethylene Oligomerization Catalysts

Doo Hyun Kwon
Brigham Young University

Computational Design and Analysis of Molecular Ethylene Oligomerization Catalysts

Doo Hyun Kwon

A dissertation submitted to the faculty of
Brigham Young University
in partial fulfillment of the requirements for the degree of

Doctor of Philosophy

Daniel H. Ess, Chair
Brian F. Woodfield
David J. Michaelis
Kara J. Stowers
Roger G. Harrison
Steven M. Bischof

Department of Chemistry and Biochemistry

Brigham Young University

ABSTRACT

Computational Design and Analysis of Molecular Ethylene Oligomerization Catalysts

Doo Hyun Kwon
Department of Chemistry and Biochemistry, BYU
Doctor of Philosophy

Linear alpha olefins (LAOs) are key petrochemical precursors for the synthesis of larger polymers, detergents, plasticizers, and lubricants. Most catalytic ethylene oligomerization processes generate a wide distribution of LAO carbon chain lengths. A major ongoing industrial challenge is to develop homogeneous catalysts that result in selective and tunable ethylene oligomerization to 1-hexene and 1-octene alkenes. Quantum mechanical calculations coupled with rapidly advancing technology have enabled the ability to calculate small molecule systems with high accuracy. Employing computational models to advance from empirical to quantitative prediction of product selectivities has become an active area of exploration. In this work, we demonstrate the development and use of a density-functional theory (DFT) transition-state model that provides highly accurate quantitative prediction of phosphinoamidine (P,N) Cr catalysts for controllable selective ethylene trimerization and tetramerization. This model identified a new family of highly selective catalysts that through computational-based ligand design results in a predictable shift from 1-hexene selectivity to 1-octene. Subsequent experimental ligand synthesis and catalyst testing verified the quantitative computational predictions. DFT calculations also provide key insights to factors controlling catalytic activity and present important design criteria for the development of active Cr-based ethylene oligomerization systems. Non-selective ethylene transformations, referred to as full range processes, provide access to a range of LAOs (C_4-C_{20}) that are used to produce polyethylene, surfactants, and other commercial products. During full-range oligomerizations, undesired byproducts degrade the purity of LAOs mostly consisting of branched oligomers. Computational mechanistic investigations reveal the origin of linear versus branched selectivity in Fe-catalyzed ethylene oligomerization reactions.

Keywords: computational predictions, transition-state design, DFT, molecular catalysis, chromium catalysis, ethylene trimerization, ethylene tetramerization, iron catalysis, full range oligomerization

ACKNOWLEDGEMENTS

Words cannot express the gratitude and love I have for the individuals that have helped me get to this point in my journey. I need to thank Dr. Daniel Ess who has instilled in me deep knowledge and understanding of chemistry, unveiling a sliver of how our marvelous world works. I now often dream about traversing through a range of mountain passes only to find myself ending up where I first started. In all seriousness, Dan's perpetual patience, enthusiasm for solving challenging problems, and mentorship to groom students to become independent scientists are a select few characteristics that I hope to mirror one day. Dan is truly a giant with shoulders, and none of this work would have been possible without him.

I'm especially thankful for a highly collaborative endeavor with researchers at Chevron Phillips Chemical Co. LP. Much gratitude to the CPChem folks for not only funding me throughout the entirety of the doctoral program, but for their mentorship and friendship. Drs. Steven Bischof, Orson Sydora, and Uriah Kilgore have been instrumental puppeteers molding me to become the scientist I am today.

I would also like to thank Dr. Woodfield, Dr. Michaelis, Dr. Stowers, and Dr. Harrison for not only serving as committee members, but always taking time to answer my questions and treating me as a colleague. I also want to thank the folks at Fulton Supercomputing Lab for providing state of the art computational resources without whom, I would still be sitting in the lab calculating nasty integrals. I have been very fortunate to make such great friends who have positively influenced me throughout my time at BYU: Deepa, Samantha, Ying, Steven, Madhu, Clinton, Jack, Ryan, Kyle, Josh, and all the undergraduate students who took on the blunt of the grunt work; I sincerely appreciate you.

Lastly, I want to thank my family. My parents have sacrificed so much for me, and I'm grateful I was able to grow up in the states and pursue higher education. I appreciate my younger brother, Doo-Hee, for putting up with me and helping me whenever I needed it. Special thanks and love to my amazing wife, Eunsol, who worked full-time, had her hands full as a full-time wife and mother, and for always encouraging me to do better and brightening my life. Our daughter, Narin, has also carried a lot of weight on her tiny shoulders with mom and dad not being around as often as we would have liked. Now that Narin can run and jump to new places, I'm excited to see what awaits us on the next part of the journey.

Chapter 3 was reprinted (adapted) with permission from Kwon, D. –H.; Fuller, J. T., III; Kilgore, U. J.; Sydora, O. L.; Bischof, S. M.; Ess, D. H. *ACS Catal.* **2018**, *8*, 1138. DOI: 10.1021/acscatal.7b04026. Copyright 2018 American Chemical Society.

Chapter 5 was reprinted (adapted) with permission from Kwon, D. –H.; Small, B. L.; Sydora, O. L.; Bischof, S. M.; Ess, D. H. *J. Phys. Chem. C* **2019**, *123*, 3727. DOI: 10.1021/acs.jpcc.9b00129. Copyright 2019 American Chemical Society.

"If I have seen further, it is by standing on the shoulder of giants." - Isaac Newton

TABLE OF CONTENTS

LIST OF FIGURES

LIST OF TABLES

LIST OF SCHEMES

1 INTRODUCTION

1.1 Ethylene Oligomerization Overview

Formation of linear α-olefins (LAOs) through ethylene oligomerization is an important industrial scale reaction produced on the million ton scale annually.[1,2] LAOs are in high demand as precursors for the synthesis of plasticizers, lubricants, detergents, surfactants, and used as a co-monomer in ethylene co-polymerization to form linear-low density polyethylene (LLDPE).[3] Often, LAOs are produced through full range catalysis where a distribution of both short-chain and long-chain LAOs are formed. However, approximately 50% of LAOs produced worldwide, mainly 1-butene, 1-hexene, and 1-octene were used as co-monomers with ethylene to produce LLDPE (Scheme 1-1).[4] Because of the utility of LAOs, there has been a surge in developing new catalysts for selective ethylene oligomerization to generate short-chain LAOs. In particular, 1-hexene and 1-octene are highly attractive short-chain LAOs that exhibit desirable co-polymer characteristics such as greater stress-crack and tear resistance compared to co-polymers made with 1-butene.[5]

Scheme 1-1. a) Overview of full-range ethylene oligomerization that generates short-chain and long-chain LAOs. b) Illustration of 1-hexene co-monomer co-polymerization with ethylene forming LLDPE. The bolded line denotes a chain of ethylene units.

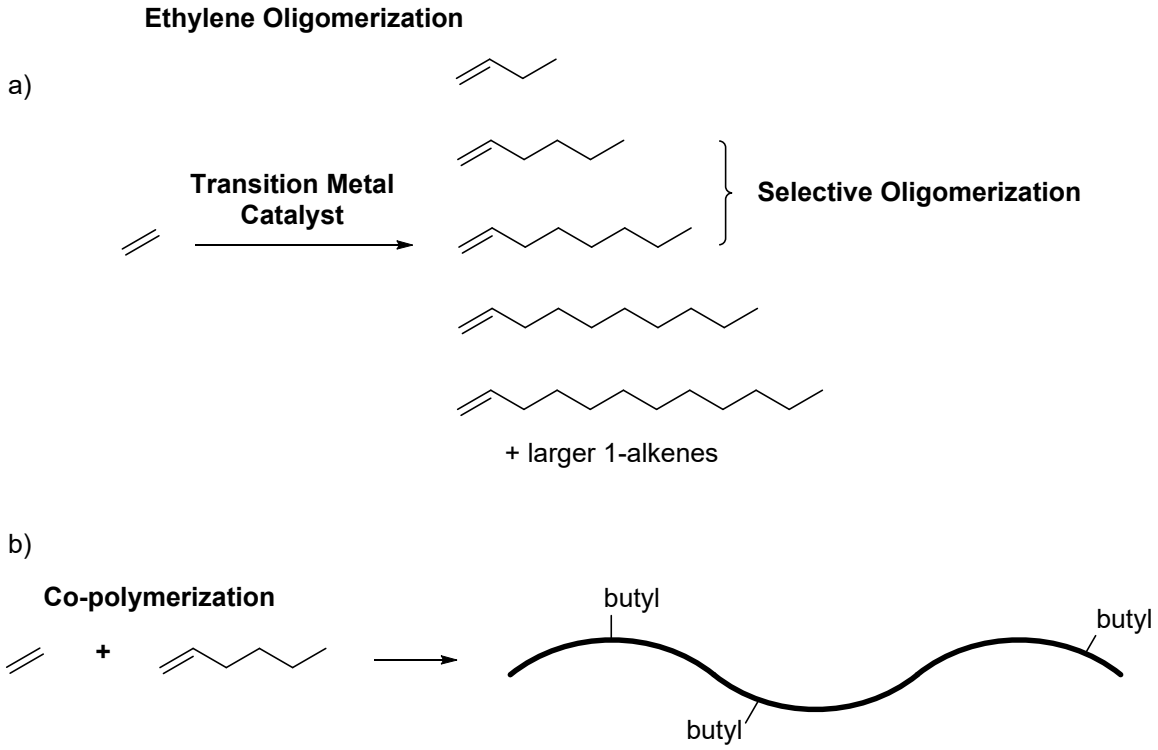

Transition-metal catalyzed polymerization began with the independent discoveries by Hogan and Banks (Phillips Petroleum) and Ziegler and Natta in the early 1960s. Phillips Petroleum technology used a silica based chromium system that produced crystalline polyethylene while Ziegler and Natta utilized titanium-based catalysts, which resulted in the 1963 Nobel Prize. The heterogeneous, multinuclear nature of both catalyst systems, the value in commodity chemicals, and advancements in organometallic chemistry enabled the discovery of homogeneous complexes also capable of oligomerizing ethylene with high activity and selectivity. There are numerous examples of transition metals and lanthanides catalysis facilitating full range ethylene oligomerization with various activities and selectivities. [6-9]

Full range ethylene oligomerization reactions are generally proposed to occur via a Cossee-Arlman mechanism[10] that produce a Schulz-Flory distribution of short chain oligomers (C_4-C_{20}). The Cossee-Arlman mechanism is outlined in Scheme 1-2. Homogeneous full range processes are typically catalyzed with a transition metal catalyst and aluminum activator. Select industrial examples include a nickel catalyst used by Shell, which is referred to as the Shell higher olefin process (SHOP),[11] Zr based metallocene catalysts developed by Idemitsu,[12] and Zr carboxylate complexes practiced at SABIC-Linde.[13] A prominent example of molecular catalysis for LAO production with potential commercial application was reported in 1998 by Small and Brookhart where modified-methylaluminoxanes (MMAO) activated a Fe tridentate pyridine bisimine (PBI) complex catalyzed ethylene oligomerization with a general distribution range of C_4-C_{20}.[14] Later, Small at Chevron Phillips Chemical Co. LP discovered Fe pendant donor diimine complexes ((PDD)Fe) that greatly enhanced linear selectivity with almost no branching, albeit with reduced catalytic rates.[15] The high terminal alkene selectivity with no branching is the subject discussed in chapter 5.

Scheme 1-2. Cosse-Arlman mechanism for full range ethylene oligomerization. Squares denote a vacant site on the Fe.

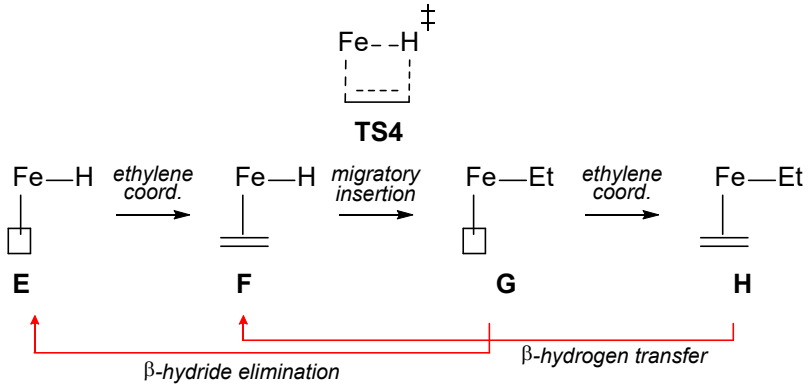

Instead of producing a distribution of oligomers, current market needs have placed heavy demand on selectively forming oligomer fragments.[4] The selective transformation of ethylene to 1-hexene oligomers has been demonstrated with several transition metals, with chromium being the most active, selective, and studied. The first example of selective ethylene trimerization was discovered by Union Carbide Corporation (UCC) employing a 2-ethylhexanoate-chromium complex and an aluminum co-catalyst.[16] They observed 1-hexene as the major byproduct oligomer during polyethylene production. Phillips Petroleum was the first to develop a trimerization catalyst which achieved greater 90% 1-hexene selectivity.[16]

Chevron Phillips Chemical was the first to commercialize a selective 1-hexene process,[17] and several other companies quickly followed with their own process.[18] Sasol,[19] DowDuPont,[20] French Institute of Petroleum,[21] and British Petroleum[22] are several companies that developed selective ethylene trimerization and tetramerization processes. In most of their processes, selective oligomerization to 1-hexene and/or 1-octene is typically catalyzed by a Cr transition metal catalyst with an aluminum activator. The putative mechanism involves the formation of metallacycle intermediates, which provides an explanation for the observed LAO selectivity along with the formation of undesirable side products, such as methylcyclopentane and methylenecyclopentane (see below).[23-25]

The commercial Chevron Phillips 1-hexene process is ~99% selective and therefore no 1-octene is produced. In 2012, Sydora and co-workers at Chevron Phillips demonstrated the generation of a mixture of 1-hexene and 1-octene by using molecular phosphinonamidine Cr catalysts.[26] Through modification of the phosphinoamidine ligand architecture, 1-hexene Cr catalysts were found to give moderate amounts (~30%) of 1-octene. The computational-

experimental collaboration described in Chapter resulted in the discovery of new, more 1-octene selective Cr catalysts.

1.2 Cr-Catalyzed Ethylene Trimerization

As mentioned above, the first example of selective ethylene trimerization formation was discovered by Union Carbide Corporation (UCC) employing a 2-ethylhexanoate-chromium species and an aluminum co-catalyst.[16] They observed 1-hexenes as the major byproduct oligomer during the production of polyethylene.[27] A metallacycle mechanism rather than a linear chain growth Cossee-Arlman mechanism was proposed to account for differences in second order rate dependence for the formation of 1-hexene (Scheme 1-3). A chromacycle mechanism also provided an explanation for the branched decene side products that was formed by the co-trimerization of two ethylenes and one 1-hexene oligomer.

The mechanism of ethylene trimerization via metallacycle intermediates is illustrated in Scheme 1-3. MMAO activates the chromium catalyst allowing the formation of the di-ethylene coordinated Cr^{I} intermediate **A**. Oxidative carbon-carbon coupling forms the chromacyclopentane **B** with Cr^{I} oxidizing to Cr^{III}. A third ethylene coordinates to form intermediate **C** followed by migratory insertion to form the metallacycloheptane intermediate **D**. From D, β-hydrogen transfer, **TS1**, produces the 1-hexene product and regenerates the Cr^{I} catalyst. β -hydrogen transfer is akin to a concerted β-hydride elimination followed by reductive elimination. The chromacycle pathway offered a rationale for the observed 1-hexene selectivity while the Cossee-Arlman mechanism does not provide a reasonable explanation.

Scheme 1-3. Outline of catalytic ethylene trimerization by a chromacycle mechanism. Spectator ligands have been removed for visual clarity.

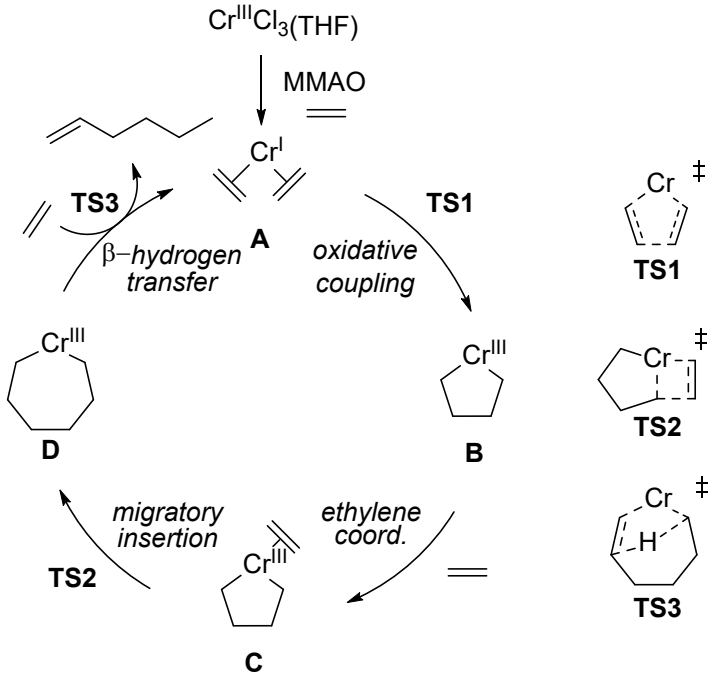

In this chromacycle mechanism, Cr must access M^n and M^{n+2} oxidation states during oxidative coupling and reductive elimination reaction steps. Because direct observation of catalytic Cr species is difficult for a variety of reasons, such as access to high spin states, experimental and computational studies have suggested both Cr^I/Cr^{III} and Cr^{II}/Cr^{IV} cycles, although the majority of studies a a $Cr^{I/III}$ pathway.[28-30] Early evidence establishing the chromacycle mechanism along with characterizing the oxidation state was demonstrated by Jolly who isolated a Cr^{III}-alkanediyl chromacyclopentane and chromacycloheptane intermediates.[24] However, it is important to note that these Cr^{III}-alkanediyl species are not catalytically active. Considering supporting ligands relevant to catalytic oligomerization, Bercaw isolated and characterized a Cr^{III}(PNP)Br(biphenyldiyl) complex by x-ray diffraction.[31] The bromochromium biphenyldiyl species were activated by $NaBAr^F_4$ in the presence of ethylene, producing both 1-hexene and

vinylbiphenyl supporting the $Cr^{I/III}$ cycle. Magnetic susceptibility measurements of a 1,3,5-triazacyclohexane-Cr species resulted in $\mu_{eff} = 3.1 - 4.1\ \mu_B$ indicating the presence of a mono and dinuclear Cr^{III} species.[32] Cr^0 and Cr^I carbonyl complexes containing a bidentate diphosphinoamine (PNP) ligands were examined by Wass[33] and Hanton[34] that revealed the Cr^I species with a weakly coordinating anion was necessary to produce an active catalytic system. Electron paramagnetic resonance studies observed a Cr^I(PNP) complex; however, this only accounts for a small amount of the active species in solution.[35] Regardless, with the addition of ethylene, the signal corresponding to the active species broadens, indicating the redox cycle between $Cr^{I/III}$ during catalysis. Theopold has shown that neutral Cr^I dinitrogen complexes catalyzes ethylene trimerization as well as the corresponding monomeric Cr^{III} chromacyclopentadiene.[36] These complexes are quite sluggish in activity, consistent with highly active cationic systems. McGuinness, based on computations propsoed a Cr^I/Cr^{III} redox cycle with the M06L functional best replicating experimental values. [37]

As mentioned earlier, Jolly successfully isolated chromacyclopentane and chromacycloheptane derivatives containing η^5 cyclopentadienyl stabilized Cr complexes lending support of a metallacycle mechanism.[24] Deuterium labeling studies using a 1:1 C_2H_4 and C_2D_4 trimerization reaction was the first study to distinguish between the metallacycle and Cossee-Arlman mechanisms.[31] Bercaw demonstrated the trimerization reaction produces only the isotopomers C_6D_{12}, $C_6D_8H_4$, $C_6D_4H_8$, and C_6H_{12} in a 1:3:3:1 ratio, indicative of a chromacycle pathway. Further investigations with cis and trans ethylene-d_2, revealed only scrambling at the terminal position supporting rapid reductive elimination or a 3,7 hydride shift (β-hydrogen transfer) with no product 2,1 reinsertion.[38] Although difficult to pinpoint the product forming pathway, theoretical studies support a concerted β-hydrogen transfer pathway to be most likely as

opposed to stepwise alternatives such as β-hydride elimination followed by reductive elimination.[39-43]

Improving upon the Cr system developed by UCC, Phillips Petroleum was the first to demonstrate a catalyst capable of trimerizing ethylene to 1-hexene with selectivity greater than 90%.[44] The Phillips trimerization catalyst system includes a Cr^{III} 2-ethylhexanoate complex, 2,5-dimethylpyrrole, $AlEt_2Cl$, and triethylaluminum in toluene in molar ratios of 1:3.3:7.8:10.8 at 25°C which produces 99.9% liquid oligomers containing 93.8% hexene of which were 99.2% 1-hexenes.[45] Impurities consisted of linear and branched decene oligomers. There are conflicting mechanistic studies of the Phillips trimerization catalyst where both a $Cr^{I/III}$, $Cr^{II/IV}$, and an interplay of the two redox cycles are proposed.[30,46-48]

Mixed phosphine, sulfur, and amine donor ligands have emerged as highly desirable ligands for Cr in catalyzing selective ethylene trimerization. In 2002, BP developed a highly active and selective 1-hexene Cr catalysts utilizing diphosphazane ligands.[49] Catalyst **1** reached activities as high as 1 x 10^6 g/g Cr per hour with 90% 1-hexene selectivity and no polyethylene products were observed. The major byproduct consisted of C_{10} oligomers from co-oligomerization of two ethylene units and one 1-hexene fragment. A year later, McGuinness reported bis(phosphino)amine (**2**) and bis(sulfanyl)amine (**3**) tridentate Cr complexes achieved 1-hexene selectivities >97% shown in Scheme 1-4.[29,50]

Scheme 1-4. Examples of Cr ligands Selective ethylene trimerization ligands.

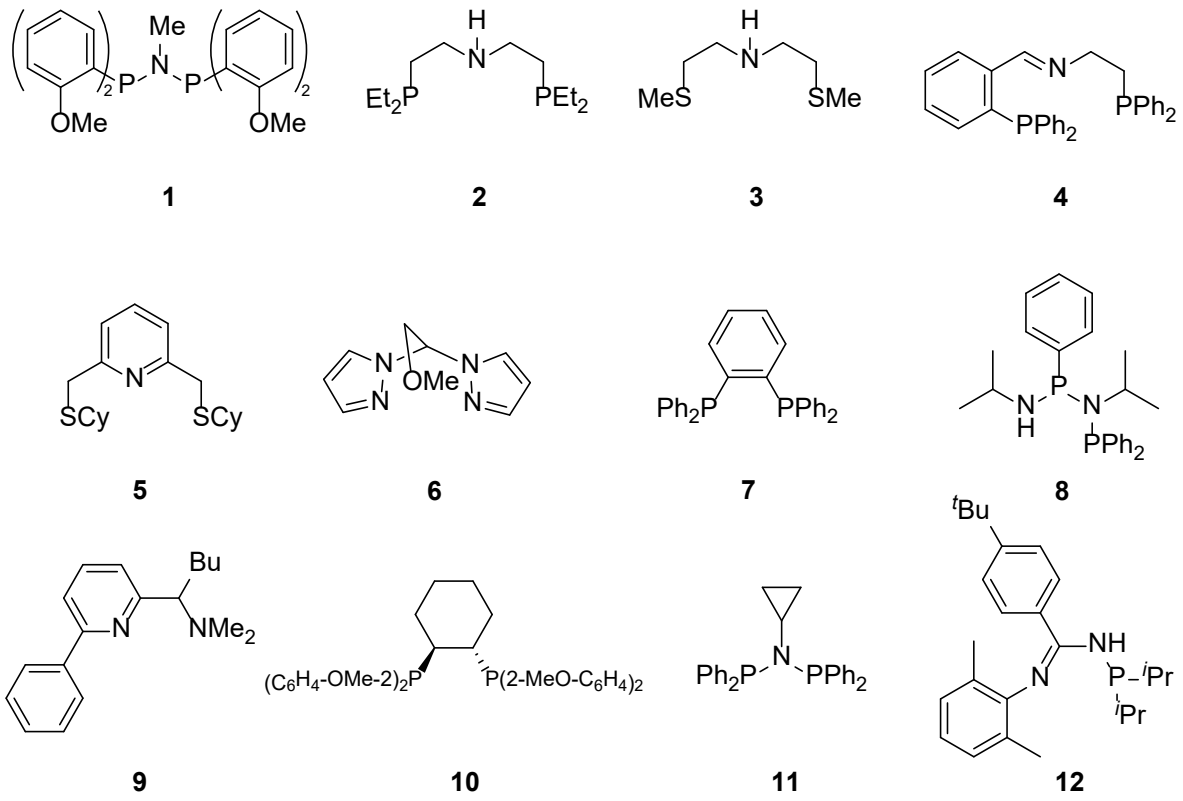

The anionic PNP and SNS Cr complexes were tested and observed to be active and selective for ethylene trimerization, suggesting the ligands are deprotonated during catalysis.[19] However, Gambarotta provided evidence the N-H group remains intact by isolating a deprotonated ligand Cr^{II} dimer species that did not produce oligomers.[51,52] The N-H group is potentially important for selective catalysis because Sasol reported an alkylated amine ligand with low catalytic activity and selectivity with the reaction forming mostly polyethylene products. The effect of chelate size was also investigated by elongating one of the PCCN linkers with an extra methylene spacer group. This modification also reduced activity and selectivity highlighting the importance of relatively close binding modes.

Bluhm reported tridentate imine and amine ligands and examined the effects of changing the N-donor groups with P, O, and S (Ligand 4, Scheme 1-4).[53] By varying reaction conditions

such as temperature, the selectivity could be tuned from polyethylene to 1-hexenes. Other tridentate ligands featuring a central imine or amine group have also been reported to facilitate selective ethylene trimerization (Ligand 5, Scheme 1-4),[54] along with heteroscorpionate pyrazolyl Cr complexes reported by Braunstein and Hor (Ligand 6, Scheme 1-4)[55] although with much less activity and selectivity for 1-hexene compared to **1**, **2**, and **3**. Further modifications of the diphosphinoamine ligands have been reported by Rosenthal featuring aminodiphosphinoamine (PNPN) type ligands; these systems are also sluggish and less selective compared to **1**, **2**, and **3**.[56]

In 2012, Chevron Phillips reported highly active and selective trimerization catalysts based on *N*-phosphinoamidine Cr complexes.[26] A potential advantage of the unsymmetrical P,N ligand framework is that it provides significant steric and electronic tunability compared to homoditopic parent compounds. Catalyst **4** in Scheme 1-4 achieved catalytic activity of 1 x 10^6 g/g Cr · hr with greater than 99% 1-hexene selectivity. This was somewhat unexpected since many highly active ethylene trimerization catalysts have tridentate ligand frameworks and the tridentate catalyst synthesized by Chevron Phillips showed no catalysis.

1.3 Ethylene Tetramerization

Developing Cr catalysts for selective ethylene tetramerization has been significantly more challenging than selective 1-hexene catalysts.[57] An abbreviated mechanism for the formation of 1-octene through the chromoacycle mechanism is shown in Scheme 1-5. At the chromacycloheptane intermediate **D**, instead of *β*-hydrogen transfer, a fourth ethylene coordinates to the Cr metal and undergoes migratory insertion to form the chromacyclononane intermediate **E** which then goes through a β-hydrogen transfer transition state to form the 1-octene product.

Scheme 1-5. Abbreviated outline of ethylene tetramerization mechanism starting from the chromacycloheptane intermediate.

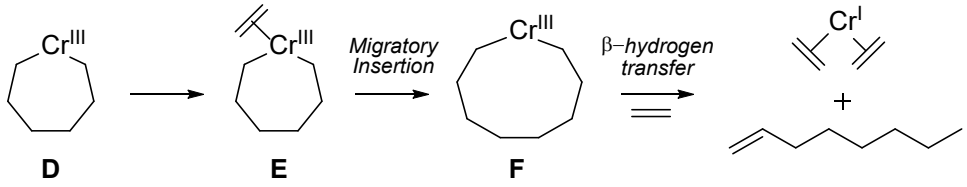

Sasol was the first to report a catalyst showing high activity and relatively high selectivity for 1-octene. By removing the ortho-substitution on the aryl phosphine groups and changing the methyl on the amine to an isopropyl (ligand **18** on Scheme 1-6), Bollmann demonstrated high activities (2.7 x 10^5 g/g Cr per hour) and relatively high 1-octene selectivities (70%) could be achieved.[58] The other major product formed was the 1-hexene. However, depending on the ligand, significant amounts of non LAO isomers reduced the purity of 1-hexene oligomers. Methylcyclopentane and methylenecyclopentane isomers were observed to make up as much as 60% of the C_6 fraction. The difference in trimer and tetramer selectivities can be rationalized with steric interactions and coordination effects. The BP ligands contain ortho-substituted ether donors that can bind to a metal vacant site adopting a pseudo-tridentate chelate framework and occupies the metal coordination sphere compared to a more accessible metal center in κ^2 tetramerization ligand **18**. Both of these factors potentially enhance 1-hexene selectivity by suppressing the ability of more ethylene units to bind to the metal; whereas, **18** reduces the steric interactions and enables an extra metal coordination site.

Several efforts have examined modification of the diphosphinoamine ligand. Overett investigated electronic and steric effects of polar functional groups substituted on various positions of the aryl groups. As expected, modifying the methoxy group from ortho to meta to para positions progressively shifted the oligomer selectivity from 1-hexene to 1-octene.[59] Jiang investigated

substituent effects on the central amine by changing the isopropyl (iPr) group to a cyclopentane. The cyclopentylamine group improved 1-octene selectivity up to ~75% with moderate catalytic activity.[60] Wass explored ligand backbone alkylation effects in bis(diphenylphosphino)methane, referred to as dppm, Cr complexes.[61] Modifying the carbon substituents with short and long aliphatic chains and benzyl groups, selective ethylene transformation was enhanced compared to the unsubstituted dppm catalysts suggesting increased stability against deprotonation and decomplexation. However, the various C-substituted ligands did not match the performance of the diphosphinoamine counterparts.

Gambarotta and Duchateau reported several selective ethylene oligomerization catalysts. A few select examples include the development of aminophosphine-based ligand such as PNPy, PNN, and PNP. Ligand PNP exhibited the best performance, achieving 89% 1-octene selectivity. Ligand PNPy was slightly lower at 75% 1-octene selectivity while surprisingly the PNP ligand switches toward nonselective, full range oligomerization.[62] Cr complexes bearing a series of pyridine-phosphine ligands have also been investigated (Ligands PNCN, PNCCP). The highest 1-octene achieved was 58%, but catalytic activity was significantly slower compared to previous generation bidentate phosphinoamine Cr complexes.[63]

Sasol also developed bis(phosphanyl)amine ligands capable of selective ethylene tetramerization.[64] Ligand **19** achieved 61% 1-octene selectivity with 4.9 x 10^5 g/g Cr per hour activity. Similar steric influences were observed with the bis(phosphanyl)amines; modifying the 2,6 methyl groups on the aniline to isopropyl groups switched the selectivity toward 1-hexene. Many adjustments to the diphosphazane and bis(phosphanyl)amine ligands have been investigated.[4]

Scheme 1-6. Selective tetramerization catalysts

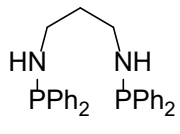

13

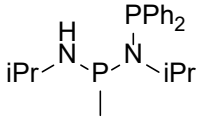

14

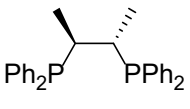

15

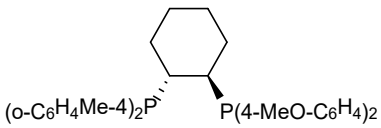

16

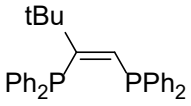

17

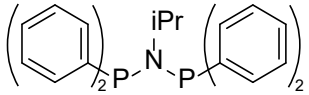

18

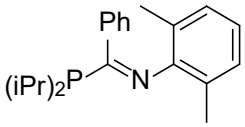

19

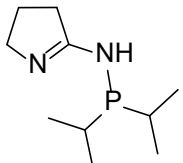

20

As mentioned earlier, generally the most significant impurities during catalysis result from in formation of alkylcyclopentanes and alkenylcyclopentanes. Although these undesired cyclic byproducts provide additional evidence that support a chromacycle mechanism, these off-cycle pathways can become more prevalent as the catalysts become more selective for 1-octene. Therefore, a key challenge to overcome in selective ethylene tetramerization is to develop selective 1-octene catalysts where the off-cycle pathways resulting on products other than LAOs are non-competitive.

1.4 Computational Studies on Selective Ethylene Tri-/Tetramerization

Several density functional theory (DFT) studies have been conducted to elucidate the mechanism, metal oxidation state and spin state, and ligand effects of chromium catalyzed selective ethylene trimerization and tetramerization. One of the first computational studies employing DFT was reported by van Rensburg,[46] investigating the Phillips trimerization catalyst. The authors proposed a $Cr^{II/IV}$ redox cycle with the triplet spin state as the lowest energy pathway, and proposed that no spin state crossing is likely to occur. In a related study, Blom computationally examined cyclopentadienyl Cr complexes and also concluded a catalytically reactive Cr^{IV}

oxidation state containing a triplet spin configuration is most likely.[65] Mukhopadhyay investigated neutral and cationic Cr complexes using chloro groups and B3LYP level of theory and also concluded the $Cr^{II/IV}$ pathway was most likely.[66]

Contrary to these reports, Budzelaar proposed a $Cr^{I/III}$ pathway using indolyl as a model for a tetrahydrocarbozolyl ligand.[67] Based on B3LYP calculations, it was proposed that the quartet spin state is the lowest in energy and spin crossing is unlikely to occur. In 2011, Liu performed DFT calculations on Ligand **3** from Scheme 1-4 and was the first to propose that spin crossing is viable.[68] Liu's calculations indicated that a Cr^{I} diethylene coordinated sextet spin state initiated catalysis and subsequent oxidation to Cr^{III} facilitated spin surface crossing through a minimum energy crossing point (MECP) onto the quartet surface. The sextet to quartet spin crossing allowed access to lower energy pathways illustrated in Scheme 1-7. It is worth noting the authors also examined $Cr^{II/IV}$ dicationic species and concluded the cationic $Cr^{I/III}$ was the most likely redox cycle. They also examined the acidity of the amine proton and found the ligands were unlikely to be deprotonated by MAO. Although B3LYP may correctly predict the ability of the Cr complexes to undergo spin crossing and access lower energy pathways, the reported free energy barriers are relatively high (33 kcal/mol) for this very efficient catalytic process, which suggests the computed B3LYP barriers do not quantitatively model experimental rates.

Scheme 1-7. Spin state crossing allows access to lower energy pathways. Ligands are omitted for clarity.

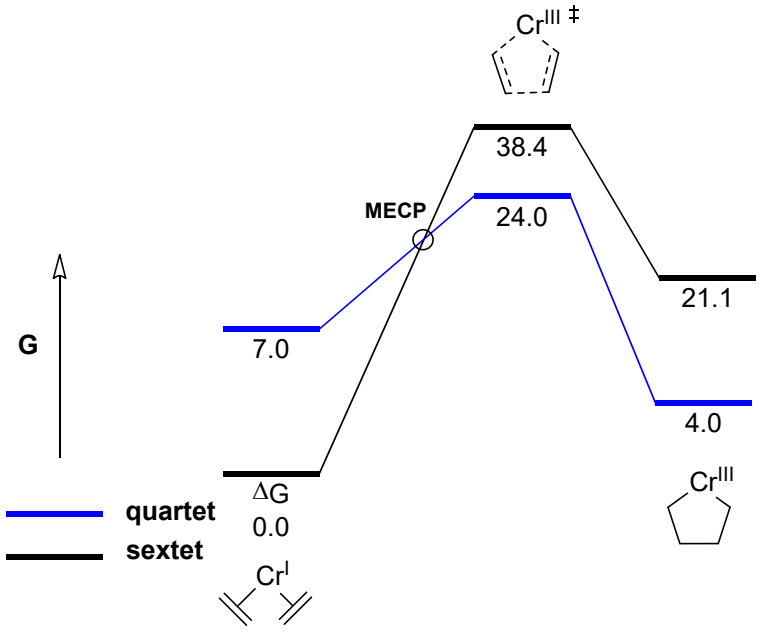

In 2014, McGuinness performed a computational DFT benchmark study versus wavefunction methods and identified the M06L functional accurately models spin state energy gaps better than other commonly used functionals such as B3LYP.[37] Employing the M06L functional, McGuinness computed a model system of Ligand **6** where the aryl and isopropyl groups on the phosphine and amine respectively were truncated to methyl groups.[43] The authors proposed a similar $Cr^{I/III}$ pathway to previous works of Liu,[68] where spin state crossing from sextet to quartet surfaces facilitate catalysis. McGuinness followed up a computational report by investigating the complete Ligand **6** and provided mechanistic insights for cyclic impurities in the C_6 olefins.[69]

1.5 Overview of Dissertation Chapters 2-5

Chapter 2 provides a brief introduction to density functional theory (DFT) methods and the general computational approaches used in this work.

Chapter 3 presents a computational study where a transition-state model was developed to quantitatively predict ethylene trimerization versus tetramerization selectivity. This resulted in the prediction and experimental testing of a new family of Cr phosphine monocyclic imine catalysts.

Chapter 4 reports a computational study examining the mechanism and relative reactivity of several didentate and tridentate ligands for Cr-catalyzed 1-hexene.

Chapter 5 presents a computational investigation examing Fe-catalyzed full-range oligomerization.

1.6 References

1. Green, M. M.; Wittcoff, H. A. *Organic Chemistry Principles and Industrial Practice,* Wiley-VCH Verlag GmbH & Co., 2003.
2. Weissermel, K.; Arpe, H.-J. *Industrial Organic Chemistry,* Chapter 3, 5th ed. Wiley-VCH Verlag GmbH & Co., 2010.
3. Kissin, Y. V. Polyethylene, Linear Low Density, *Kirk-Othmer Encyclopedia of Chemical Technology* pp.
4. Alferov, K. A.; Belov, G. P.; Meng, Y. Chromium catalysts for selective ethylene oligomerization to 1-hexene and 1-octene: Recent results. *Appl. Catal., A* **2017,** *542*, 71.
5. Breuil, P.-A. R.; Magna, L.; Olivier-Bourbigou, H. Role of Homogeneous Catalysis in Oligomerization of Olefins : Focus on Selected Examples Based on Group 4 to Group 10 Transition Metal Complexes. *Catal. Lett.* **2015,** *145*, 173.
6. Bianchini, C.; Giambastiani, G.; Rios, I. G.; Mantovani, G.; Meli, A.; Segarra, A. M. Ethylene oligomerization, homopolymerization and copolymerization by iron and cobalt catalysts with 2,6-(bis-organylimino)pyridyl ligands. *Coord. Chem. Rev.* **2006,** *250*, 1391.
7. Gibson, V. C.; Redshaw, C.; Solan, G. A. Bis(imino)pyridines: Surprisingly Reactive Ligands and a Gateway to New Families of Catalysts. *Chem. Rev.* **2007,** *107*, 1745.
8. Bianchini, C.; Giambastiani, G.; Luconi, L.; Meli, A. Olefin oligomerization, homopolymerization and copolymerization by late transition metals supported by (imino)pyridine ligands. *Coord. Chem. Rev.* **2010,** *254*, 431.
9. Small, B. L. Discovery and Development of Pyridine-bis(imine) and Related Catalysts for Olefin Polymerization and Oligomerization. *Acc. Chem. Res* **2015,** *48*, 2599.

10. Cossee, P. Ziegler-Natta catalysis I. Mechanism of polymerization of α-olefins with Ziegler-Natta catalysts. *J. Catal.* **1964,** *3*, 80.

11. Keim, W. Oligomerization of Ethylene to α-Olefins: Discovery and Development of the Shell Higher Olefin Process (SHOP). *Angew. Chem. Int. Ed.* **2013,** *52*, 12492.

12. Shiraki, Y.; Tamura, T. Production of Linear Alpha-Olefins. US Patent 4886933, 1989.

13. Aliyev, V.; Mosa, F.; Al-Hazmi, M. Catalyst Composition for Oligomerization of Ethylene Oligomerization Process and Method for its Preparation. US Patent 8481444, 2013.

14. Small, B. L.; Brookhart, M. Iron-Based Catalysts with Exceptionally High Activities and Selectivities for Oligomerization of Ethylene to Linear α-Olefins. *J. Am. Chem. Soc.* **1998,** *120*, 7143.

15. Small, B. L.; Rios, R.; Fernandez, E. R.; Carney, M. J. Oligomerization of Ethylene Using New Iron Catalysts Bearing Pendant Donor Modified α-Diimine Ligands. *Organometallics* **2007,** *26*, 1744.

16. Hurley, G. F.; Manyik, R. M.; Walker, W. E.; Wilson, T. P., Olefin polymerization catalysts. U. S. Patent 3,242,099A.

17. Reagen, W. K.; McDaniel, M. P., Chromium compounds and uses in trimerization or oligomerization. U.S. Patent 5,382,738A.

18. Dixon, J. T.; Green, M. J.; Hess, F. M.; Morgan, D. H. Advances in selective ethylene trimerisation – a critical overview. *J. Organomet. Chem.* **2004,** *689*, 3641.

19. McGuinness, D. S. Olefin Oligomerization via Metallacycles: Dimerization, Trimerization, Tetramerization, and Beyond. *Chem. Rev.* **2011,** *111*, 2321.

20. Al-Jarallah, A. M.; Anabtawi, J. A.; Siddiqui, M. A. B.; Aitani, A. M.; Al-Sa'doun, A. W. Ethylene dimerization and oligomerization to butene-1 and linear α-olefins: A review of catalytic systems and processes. *Catal. Today* **1992,** *14*, 1.

21. Al-Sa'doun, A. W. Dimerization of ethylene to butene-1 catalyzed by Ti(OR')4-AlR3. *Appl. Catal., A* **1993,** *105*, 1.

22. Wu, F. J. Ethylene trimerization. US Patent, 5968866A, October 19, 1999.

23. Stockis, A.; Hoffmann, R. Metallacyclopentanes and bisolefin complexes. *J. Am. Chem. Soc.* **1980,** *102*, 2952.

24. Emrich, R.; Heinemann, O.; Jolly, P. W.; Krüger, C.; Verhovnik, G. P. J. The Role of Metallacycles in the Chromium-Catalyzed Trimerization of Ethylene. *Organometallics* **1997,** *16*, 1511.

25. Zheng, F.; Sivaramakrishna, A.; Moss, J. R. Thermal studies on metallacycloalkanes. *Coord. Chem. Rev.* **2007,** *251*, 2056.

26. Sydora, O. L.; Jones, T. C.; Small, B. L.; Nett, A. J.; Fischer, A. A.; Carney, M. J. Selective Ethylene Tri-/Tetramerization Catalysts. *ACS Catal.* **2012,** *2*, 2452.

27. Manyik, R. M.; Walker, W. E.; Wilson, T. P. A soluble chromium-based catalyst for ethylene trimerization and polymerization. *J. Catal.* **1977,** *47*, 197.

28. Jabri, A.; Crewdson, P.; Gambarotta, S.; Korobkov, I.; Duchateau, R. Isolation of a Cationic Chromium(II) Species in a Catalytic System for Ethylene Tri- and Tetramerization. *Organometallics* **2006,** *25*, 715.

29. McGuinness, D. S.; Wasserscheid, P.; Keim, W.; Morgan, D.; Dixon, J. T.; Bollmann, A.; Maumela, H.; Hess, F.; Englert, U. First Cr(III)−SNS Complexes and Their Use as Highly

Efficient Catalysts for the Trimerization of Ethylene to 1-Hexene. *J. Am. Chem. Soc.* **2003,** *125*, 5272.

30. Venderbosch, B.; Oudsen, J.-P. H.; Wolzak, L. A.; Martin, D. J.; Korstanje, T. J.; Tromp, M. Spectroscopic Investigation of the Activation of a Chromium-Pyrrolyl Ethene Trimerization Catalyst. *ACS Catal.* **2019,** *9*, 1197.
31. Agapie, T.; Schofer, S. J.; Labinger, J. A.; Bercaw, J. E. Mechanistic Studies of the Ethylene Trimerization Reaction with Chromium−Diphosphine Catalysts: Experimental Evidence for a Mechanism Involving Metallacyclic Intermediates. *J. Am. Chem. Soc.* **2004,** *126*, 1304.
32. Köhn, R. D.; Haufe, M.; Kociok-Köhn, G.; Grimm, S.; Wasserscheid, P.; Keim, W. Selective Trimerization of α-Olefins with Triazacyclohexane Complexes of Chromium as Catalysts. *Angew. Chem. Int. Ed.* **2000,** *39*, 4337.
33. Bowen, L. E.; Haddow, M. F.; Orpen, A. G.; Wass, D. F. One electron oxidation of chromium N,N-bis(diarylphosphino)amine and bis(diarylphosphino)methane complexes relevant to ethene trimerisation and tetramerisation. *Dalton Trans.* **2007**, 1160.
34. Rucklidge, A. J.; McGuinness, D. S.; Tooze, R. P.; Slawin, A. M. Z.; Pelletier, J. D. A.; Hanton, M. J.; Webb, P. B. Ethylene Tetramerization with Cationic Chromium(I) Complexes. *Organometallics* **2007,** *26*, 2782.
35. Brückner, A.; Jabor, J. K.; McConnell, A. E. C.; Webb, P. B. Monitoring Structure and Valence State of Chromium Sites during Catalyst Formation and Ethylene Oligomerization by in Situ EPR Spectroscopy. *Organometallics* **2008,** *27*, 3849.
36. Monillas, W. H.; Young, J. F.; Yap, G. P. A.; Theopold, K. H. A well-defined model system for the chromium-catalyzed selective oligomerization of ethylene. *Dalton Trans.* **2013,** *42*, 9198.

37. McGuinness, D. S.; Chan, B.; Britovsek, G. J. P.; Yates, B. F. Ethylene Trimerisation with Cr-PNP Catalysts: A Theoretical Benchmarking Study and Assessment of Catalyst Oxidation State. *Aust. J. Chem.* **2014,** *67*, 1481.

38. Agapie, T.; Labinger, J. A.; Bercaw, J. E. Mechanistic Studies of Olefin and Alkyne Trimerization with Chromium Catalysts: Deuterium Labeling and Studies of Regiochemistry Using a Model Chromacyclopentane Complex. *J. Am. Chem. Soc.* **2007,** *129*, 14281.

39. Blok, A. N. J.; Budzelaar, P. H. M.; Gal, A. W. Mechanism of Ethene Trimerization at an ansa-(Arene)(cyclopentadienyl) Titanium Fragment. *Organometallics* **2003,** *22*, 2564.

40. de Bruin, T. J. M.; Magna, L.; Raybaud, P.; Toulhoat, H. Hemilabile Ligand Induced Selectivity: a DFT Study on Ethylene Trimerization Catalyzed by Titanium Complexes. *Organometallics* **2003,** *22*, 3404.

41. Robinson, R.; McGuinness, D. S.; Yates, B. F. The Mechanism of Ethylene Dimerization with the Ti(OR′)4/AlR3 Catalytic System: DFT Studies Comparing Metallacycle and Cossee Proposals. *ACS Catal.* **2013,** *3*, 3006.

42. Tobisch, S.; Ziegler, T. Catalytic Oligomerization of Ethylene to Higher Linear α-Olefins Promoted by Cationic Group 4 Cyclopentadienyl-Arene Active Catalysts: Toward the Computational Design of Zirconium- and Hafnium-Based Ethylene Trimerization Catalysts. *Organometallics* **2004,** *24*, 256.

43. Britovsek, G. J. P.; McGuinness, D. S.; Wierenga, T. S.; Young, C. T. Single- and Double-Coordination Mechanism in Ethylene Tri- and Tetramerization with Cr/PNP Catalysts. *ACS Catal.* **2015,** *5*, 4152.

44. Reagan, W. EP 0417477 (Phillips Petroleum Company). 1991.

45. Buster, J.; Knudsen, R. US 5,856,257, 1999.

46. Janse van Rensburg, W.; Grové, C.; Steynberg, J. P.; Stark, K. B.; Huyser, J. J.; Steynberg, P. J. A DFT Study toward the Mechanism of Chromium-Catalyzed Ethylene Trimerization. *Organometallics* **2004,** *23*, 1207.

47. Jabri, A.; Mason, C. B.; Sim, Y.; Gambarotta, S.; Burchell, T. J.; Duchateau, R. Isolation of Single-Component Trimerization and Polymerization Chromium Catalysts: The Role of the Metal Oxidation State. *Angew. Chem. Int. Ed.* **2008,** *47*, 9717.

48. Skobelev, I. Y.; Panchenko, V. N.; Lyakin, O. Y.; Bryliakov, K. P.; Zakharov, V. A.; Talsi, E. P. In Situ EPR Monitoring of Chromium Species Formed during Cr−Pyrrolyl Ethylene Trimerization Catalyst Formation. *Organometallics* **2010,** *29*, 2943.

49. Carter, A.; Cohen, S. A.; Cooley, N. A.; Murphy, A.; Scutt, J.; Wass, D. F. High activity ethylene trimerisation catalysts based on diphosphine ligands. *Chem. Commun.* **2002**, 858.

50. McGuinness, D. S.; Wasserscheid, P.; Keim, W.; Hu, C.; Englert, U.; Dixon, J. T.; Grove, C. Novel Cr-PNP complexes as catalysts for the trimerisation of ethylene. *Chem. Commun.* **2003**, 334.

51. Jabri, A.; Temple, C.; Crewdson, P.; Gambarotta, S.; Korobkov, I.; Duchateau, R. Role of the Metal Oxidation State in the SNS−Cr Catalyst for Ethylene Trimerization: Isolation of Di- and Trivalent Cationic Intermediates. *J. Am. Chem. Soc.* **2006,** *128*, 9238.

52. Temple, C.; Jabri, A.; Crewdson, P.; Gambarotta, S.; Korobkov, I.; Duchateau, R. The Question of the Cr Oxidation State in the {Cr(SNS)} Catalyst for Selective Ethylene Trimerization: An Unanticipated Re-Oxidation Pathway. *Angew. Chem. Int. Ed.* **2006,** *45*, 7050.

53. Bluhm, M. E.; Walter, O.; Döring, M. Chromium imine and amine complexes as homogeneous catalysts for the trimerisation and polymerisation of ethylene. *J. Organomet. Chem.* **2005,** *690*, 713.

54. Temple, C. N.; Gambarotta, S.; Korobkov, I.; Duchateau, R. New Insight into the Role of the Metal Oxidation State in Controlling the Selectivity of the Cr-(SNS) Ethylene Trimerization Catalyst. *Organometallics* **2007,** *26*, 4598.

55. Zhang, J.; Braunstein, P.; Hor, T. S. A. Highly Selective Chromium(III) Ethylene Trimerization Catalysts with [NON] and [NSN] Heteroscorpionate Ligands. *Organometallics* **2008,** *27*, 4277.

56. Reddy Aluri, B.; Peulecke, N.; Peitz, S.; Spannenberg, A.; Müller, B. H.; Schulz, S.; Drexler, H.-J.; Heller, D.; Al-Hazmi, M. H.; Mosa, F. M.; Wöhl, A.; Müller, W.; Rosenthal, U. Coordination chemistry of new selective ethylene trimerisation ligand Ph2PN(iPr)P(Ph)NH(R) (R = iPr, Et) and tests in catalysis. *Dalton Trans.* **2010,** *39*, 7911.

57. Sydora, O. L. Selective Ethylene Oligomerization. *Organometallics* **2019,** *38*, 997.

58. Bollmann, A.; Blann, K.; Dixon, J. T.; Hess, F. M.; Killian, E.; Maumela, H.; McGuinness, D. S.; Morgan, D. H.; Neveling, A.; Otto, S.; Overett, M.; Slawin, A. M. Z.; Wasserscheid, P.; Kuhlmann, S. Ethylene Tetramerization: A New Route to Produce 1-Octene in Exceptionally High Selectivities. *J. Am. Chem. Soc.* **2004,** *126*, 14712.

59. Overett, M. J.; Blann, K.; Bollmann, A.; Dixon, J. T.; Hess, F.; Killian, E.; Maumela, H.; Morgan, D. H.; Neveling, A.; Otto, S. Ethylene trimerisation and tetramerisation catalysts with polar-substituted diphosphinoamine ligands. *Chem. Commun.* **2005**, 622.

60. Jiang, T.; Ning, Y.; Zhang, B.; Li, J.; Wang, G.; Yi, J.; Huang, Q. Preparation of 1-octene by the selective tetramerization of ethylene. *J. Mol. Catal. A: Chem.* **2006,** *259*, 161.

61. Dulai, A.; de Bod, H.; Hanton, M. J.; Smith, D. M.; Downing, S.; Mansell, S. M.; Wass, D. F. C-Substituted Bis(diphenylphosphino)methane-Type Ligands for Chromium-Catalyzed Selective Ethylene Oligomerization Reactions. *Organometallics* **2009,** *28*, 4613.

62. Shaikh, Y.; Gurnham, J.; Albahily, K.; Gambarotta, S.; Korobkov, I. Aminophosphine-Based Chromium Catalysts for Selective Ethylene Tetramerization. *Organometallics* **2012,** *31*, 7427.

63. Yang, Y.; Gurnham, J.; Liu, B.; Duchateau, R.; Gambarotta, S.; Korobkov, I. Selective Ethylene Oligomerization with Chromium Complexes Bearing Pyridine–Phosphine Ligands: Influence of Ligand Structure on Catalytic Behavior. *Organometallics* **2014,** *33*, 5749.

64. Radcliffe, J. E.; Batsanov, A. S.; Smith, D. M.; Scott, J. A.; Dyer, P. W.; Hanton, M. J. Phosphanyl Methanimine (PCN) Ligands for the Selective Trimerization/Tetramerization of Ethylene with Chromium. *ACS Catal.* **2015,** *5*, 7095.

65. Blom, B.; Klatt, G.; Fletcher, J. C. Q.; Moss, J. R. Computational investigation of ethene trimerisation catalysed by cyclopentadienyl chromium complexes. *Inorg. Chim. Acta.* **2007,** *360*, 2890.

66. Bhaduri, S.; Mukhopadhyay, S.; Kulkarni, S. A. Density functional studies on chromium catalyzed ethylene trimerization. *J. Organomet. Chem.* **2009,** *694*, 1297.

67. Budzelaar, P. H. M. Ethene trimerization at CrI/CrIII — A density functional theory (DFT) study. *Canadian Journal of Chemistry* **2009,** *87*, 832.

68. Yang, Y.; Liu, Z.; Zhong, L.; Qiu, P.; Dong, Q.; Cheng, R.; Vanderbilt, J.; Liu, B. Spin Surface Crossing between Chromium(I)/Sextet and Chromium(III)/Quartet without Deprotonation in SNS-Cr Mediated Ethylene Trimerization. *Organometallics* **2011,** *30*, 5297.

69. Britovsek, G. J. P.; McGuinness, D. S. A DFT Mechanistic Study on Ethylene Tri- and Tetramerization with Cr/PNP Catalysts: Single versus Double Insertion Pathways. *Chem. Eur. J.* **2016,** *22*, 16891.

2 COMPUTATIONAL METHODS

2.1 Density Functional Theory

For organometallic molecular modeling, quantum-mechanical density functional theory (DFT) methods remain the optimal compromise between computational efficiency and accuracy.[1] DFT utilizes the electron density (ρ) of a molecular system rather than a wavefunction. It has been demonstrated that the total energy of a molecular system can be calculated exactly if the electron density of the system is known. DFT states two theorems: 1) The ground state electron density of a system of electrons determines the Hamiltonian and that the total electronic energy of the system is a functional of the density

$$E = E[\rho] \qquad \text{(Eq 2.1.1)}$$

and 2) the ground state electronic density minimizes the electronic energy of the system.[2-3] While this density-based approach to evaluation of the total energy of a many-body system appears straightforward, the exact functional $E[\rho]$ is unknown. Therefore, DFT methods are approximate and many recipes for the exchange and correlation terms have led to variety of functionals.[4]

A hierarchy exists within DFT methods where different levels of theory approximating the exact functional is sometimes referred to as the "Jacob's ladder." The lowest rung of the ladder is

comprised of the local spin density approximations (LSDA).[5] LSDA is the simplest approximation to the exchange-correlation functional where it is assumed that the electron density has such minimal variability that it can be treated as a uniform electron gas or that the density is a slowly varying function. The LSDA method is known not to be quantitatively accurate but is commonly employed in describing extended metal systems. The next rung on the ladder includes treatment of a non-uniform gas or gradient corrected functionals that allow the electron density to vary in space referred to as the generalized gradient approximation (GGA).[5] Select examples of GGA functionals include BLYP and PBE. Another step up the ladder is referred to as the meta functionals which include functional dependence on the up and down spin kinetic energy densities by taking a second derivative of the density, or the Laplacian. Much of the work performed in this study utilizes the meta-GGA DFT functionals such as M06-L.[6]

The highest rung of the ladder used in this work includes hybrid functionals that include some fraction of the exact Hartree-Fock (HF) exchange. Popular functionals include the so called B3LYP[6] and M06[6-7] functionals and the Minnesota suite of functionals are heavily used throughout this study. B3LYP and M06 include 20% and 27% HF exchange respectively. The variation of the HF exchange (1-100%) results in a myriad of hybrid functionals available today. M06-L and M06 have been examined to access their ability to reproduce experimental values of transition metal complexes with multiple accessible spin states.[6, 8] The binding energies of four complexes containing both covalent and noncovalent bonding modes of zeolite model complexes benchmarked on high level wavefunction methods (CCSD(T)) calculations were tested against the M06 family density functionals.[9] The M06-2X, M06-L, and M06 showed great performance (mean unsigned error ~5 kcal/mol). Bond energies and barrier height benchmarking studies in homogeneous catalysis that included calculation of metal-metal, metal-ligand, alkyl bond

homolysis, and atomization energies of small main group molecules demonstrated the accuracy of the M06 suite and illustrated their applicability in catalytic reactions.[10] Harvey and co-workers demonstrated the M06 suite can accurately predict the trend of phosphine binding energies of Grubbs ruthenium precatalysts in olefin metathesis reactions.[11] Furthermore, Hillier and co-workers computed ring closing metathesis catalyzed by Ru complexes, and the M06 and M06-L functionals agreed with CCSD(T) methods within 1.6 kcal/mol.[12] Buhl has also computed the binding enthalpy of triphenylphosphine ligand in with Ru catalysts, which requires an accurate treatment of noncovalent interactions, and discovered the M06 class of functionals along with dispersion corrected, B97-D, had the best performance.[13] Jensen and co-workers tested a series of functionals for predicting metal-phosphine bond strengths bound to Cr, Ni, Mo, and Ru and found the M06 suite along with dispersion corrected perform quite well.[14] We have demonstrated the M06-L functional accurately predicts singlet-triplet gaps (within 1 kcal/mol) in dinuclear Ni-Ni complexes whereas other functionals differed by as much as ~9 kcal/mol.[15] Specifically for selective ethylene oligomerization processes catalyzed by a Cr metal, M06-L has been shown to accurately model experiment. McGuinness and co-workers performed a theoretical benchmarking study showcasing the M06-L functional to accurately favor a $Cr^{I/III}$ redox cycle consistent with experiments,[16-17] favorable spin state crossing to access lower energy pathways, and overall thermodynamics which mirror highly active Cr oligomerization catalysts.[18] We have also demonstrated ability to quantitatively predict the amount of 1-hexene versus 1-octene oligomers in ethylene oligomerization reactions employing a transition state selectivity model with the M06-L functional.[19] For full range processes, the choice of DFT functional is not as straight-forward and the computational analysis reveals the challenges in modeling these systems.[20]

Higher rungs, such as double hybrid functionals were not used because of the increase in computational cost which does not necessarily improve computational accuracy. These methods scale as N^5 whereas other methods mentioned above scale between N^3-N^4 and depending on the molecular system, the cost and accuracy of single hybrid or local functionals outcompete the double hybrid methods.[4]

2.2 Basis Sets

After choosing a DFT functional, it is necessary to represent the electron density by expanding a set of functions, referred to as a basis set, to approximate the unknown molecular orbitals as a set of one electron functions.[4] Molecular orbitals (MOs) are an approximate mathematical function consisting of a linear combination of atomic orbitals (AOs). There are typically two types of functions to construct atomic orbitals. Slater-type orbitals (STOs) closely resemble atomic orbitals and may seem like a straight forward approach. However, STOs are ill-suited since there are no analytical solutions over multiple STO integrals. Numerical methods severely limit the ability to employ STO basis sets in molecular systems of any significant size. In contrast, an analytical solution can be achieved if the AO functions are chosen to be Gaussian-type. Gaussian-type orbitals (GTOs) are considerably easier to compute and the addition of more GTO functions are more than compensated by its efficiency.[21] GTOs also include contracted GTOs (CGTOSs). CGTOs are typically used for the core electrons and GTOs for valence electrons. Only GTO basis sets are used in this study.

The number of basis functions can significantly affect the speed and accuracy of quantum mechanical calculations. The smallest basis set referred to as the single zeta (SZ) contains only a minimum description of the occupied orbitals. For first row of the periodic table, a SZ basis set only has a single *s*-function.[4] For the second row elements, there are two s-functions and one set

of *p*-functions. The SZ basis set can be improved by doubling the amount of basis functions referred to as double-zeta (DZ) basis set. For hydrogen and helium, a DZ basis set contains two *s*-functions while the second row elements contains four *s*-functions and two *p*-functions. The next improvement triples the number of functions within SZ basis sets. A triple-zeta (TZ) therefore has 3 *s*-functions for first row elements, and 6 *s*-functions and 3 *p*-functions for the second row. The number of functions can continue multiply and create larger basis sets. TZ basis sets are the extent of basis sets used in this study. To accurate model chemical bonding, polarization functions are required. Polarization adds higher angular momentum functions for greater orbital flexibility. Therefore, *p* and *d*-functions are added for the first and second row elements respectively. A commonly used basis set in this study are the 6-31G(d,p)[22-23] and def2-TZVP[24] basis sets. The "6" denotes the number of CGTOs for the core electrons, the "3" and "1" show there are three CGTOs and one GTOs for the valence electrons. The "G" denotes the basis set consists of GTOs. The "d" and "p" indicate polarization functions on the heavy and hydrogen atoms respectively.[25] The def2-TZVP basis set includes polarization functions as well and contains more basis functions than the 6-31G(d,p). For example, the phosphorus atom contains 5 *s*-functions, 5 *p*-functions, 2 *d*-functions and 1 *f*-function. The def2-TZVP basis set was tested on a set of more than 300 molecules in their most common oxidation states and molecular properties such as atomization energies and dipole moments were used for experimental validation. The def2-TZVP basis set coupled with DFT level of theory demonstrated highly accurate quantitative results.[24]

Many basis set functions are required for modeling atoms that contain many core electrons (e.g. transition metals) that do not participate in the chemistry. Relativistic effects further complicate matters as the core electrons are moving at a much greater speed compared to the valence electrons. These problems are addressed in a model called the effective core potential

(ECP) or pseudo-potential (PP).[26] In the ECP, the core electrons are treated by a suitable function to reduce computational cost while treating the valence electrons are treated explicitly. LANL2DZ[27] is a common ECP used in this study to model transition metal complexes.

2.3 Solvation Model

Since the reactions examined in this work were carried out in solution, a solvation method is potentially important to accurately the model the chemical environment. The solution environment can have a significant effect on chemical properties such as reaction barriers or intermediates that affect reactivity or selectivity. Self-consistent reaction field (SCRF) models of solvation allow a solute to be placed in an empty cavity within a solvent, and the solvent itself is treated as a continuous, uniform dielectric medium with surface tension at the solute-solvent boundary along with their mutual polarization. Parameters such as the size and shape of the cavity and solvation medium, dielectric constant, and non-electrostatic interactions define a continuum solvation model. The use of explicit solvent for modeling solvent effects for large organometallic complexes is generally not feasible, and may not necessarily be more accurate than using a continuum model.

Cramer and Truhlar jointly developed a continuum solvent model referred to as the solvent model density (SMD).[28] SMD describes the charge density of a solute molecule interacting with its solvent or a dielectric medium. Parameterized with a training data set that includes dielectric constant, refractive index, bulk surface tension, and acidity experimental values, SMD was designed to be universally applicable to both charged and uncharged solutes in any medium. Various solvents were modeled using the SMD method in this study. Figure 2-1 displays an example of a tessellated Cr phosphinoamidine van der Waals molecular surface used in a typical SMD solvation calculation.

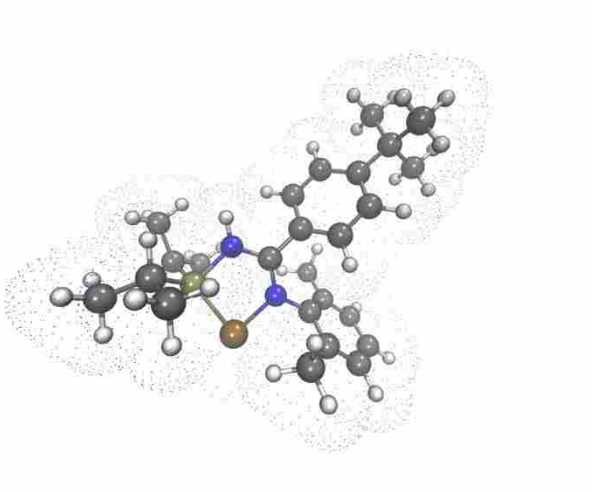

Figure 2-1. 3D illustration of a Cr phosphinoamidine molecular surface representing the solute-solvent boundary utilized in a SMD solvation model.

2.4 Computational Methodology

All calculations were performed in Gaussian 09.[29] Geometry optimizations were carried out with M06L/6-31G(d,p)[LANL2DZ for Cr and Fe].[6,6,27,30] Vibrational frequencies were calculated to verify stationary points as minima or first-order saddle points (transition states). Intrinsic reaction coordinate (IRC) calculations were used to verify connection between transition states and intermediates. The M06L functional was chosen because it provides an accurate estimate of relative spin-state energies and reaction energies for first-row transition metal complexes. The cyclohexane solvent was modeled using an implicit SMD solvation model,[28] which provides an estimate of ΔG_{solv}. Optimized energies were further refined with single point calculations using a def2-TZVP[24] basis set so that final free energies are considered M06L/def2-TZVP//M06L/6-31G(d,p)[LANL2DZ for Cr and Fe]. Free energies are the sum of $E_{(large)} + \Delta E_{ZPE(small)} + \Delta U_{vib(small)} + \Delta U_{rot(small)} + \Delta U_{trans(small)} + n\mathrm{RT} - \mathrm{T}\Delta S_{vib(small)} - \mathrm{T}\Delta S_{rot(small)} - \mathrm{T}\Delta S_{trans(small)} + \Delta G_{solv(large)}$. E is the total SCF energy. $\Delta E_{ZPE(small)}$ is the zero point energy correction. $\Delta U_{vib(small)}$, $\Delta U_{rot(small)}$, and

$\Delta U_{trans(small)}$ are thermal energy vibrational, rotational, and translational corrections. R is the gas constant. T is the temperature. $T\Delta S_{vib(small)}$, $T\Delta S_{rot(small)}$, and $T\Delta S_{trans(small)}$ are temperature-dependent entropy vibrational, rotational, and translational corrections. $\Delta G_{solv(large)}$ is the standard state solvation free energy change. Large = M06L/def2-TZVP. Small = M06L/6-31G(d,p)[LANL2DZ for Cr and Fe]. 3-D structures were generated using CYLview.[31]

2.5 Conclusions

DFT methods must be judiciously chosen to accurately model organometallic complexes especially those containing first-row transition metals that can readily access different oxidation states and spin states.[32-39] With regard to Cr and Fe-catalyzed ethylene oligomerization reactions, the M06L functional replicated experimental results with the best performance.[19-20]

2.6 References

1. Szabo, A.; Ostlund, N. S., *Modern quantum chemistry: introduction to advanced electronic structure theory*. Courier Corporation: 2012.

2. Kohn, W.; Sham, L. J. Self-Consistent Equations Including Exchange and Correlation Effects. *Physical Review* **1965,** *140*, A1133-A1138.

3. Koch, W.; Holthausen, M. C., *A chemist's guide to density functional theory*. John Wiley & Sons: 2015.

4. Jensen, F., *Introduction to computational chemistry*. John wiley & sons: 2017.

5. Cramer, C. J., *Essentials of Computational Chemistry: Theories and Models (2nd Edition)*. John Wiley & Sons: 2004.

6. Zhao, Y.; Truhlar, D. G. Density Functionals with Broad Applicability in Chemistry. *Acc. Chem. Res.* **2008,** *41*, 157-167.

7. Becke, A. D. Density-functional exchange-energy approximation with correct asymptotic behavior. *Physical Review A* **1988,** *38*, 3098-3100.

8. Valero, R.; Costa, R.; de P. R. Moreira, I.; Truhlar, D. G.; Illas, F. Performance of the M06 family of exchange-correlation functionals for predicting magnetic coupling in organic and inorganic molecules. *J. Chem. Phys.* **2008,** *128*, 114103.

9. Zhao, Y.; Truhlar, D. G. Benchmark Data for Interactions in Zeolite Model Complexes and Their Use for Assessment and Validation of Electronic Structure Methods. *The Journal of Physical Chemistry C* **2008,** *112*, 6860-6868.

10. Yang, K.; Zheng, J.; Zhao, Y.; Truhlar, D. G. Tests of the RPBE, revPBE, τ-HCTHhyb, ωB97X-D, and MOHLYP density functional approximations and 29 others against representative databases for diverse bond energies and barrier heights in catalysis. *J. Chem. Phys.* **2010,** *132*, 164117.

11. Tsipis, A. C.; Orpen, A. G.; Harvey, J. N. Substituent effects and the mechanism of alkene metathesis catalyzed by ruthenium dichloride catalysts. *Dalton Trans.* **2005**, 2849-2858.

12. Pandian, S.; Hillier, I. H.; Vincent, M. A.; Burton, N. A.; Ashworth, I. W.; Nelson, D. J.; Percy, J. M.; Rinaudo, G. Prediction of ring formation efficiency via diene ring closing metathesis (RCM) reactions using the M06 density functional. *Chemical Physics Letters* **2009,** *476*, 37-40.

13. Sieffert, N.; Bühl, M. Noncovalent Interactions in a Transition-Metal Triphenylphosphine Complex: a Density Functional Case Study. *Inorganic Chemistry* **2009,** *48*, 4622-4624.

14. Minenkov, Y.; Occhipinti, G.; Jensen, V. R. Metal−Phosphine Bond Strengths of the Transition Metals: A Challenge for DFT. *The Journal of Physical Chemistry A* **2009,** *113*, 11833-11844.

15. Kwon, D.-H.; Proctor, M.; Mendoza, S.; Uyeda, C.; Ess, D. H. Catalytic Dinuclear Nickel Spin Crossover Mechanism and Selectivity for Alkyne Cyclotrimerization. *ACS Catal.* **2017,** *7*, 4796-4804.

16. Agapie, T.; Labinger, J. A.; Bercaw, J. E. Mechanistic Studies of Olefin and Alkyne Trimerization with Chromium Catalysts: Deuterium Labeling and Studies of Regiochemistry Using a Model Chromacyclopentane Complex. *J. Am. Chem. Soc.* **2007,** *129*, 14281-14295.

17. Sydora, O. L. Selective Ethylene Oligomerization. *Organometallics* **2019,** *38*, 997-1010.

18. McGuinness, D. S.; Chan, B.; Britovsek, G. J. P.; Yates, B. F. Ethylene Trimerisation with Cr-PNP Catalysts: A Theoretical Benchmarking Study and Assessment of Catalyst Oxidation State. *Aust. J. Chem.* **2014,** *67*, 1481-1490.

19. Kwon, D.-H.; Fuller, J. T.; Kilgore, U. J.; Sydora, O. L.; Bischof, S. M.; Ess, D. H. Computational Transition-State Design Provides Experimentally Verified Cr(P,N) Catalysts for Control of Ethylene Trimerization and Tetramerization. *ACS Catal.* **2018,** *8*, 1138-1142.

20. Kwon, D.-H.; Small, B. L.; Sydora, O. L.; Bischof, S. M.; Ess, D. H. Challenge of Using Practical DFT to Model Fe Pendant Donor Diimine Catalyzed Ethylene Oligomerization. *The Journal of Physical Chemistry C* **2019,** *123*, 3727-3739.

21. Hehre, W. J.; Ditchfield, R.; Pople, J. A. Self—Consistent Molecular Orbital Methods. XII. Further Extensions of Gaussian—Type Basis Sets for Use in Molecular Orbital Studies of Organic Molecules. *J. Chem. Phys.* **1972,** *56*, 2257-2261.

22. Petersson, G. A.; Bennett, A.; Tensfeldt, T. G.; Al-Laham, M. A.; Shirley, W. A.; Mantzaris, J. A complete basis set model chemistry. I. The total energies of closed-shell atoms and hydrides of the first-row elements. *J. Chem. Phys.* **1988,** *89*, 2193-2218.

23. Petersson, G. A.; Tensfeldt, T. G.; Jr., J. A. M. A complete basis set model chemistry. III. The complete basis set-quadratic configuration interaction family of methods. *J. Chem. Phys.* **1991,** *94*, 6091-6101.

24. Weigend, F.; Ahlrichs, R. Balanced basis sets of split valence, triple zeta valence and quadruple zeta valence quality for H to Rn: Design and assessment of accuracy. *Physical Chemistry Chemical Physics* **2005,** *7*, 3297-3305.

25. Hariharan, P. C.; Pople, J. A. The influence of polarization functions on molecular orbital hydrogenation energies. *Theoretica chimica acta* **1973,** *28*, 213-222.

26. Hellmann, H. A new approximation method in the problem of many electrons. *J. Chem. Phys.* **1935,** *3*, 61-61.

27. Hay, P. J.; Wadt, W. R. Ab initio effective core potentials for molecular calculations. Potentials for the transition metal atoms Sc to Hg. *J. Chem. Phys.* **1985,** *82*, 270-283.

28. Marenich, A. V.; Cramer, C. J.; Truhlar, D. G. Universal solvation model based on solute electron density and on a continuum model of the solvent defined by the bulk dielectric constant and atomic surface tensions. *The Journal of Physical Chemistry B* **2009,** *113*, 6378-6396.

29. Frisch, M.; Trucks, G.; Schlegel, H.; Scuseria, G.; Robb, M.; Cheeseman, J.; Scalmani, G.; Barone, V.; Mennucci, B.; Petersson, G. Gaussian 09, revision B. 01. *Gaussian, Inc., Wallingford, CT* **2010**.

30. Zhao, Y.; Truhlar, D. G. A new local density functional for main-group thermochemistry, transition metal bonding, thermochemical kinetics, and noncovalent interactions. *J. Chem. Phys.* **2006,** *125*, 194101.

31. Legault, C. Y. *CYLview, 1.0b*, (http://www.cylview.org): Universite de Sherbrooke, 2009.

32. Swart, M.; Groenhof, A. R.; Ehlers, A. W.; Lammertsma, K. Validation of Exchange−Correlation Functionals for Spin States of Iron Complexes. *The Journal of Physical Chemistry A* **2004,** *108*, 5479-5483.

33. Conradie, J.; Ghosh, A. DFT Calculations on the Spin-Crossover Complex Fe(salen)(NO): A Quest for the Best Functional. *The Journal of Physical Chemistry B* **2007,** *111*, 12621-12624.

34. Swart, M. Accurate Spin-State Energies for Iron Complexes. *Journal of Chemical Theory and Computation* **2008,** *4*, 2057-2066.

35. Jensen, K. P.; Cirera, J. Accurate Computed Enthalpies of Spin Crossover in Iron and Cobalt Complexes. *The Journal of Physical Chemistry A* **2009,** *113*, 10033-10039.

36. Hughes, T. F.; Friesner, R. A. Correcting Systematic Errors in DFT Spin-Splitting Energetics for Transition Metal Complexes. *Journal of Chemical Theory and Computation* **2011,** *7*, 19-32.

37. Kepp, K. P. Consistent descriptions of metal–ligand bonds and spin-crossover in inorganic chemistry. *Coord. Chem. Rev.* **2013,** *257*, 196-209.

38. Mortensen, S. R.; Kepp, K. P. Spin Propensities of Octahedral Complexes From Density Functional Theory. *The Journal of Physical Chemistry A* **2015,** *119*, 4041-4050.

39. Ashley, D. C.; Jakubikova, E. Ironing out the photochemical and spin-crossover behavior of Fe(II) coordination compounds with computational chemistry. *Coord. Chem. Rev.* **2017,** *337*, 97-111.

3 COMPUTATIONAL TRANSITION-STATE DESIGN PROVIDES EXPERIMENTALLY VERIFIED Cr(P,N) CATALYSTS FOR CONTROL OF ETHYLENE TRIMERIZATION AND TETRAMERIZATION

3.1 Introduction

Linear α-olefins (LAOs, 1-alkenes) are produced from ethylene oligomerization at ~3,000,000 tons/year worldwide.[1,2] LAOs are key petrochemical precursors for the synthesis of larger polymers, detergents, plasticizers, and lubricants. Several manufacturers such as Shell, Ineos, Idemitsu, SABIC, and Chevron Phillips Chemical Company LP (CPChem) use metal-catalyzed multi-step ethylene oligomerization processes to produce LAOs. Most of these processes generate a wide distribution of LAO carbon chain lengths from C_4 (1-butene) to C_{20} (1-eicosene).[1,3] Sasol also recovers LAOs from Fischer-Tropsch synthesis. A major ongoing industrial challenge is to develop homogeneous molecular catalysts that result in selective and tunable ethylene oligomerization to only 1-hexene and 1-octene (Scheme 3-1),[4-6] which are in demand as co-monomers for polyethylene production and elastomers. While CPChem was the first to commercialize a selective catalyst system for 1-hexene,[7] Wass/BP, and Sasol have developed technology for selective ethylene trimerization and tetramerization.[8-12] However, despite all of these efforts there is no clear empirical approach to the design of molecular homogeneous Cr-based catalysts that increase LAO selectivity towards 1-octene.

Computational molecular catalyst design has the potential to significantly impact selective ethylene oligomerization, if new metal-ligand catalysts can be identified that have predictable control of

ethylene trimerization versus tetramerization. While accurate density-functional theory (DFT) methods have the potential to predict catalysts,[13-35] there are very few cases of specific and genuine prediction followed by experimental realization for molecular organometallic catalysts.[23-29] Here, we report the development and use of a DFT transition-state model that provides quantitative prediction of phosphine imine (P,N) Cr catalysts for controllable selective ethylene trimerization and tetramerization. The DFT correlation model is based on competitive transition states from a common chromacycloheptane catalytic cycle intermediate. This model identified a new family of highly selective catalysts that through computational-based ligand design resulted in a predictable selectivity shift from 1-hexene to 1-octene. Subsequent experimental ligand and catalyst synthesis, and ethylene oligomerization reaction testing, realized the computational predictions.

Scheme 3-1. Ethylene Oligomerization Targets.

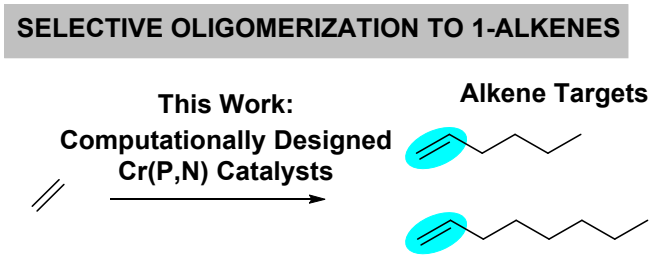

3.2 Previously Reported Cr Catalysts

Cr bidentate phosphine imine (Cr(P,N)) catalysts[36-44] (Scheme 3-2) represent a desirable class of catalysts for selective LAO production from ethylene for several reasons:[45-47] (1) (P,N) ligands can be synthesized in a modular route that is highly flexible. (2) Metalation to Cr is straightforward, and the starting (P,N)$Cr^{III}Cl_3$ catalysts can be characterized. (3) Ethylene oligomerization reactions are generally highly reproducible and lead to high purity LAOs without chain branching[36] which is generally challenging for other types of catalysts. In pursuit of controlling targeted C_6 to C_8 1-alkene selectivity with

Cr(P,N) catalysts, Sydora and co-workers reported LAO selectivity for several aryl and benzyl decorated phosphine imine catalysts (Scheme 2).[36-38] These catalysts showed moderate oligomerization activity with high purity LAO production and trace polymer production. Product purity typically exceeded >98% 1-olefin in the C_6 and C_8 fractions. It was through time consuming (several years) experimental screening that catalyst **1a** was identified that results in >90 weight % yield of C_6 (at >99% 1-hexene purity). Unfortunately, changes to the **1a** (P,N) ligand structure resulted in no more than ~30 weight % of C_8, and no systematic empirical approach was identified to further increase the LAO selectivity towards 1-octene. Therefore, we undertook the task of computational design of new Cr(P,N) catalysts with the goal of predictable control of 1-hexene and 1-octene selectivity.

Scheme 3-2. Reported Ethylene Trimerization/Tetramerization Catalysts and Relative Mass % of C_6 and C_8. [Selectivity %] = % of 1-Alkene Relative to Total Alkenes.

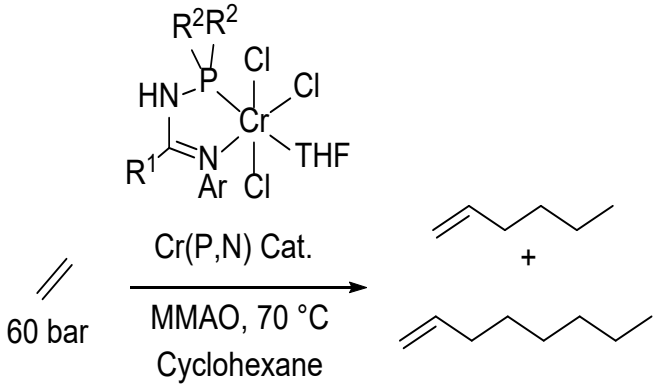

Catalyst	mass % [Selectivity %] C_6 [1-C_6]	C_8 [1-C_8]
1a Ar = 2,6-Me$_2$C$_6$H$_3$; R^1 = 4-tBuC$_6$H$_4$; R^2 = iPr	94 [>99]	1 [98]
1b Ar = 2,6-Me$_2$C$_6$H$_3$; R^1 = 4-tBuC$_6$H$_4$; R^2 = Ph	85 [99]	12 [98]
1c Ar = 2,6-Me$_2$C$_6$H$_3$; R^1 = 4-MeBn; R$_2$ = Ph	79 [99]	15 [>99]
1d Ar = 3,5-Me$_2$C$_6$H$_3$; R^1 = Ph; R$_2$ = iPr	65 [97]	31 [>99]
1e	52 [45]	34 [84]

3.3 Catalytic Cycle

To build a predictive DFT transition-state selectivity model, we undertook quantitative modeling of **1a**-**1e** LAO selectivity. This required identification of a catalytic mechanism and comparison of calculated 1-hexene:1-octene ratio selectivity to experiment. Previous computational studies by Britovsek and McGuinness,[48,49] Cheong,[50] Liu,[51-53] and others[54-56] explored possible mechanisms for ethylene oligomerization by related Sasol and Phillips Cr-type catalysts. Combined with experimental studies,[57] and our own calculations, Scheme 3-3 shows the most plausible catalytic mechanism that has emerged for ethylene trimerization and tetramerization. Pre-catalyst activation generates a low-valent Cr species **A** with ethylene coordination. Oxidative C-C bond coupling forms chromacyclopentane **B**. Another ethylene coordination gives intermediate **C** and migratory insertion leads to the key chromacycloheptane intermediate **D**. The catalytic cycle diverges into two pathways at this chromacycloheptane intermediate. In one pathway, β-hydrogen transfer, which can be considered a one-step β-hydrogen elimination/reductive elimination process, results in formation of 1-hexene and Cr catalyst reduction (blue arrows). In a second pathway, ethylene coordination by intermediate **E** and migratory insertion leads to the chromacyclononane intermediate **F** that leads to 1-octene (red arrows). Therefore, selectivity can result from competitive β-hydrogen transfer and ethylene migratory insertion from intermediate **D**.

Scheme 3-3. Mechanism for Homogeneous Cr-Catalyzed Ethylene Trimerization and Tetramerization. (Black arrows represent common reaction steps. Blue arrows represent 1-hexene pathway. Red arrows represent 1-octene pathway.)

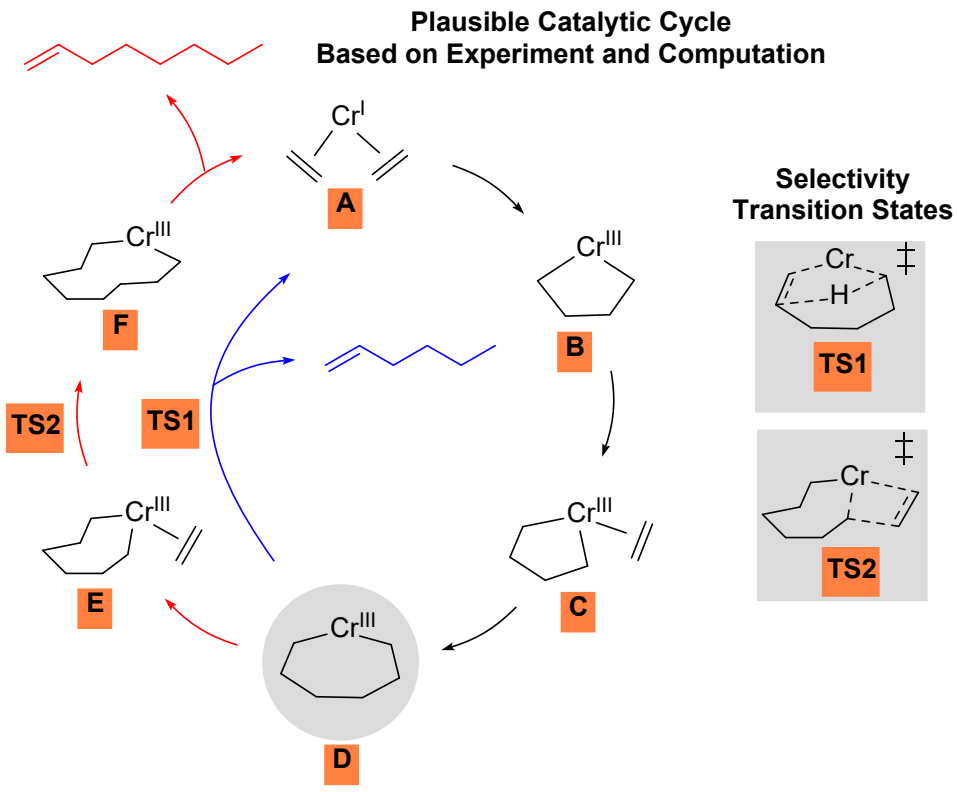

3.4 Transition State Controlled Selectivity Model

Previous computational studies[48,49] established that the M06L[58,59] density functional is accurate for treating the multiple spin states and oxidation and reduction steps involved in Cr catalytic cycles similar to that shown in Scheme 3-3. Therefore, we used unrestricted UM06L/def2-TZVP//UM06L/6-31G(d,p)(LANL2DZ) theory[60-64] combined with the SMD[65] continuum solvent model for cyclohexane to estimate free energies for intermediates and transition states. With the adoption of the mechanism shown

in Scheme 3-3, we commenced examining transition-state structures for Cr catalysts on the top of Figure 3-2 to accurately replicate the C_6 to C_8 weight % relative selectivity. We found that the lowest-energy transition-state structures arise from the low-valent high-spin quartet cationic $(P,N)Cr^{III}(C_6H_{12})$ chromacycloheptane intermediate (intermediate **D**).[66, 67] As stated above, the key transition states that control selectivity in this mechanism are β-hydrogen transfer (**TS1**) and ethylene migratory insertion (**TS2**). The top structures in Figure 3-1[68-69] show the lowest-energy structures from the ensembles of **TS1** and **TS2** for catalyst **1a**. In this case, the **TS1** ensemble is comprised of up to 25 unique transition-state conformations and the **TS2** ensemble has up to 40 unique structures. The large number of conformations in each transition-state ensemble results from the flexibility of the chromacycloheptane ring and aryl ligand groups. More details concerning conformational analysis is found below. For the relative energies of **TS1** and **TS2** to control selectivity, intermediates leading to these transition states need to be in equilibrium (i.e. Curtin-Hammett type conditions). Consistent with this assumption, ethylene coordination to the chromacycloheptane intermediate is endergonic by ~3 kcal/mol. For catalyst **1a**, the $\Delta G_{(\mathbf{TS1}\text{-}\mathbf{TS2})}$ of ~3 kcal/mol, and is quantitatively in accord with the 94%:1% C_6:C_8 relative weight ratio.

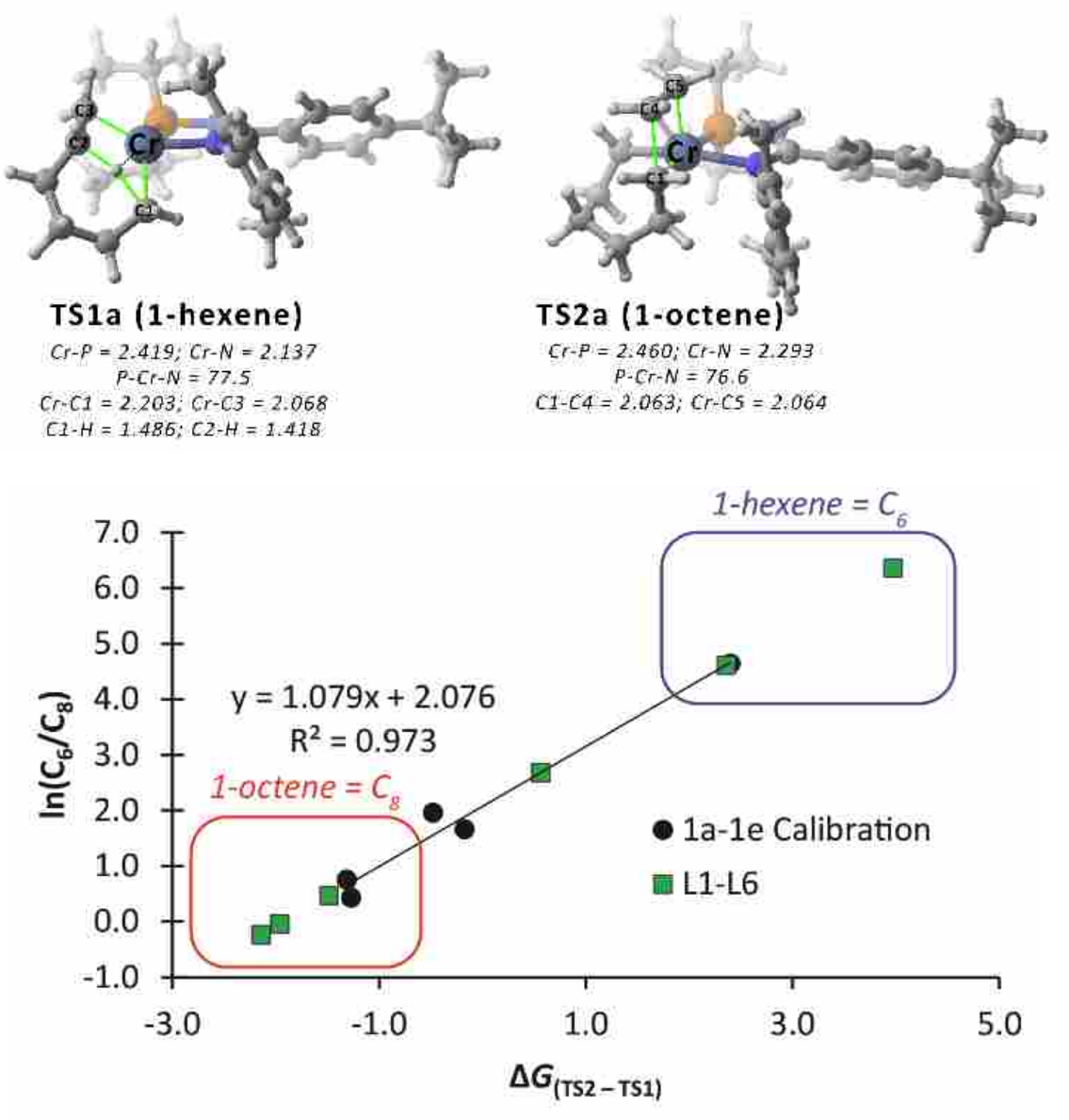

Figure 3-1. Top: TS1 and TS2 transition-state structures for catalyst 1a. Bottom: Predictive linear correlation plot between $\Delta G_{(TS1\text{-}TS2)}$ and natural log of 1-hexene:1-octene weight ratio.

3.5 Computational Design Followed by Experimental Verification

While accurate prediction for individual catalysts is important, it is potentially more powerful to correlate[70-71] $\Delta G_{(TS1\text{-}TS2)}$ values and the relative % weight of 1-hexene to 1-octene. This type of approach has the advantage of reducing errors in predicting selectivity for some experimental parameters not

directly included in this DFT transition-state model, but it may have the disadvantage of being less accurate for ligands that have large electronic or structural changes to the (P,N) core scaffold. Therefore, we explored all reasonable transition-state conformations for catalysts **1a**-**1e**. The bottom of Figure 3-1 plots the energy difference between the lowest energy structures for **TS1** and **TS2** ($\Delta G_{(\mathbf{TS1}\text{-}\mathbf{TS2})}$) for catalysts **1a**-**1e** versus their experimental relative weight % of alkenes by $\ln(C_6/C_8)$. This direct correlation approach gives a high degree of linear correlation with a slope of 1.08 ($y = 1.079x + 2.076$) and an R^2 value of 0.97.

With the correlation curve in Figure 3-1 complete, we began the design of new classes of phosphine imine Cr catalysts for predictable control of the 1-hexene to 1-octene ratio. Our calculations quickly converged on phosphine monocyclic imine catalysts (Scheme 3-4 shows the Cr (P,N) ligands). Phosphine monocyclic imines retain the (P,N) ligand core, but provide a significantly new steric and electronic environment with several ligand positions that can be readily modified. We first calculated **TS1** and **TS2** for 2-methyl-3,4-dihydro-2H-pyrrol-5-amine phosphine (**L1**, Scheme 3-4 and Figure 3-2). This 2-substituted monocyclic imine was chosen first because it was assumed based on previous experimental results that substitution at or near the imine functional group will result in high LAO purity and potential selectivity for 1-octene.[36-38] However, the calculated selectivity suggested a 94:06 relative % weight of 1-hexene:1-octene, which is a ratio similar to that observed for catalysts **1a** and **1b**. Subsequent synthesis of the (**L1**)$Cr^{III}(Cl)_3$(THF) complex and testing of ethylene oligomerization under standard conditions confirmed the prediction of C_6 selectivity with an experimental C_6:C_8 ratio of 85:15. In this case, and in some cases, C_6 selectivity is slightly overestimated. However, this overestimation of C_6 selectivity is advantageous in our DFT transition-state model since the goal is to increase selectivity towards C_8 production

Scheme 3-4. Predicted 1-Hexene:1-Octene Weight % Ratio for Cr-catalyzed Ethylene Oligomerization with Phosphine Monocyclic Imine Ligands. Experimental Weight % Ratios are Normalized for C_6+C_8 Fractions and Include All C_6 or C_8 Components. (Bottom Right-Hand Corner: X-ray Structure for $[Li(THF)_2]^+[(L2)Cr^{III}Cl_4]^-$. NA = Catalyst Not Synthesized.)

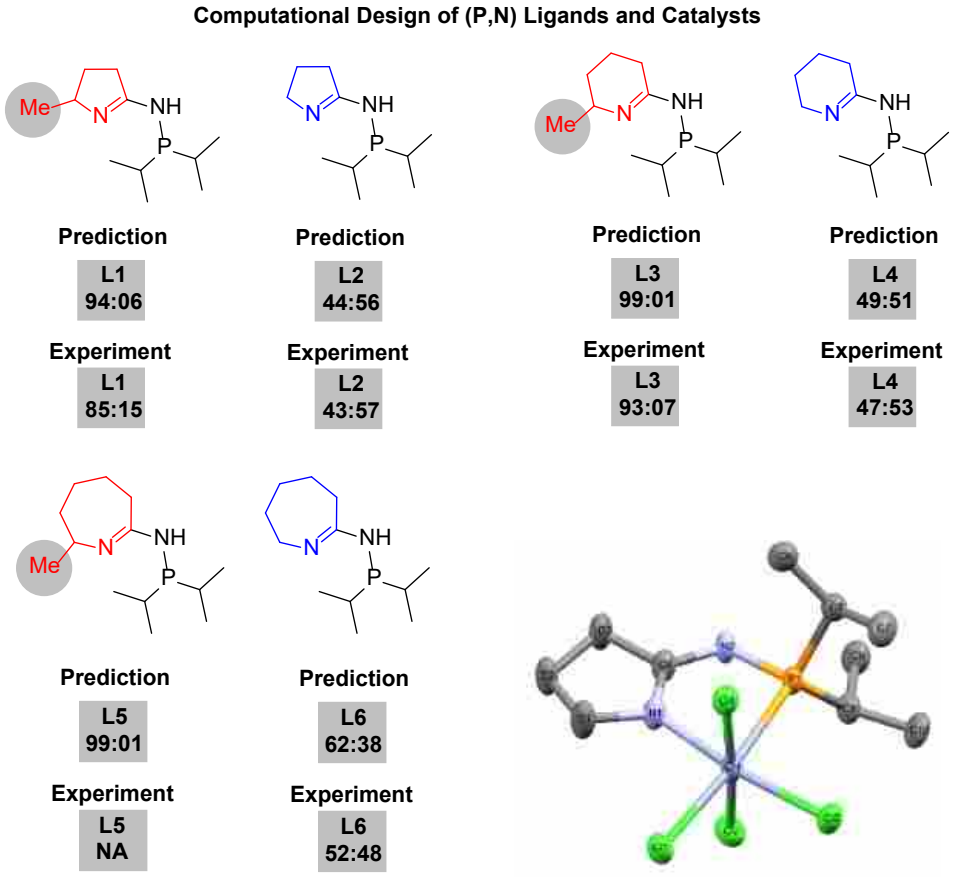

Our calculations identified that removal of the 2-methyl group in **L1** could lead to a dramatic shift in increased C_8 production. Calculation of **TS1** and **TS2** for the 3,4-dihydro-2H-pyrrol-5-amine phosphine ligand **L2** gave a prediction of 44%:56% weight C_6:C_8 ratio. Figure 3-2 shows the transition-state structures for **TS1** and **TS2** for **L1** and **L2**. Inspection of these structures shows that the 2-methyl group of **L1** resides close to the Cr catalytic pocket and intrudes in the ethylene migratory insertion transition state. Removal of this alkyl group lowers the energy of **TS2** and results in significantly greater 1-octene production. Importantly, the predicted 44:56 % weight of 1-hexene:1-octene is significantly higher in 1-

octene content than any of the catalysts **1a**-**1e** previously tested. Subsequent synthesis of the (**L2**)$Cr^{III}(Cl)_3(THF)$ complex and ethylene oligomerization reaction testing under standard conditions resulted in a quantitative confirmation of this prediction with a C_6:C_8 weight % ratio of 43:57 (Scheme 3-4), and confirms the controllable shift from C_6 selectivity towards C_8 selectivity through modification of the backbone monocyclic imine group. The (**L2**)Cr^{III} catalyst complex was confirmed with an X-ray structure of the $[Li(THF)_2]^+[$(**L2**)$Cr^{III}Cl_4]^-$ complex (bottom right-hand corner of Scheme 3-4).

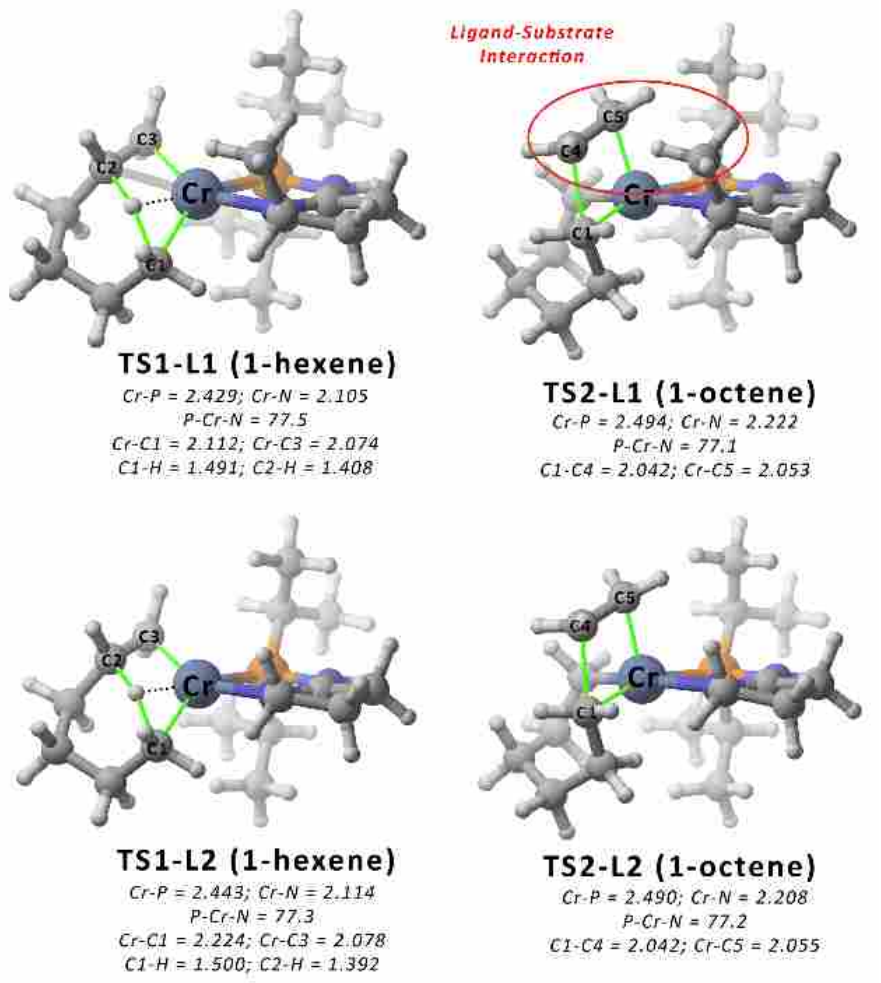

Figure 3-2. TS1 and TS2 transition-state structures for cationic (L1)$Cr^{III}(C_6H_{12})$ and (L2)$Cr^{III}(C_6H_{12})$.

To test if **L2** is a general class of ligand with the capability of 1-octene selectivity based on transition states, we computationally predicted and then experimentally examined the selectivity for the

corresponding six-membered and seven-membered monocyclic imine ligands with and without the α-methyl imine group. Indeed, tetrahydropyridin-2-amine **L3** and tetrahydro-2H-azepin-7-amine **L5** were predicted to give complete selectivity for 1-hexene while **L4** and **L6** were predicted to have 49:51 and 62:38 % weight ratios, respectively (Scheme 3-4). Experimental testing of these catalysts confirmed the quantitative predictions of the C_6 selective catalysts with **L3** and **L5** ligands. Experiments also confirmed a very close prediction for the catalysts with ligand **L4** for C_8 selectivity. The prediction for catalysis with ligand **L6** underestimated the C_8 production by ~10%.

3.6 Conclusion

This combined computational-experimental study demonstrates the successful use of a practical DFT transition-state model for quantitative prediction and experimental realization of designing new classes of Cr phosphine imine catalysts for control of ethylene trimerization/tetramerization selectivity. This begins our efforts to identify new classes of Cr catalysts and ligands by using computational design to predict catalyst selectivity and activity.

3.7 References

1. Arpe, H-J. In *Industrial Organic Chemistry*, 5th ed.; Wiley-VCH Verlag GmbH & Co., 2010.
2. Green, M. M.; Wittcoff, H. A. In *Organic Chemistry Principles and Industrial Practice,* 1st ed.; Wiley-VCH Verlag GmbH & Co., 2003.
3. Lappin, G. R.; Nemec, L. H.; Sauer, J. D.; Wagner, J. D. Higher Olefins. In *Kirk-Othmer Encyclopedia of Chemical Technology*, 5th ed.; Seidel, A., John Wiley & Sons: Hoboken, NJ, 2006; Vol. 17, p 709.
4. Agapie, T. *Coor. Chem. Rev.* **2011**, *255*, 861−880.
5. McGuinness, D. S. *Chem. Rev.* **2011**, *111*, 2321−2341.
6. Van Leeuwen, P. W. N. M.; Clément, N. D.; Tschan, J.-L. *Coor. Chem. Rev.* **2011**, *255*, 1499−1517.
7. Knudsen, R. D.; Kreischer, B. E.; Abbott, R. G.; Bridges, S. D.; Baralt, E. J. U.S. Patent 7 384 886, **2008**.
8. Carter, A.; Cohen, S. A.; Cooley, N. A.; Murphy, A.; Scutt, J.; Wass, D. F. *Chem. Commun.* **2002**, 858−859.
9. Bollmann, A.; Blann, K.; Dixon, J. T.; Hess, F. M.; Killian, E.; Maumela, H.; McGuinness, D. S.; Morgan, D. H.; Neveling, A.; Otto, S.; Overett, M.; Slawin, A. M. Z.; Wasserscheid, P.; Kuhlmann, S. *J. Am. Chem. Soc.* **2004**, *126*, 14712−14713.
10. Agapie, T.; Labinger, J. A.; Bercaw, J. E. *J. Am. Chem. Soc.* **2007**, *129*, 14281−14295.
11. Gao, X.; Carter, C. A. G.; Fan, L.; Henderson, L. D. U.S. Patent 7994363, **2011**.
12. Kuhlmann, S.; Blann, K.; Bollmann, A.; Dixon, J. T.; Killian, E.; Maumela, M. C.; Maumela, H.; Morgan, D. H.; Prétorius, M.; Taccardi, N.; Wasserscheid, P. *J. Catal.* **2007**, *245*, 279−284.
13. Golab, J. T. *Chemtech* **1998**, *28*, 17−23.

14. Allemann, C.; Gordillo, R.; Clemente, F. R.; Cheong, P. H-Y.; Houk, K. N. *Acc. Chem. Res.* **2004**, 37, 558−569.

15. Houk, K. N.; Cheong, P. H.-Y. *Nature* **2008**, *455*, 309−313. (d) Tantillo, D. J. *Angew. Chem. Int. Ed.* **2009**, *48*, 31−32.

16. Sunoj, R. B. *WIREs Comput. Mol. Sci.* **2011**, *1*, 920−931. (f) Jover, J.; Fey, N. *Chem. Asian J.* **2014**, *9*, 1714−1723.

17. Nguyen, Q. N. N.; Tantillo, D. J. *Chem. Asian J.* **2014**, *9*, 674−680.

18. Tsang, A. S-K.; Sanhueza, I. A.; Schoenebeck, F. *Chem. Eur. J.* **2014**, *20*, 16432−16441.

19. Tantillo, D. J. *Acc. Chem. Res.* **2016**, *49*, 1079.

20. Sperger, T.; Sanhueza, I. A.; Schoenebeck, *Acc. Chem. Res.* **2016**, *49*, 1311−1319.

21. Hammes-Schiffer, S. *Acc. Chem. Res.* **2017**, 50, 561−566.

22. Poree, C.; Schoenebeck, F. *Acc. Chem. Res.* **2017**, 50, 605−608.

23. Wang, Y.; Wang, J.; Su, J.; Huang, F.; Jiao, L.; Liang, Y.; Yang, D.; Zhang, S.; Wender, P. A; Yu, Z-X. *J. Am. Chem. Soc.* **2007**, *129*, 10060−10061.

24. Donoghue, P. J.; Helquist, P.; Norrby, P-O.; Wiest, O. *J. Am. Chem. Soc.* **2009**, *131*, 410−411.

25. Rowley, C. N.; Woo, T. K. *Can. J. Chem.* **2009**, *87*, 1030−1038.

26. Baik, M-H.; Mazumder, S.; Ricci, P.; Sawyer, J. R.; Song, Y-G.; Wang, H.; Evans, P. A. *J. Am. Chem. Soc.* **2011**, *133*, 7621−7623.

27. Fernandez, L. E.; Horvath, S. Hammes-Schiffer, S. *J. Phys. Chem. Lett.* **2013**, *4*, 542−546.

28. Nielsen, M. C.; Bonney, K. J.; Schoenebeck, F. *Angew. Chem. Int. Ed.* **2014**, *53*, 5903−5906.

29. Bernales, V.; League, A. B.; Li, Z.; Schweitzer, N. M.; Peters, A. W.; Carlson, R. K.; Hupp, J. T.; Cramer, C. J.; Farha, O. K.; Gagliardi, L. *J. Phys. Chem. C* **2016**, *120*, 23576−23583.

30. Kheirabadi, M.; Celebi-Olcum, N.; Parker, M. F. L.; Zhao, Q.; Kiss, G.; Houk, K. N.; Schafmeister, C. E. *J. Am. Chem. Soc.* **2012**, *134*, 18345−18353.
31. Doney, A. C.; Rooks, B. J.; Lu, T.; Wheeler, S. E. *ACS Catal.* **2016**, *6*, 7948−7955.
32. Kozlowski, M. C.; Dixon, S. L.; Panda, M.; Lauri, G. *J. Am. Chem. Soc.* **2003**, *125*, 6614−6615.
33. Ianni, J. C.; Annamalai, V.; Phuan, P.; Panda, M. Kozlowski, M. C. *Angew. Chem. Int. Ed.* **2006**, *45*, 5502−5505.
34. Mitsumori, S.; Zhang, H.; Cheong, P. H-Y.; Houk, K. N.; Tanaka, F.; Barbas, C. F., III *J. Am. Chem. Soc.* **2006**, *128*, 1040−1041.
35. Jindal, G.; Sunoj, R. B. *Org. Biomol. Chem.* **2014**, *12*, 2745−2753.
36. Sydora, O. L.; Jones, T. C.; Small, B. L.; Nett, A. J.; Fischer, A. A.; Carney, M. J. *ACS Catal.* **2012**, *2*, 2452−2455.
37. Sydora, O. L.; Carney, M.; Small, B. L.; Hutchison, S.; Gee, J. C. (CPChem) **2014**, US 8,680,003.
38. Sydora, O. L.; Carney, M.; Small, B. L.; Hutchison, S.; Gee, J. C. (CPChem) **2014**, US 9,283,555.
39. Baiget, L.; Batsanov, A. S.; Dyer, P. W.; Fox, M. A.; Hanton, M. J.; Howard, J. A. K.; Lane, P. K.; Solomon, S. A. *Dalton Trans.* **2008**, 1043−1054.
40. Dyer, P. W.; Fawcett, J.; Hanton, M. J. *Organometallics* **2008**, 27, 5082−5087.
41. Margraf, G.; Pattacini, R.; Messaoudi, A.; Braunstein, P. *Chem. Commun.* **2006**, 3098−3100.
42. Chivers, T.; McGregor, K.; Parvez, M. *Inorg. Chem.* **1993**, *32*, 5119−5125.
43. Nifant'ev, E. E.; Negrebetskii, V. V.; Grachev, M. K. Zh. *Obshch. Khim.* **1991**, *61*, 1581−1583.
44. Speiser, F.; Braunstein, P.; Saussine, L. *Acc. Chem. Res.* **2005**, *38*, 784−793.
45. Hitchcock, P. B.; Lappert, M. F.; Merle, P. G. *Dalton Trans.* **2007**, 585−594.
46. Dulai, A.; McMullin, C. L.; Tenza, K.; Wass, D. F. *Organometallics* **2011**, *30*, 935−941.

47. Peitz, S.; Peulecke, N.; Aluri, B. R.; Müller, B. H.; Spannenberg, A.; Rosenthal, U.; Al-Hazmi, M. H.; Mosa, F. M.; Wöhl, A.; Müller, W. *Organometallics* **2010**, *29*, 5263−5268.
48. Britovsek, G. J. P.; McGuinness, D. S. *Chem. Eur. J.* **2016**, *22*, 16891 – 16896.
49. Britovsek, G. J. P.; McGuinness, D. S.; Tomov, A. K. *Catal. Sci. Technol.* **2016**, *6*, 8234–8241.
50. Hossain, M. A.; Kim, H. S.; Houk, K. N. Cheong, M. *Bull. Korean Chem. Soc.* **2014**, *35*, 2835-2838.
51. Gong, M.; Liu, Z.; Li, Y.; Ma, Y.; Sun, Q.; Zhang, J.; Liu, B. *Organometallics* **2016**, *35*, 972−981.
52. Yang, Y.; Liu, Z.; Cheng, R.; He, X.; Liu, B. *Organometallics* **2014**, *33*, 2599−2607.
53. Qi, Y.; Zhong, L.; Liu, Z.; Qiu, P.; Cheng, R.; He, X.; Vanderbilt, J.; Liu, B. *Organometallics* **2010**, *29*, 1588−1602.
54. Budzelaar, P. H. M. *Can. J. Chem.* **2009**, *87*, 832−837.
55. Bhaduri, S.; Mukhopadhyay, S.; Kulkarni, S. A. *J. Organomet. Chem.* **2009**, *694*, 1297−1307.
56. van Rensburg, W. J.; Grové, C.; Steynberg, J. P.; Stark, K. B.; Huyser, J. J.; Steynberg, P. J. *Organometallics* **2004**, *23*, 1207−1222.
57. Bartlett, S. A.; Moulin, J.; Tromp, M.; Reid, G.; Dent, A. J.; Cibin, G.; McGuinness, D. S.; Evans, J. *ACS Catal.* **2014**, *4*, 4201−4204.
58. Zhao, Y.; Truhlar, D., *Theor. Chem. Acc.* **2008,** *120*, 215−241.
59. Zhao, Y.; Truhlar, D. G., *Acc. Chem. Res.* **2008,** *41*, 157−167
60. DFT calculations were carried out in Gaussian 09.
61. Frisch, M. J. et al. *Gaussian 09, Revision B.01*, Gaussian, Inc.: Wallingford, CT, USA, 2009.
62. Def2-TZVP basis sets were downloaded from https://bse.pnl.gov/bse/portal (01/01/2016).
63. Weigend, F.; Ahlrichs, R. *Phys. Chem. Chem. Phys.* **2005**, *7*, 3297−3305.

64. Andrae, D.; Haeussermann, U.; Dolg, M.; Stoll, H.; Preuss, H. *Theor. Chim. Acta.* **1990**, *77*, 123−141.

65. Marenich, A. V.; Cramer, C. J.; Truhlar, D. G., *J. Phys. Chem. B.* **2009,** *113*, 6378−6396.

66. We also examined changes to the (P,N) ligand structure due to NH activation by alkylaluminums, such as R_2'N-AlR_2, but these changes made no significant difference in predicted 1-hexene/1-octene selectivity.

67. van Rensburg, W. J.; van den Berg, J-A.; Steynberg, P. J. *Organometallics* **2007**, *26*, 1000−1013.

68. 3D structures were rendered using *CYLview*.

69. Legault, C. Y. *CYLview, 1.0b*, Université de Sherbrooke: 2009. (http://www.cylview.org).

70. QSAR-DFT methods have been used to examine bisphosphine amine (PNP) type ligands for LAO selectivity. Tang, S.; Liu, Z.; Zhan, X.; Cheng, R.; He, X.; Liu, B. *J. Mol. Model.* **2014**, *20*, 2129.

71. Karelson, M.; Lobanov, V. S.; Katritzky, A. R. *Chem. Rev.* **1996**, *96*, 1027−1043.

4 WHY LESS COORDINATION PROVIDES HIGHER REACTIVITY CHROMIUM PHOSPHINOAMIDINE ETHYLENE TRIMERIZATION CATALYSTS

4.1 Introduction

Highly selective ethylene oligomerization can produce short-chain, linear α-olefins (LAOs) used in the manufacture of plasticizers, lubricants, detergents, plastomers/elastomers, and linear-low density polyethylene (Scheme 4-1a).[1-2] Cr-phosphine molecular catalysts have emerged as being uniquely suited for industrial large-scale use.[3-6] However, catalyst reactivity, here generally used synonymously with activity and productivity, is highly dependent on the exact ligand structure coordinated to Cr, and unfortunately there are currently no simple set of empirical parameters or design principles that provide prediction of very high catalyst activity while maintaining LAO trimerization selectivity.

Scheme 4-1. a) Overview of selective ethylene oligomerization to 1-hexene. b) Chevron Phillips Chemical Co. LP **(P,N)Cr** selective ethylene trimerization catalysts reported by Sydora and coworkers.[7]

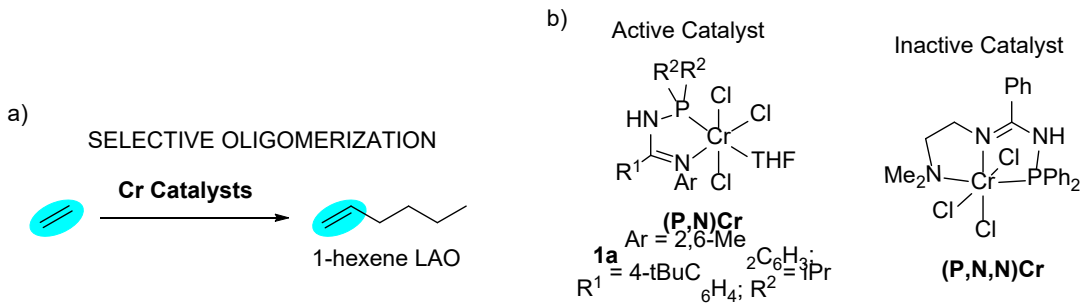

In 2012, Sydora and coworkers reported a new class of aryl and benzyl *N*-phosphinamidine (P,N) Cr 1-hexene selective catalysts (**(P,N)Cr**, Scheme 4-1b).[7] This type of bidentate (P,N) ligand provides a useful platform for catalyst optimization because the ligand can be synthesized in a flexible and modular route, metalation to Cr and characterization is straightforward, and more importantly, ethylene oligomerization reactions are generally highly reproducible and lead to high purity LAOs with only trace co-polymer production. For example, catalyst **1a** (Scheme 4-1b) results in 94% mass selectivity for C_6 products with 1-hexene purity >99%. A new innovation is that these **(P,N)Cr** catalysts can be modified to produce a roughly equal mixture of 1-hexene and 1-octene. Using a quantitative density functional theory (DFT) transition-state model, we predicted and then experimentally verified, new phosphine monocyclic imine catalysts that resulted in >50% 1-octene production.[8]

These bidentate **(P,N)Cr** catalysts are highly reactive with activity generally between 10^4 to 10^6 g of oligomerization product per gram of Cr catalyst per hour (g product/g Cr·h). While the high reactivity of this **(P,N)Cr** catalyst is consistent with the active bidentate **(PNP)Cr** catalysts (PNP = $Ar_2PN(R)PAr_2$; R = alkyl),[9-10] the ortho-methoxy aryl substituted PNP ligand is often considered a tridentate ligand,[11] and most previously disclosed ethylene trimerization catalysts contain tridentate ligand coordination.[12-13] For example, Sasol **(S,N,S)Cr** (S,N,S = $RSCH_2CH_2)_2NH$; R = alkyl) and **(P,N,P)Cr** catalysts (P,N,P = $R_2PCH_2CH_2)_2NH$; R = Ar or alkyl) resulted in productivities $>10^3$ g/g Cr·h.[14-15] With the known reactivity of these tridentate **(S,N,S)Cr** and **(P,N,P)Cr** catalysts, it was surprising that modification of the (P,N) ligand core with a third donor group to give a tridentate (P,N,N) ligand (defined in Scheme 4-1b) resulted in no ethylene oligomerization when subjected to similar conditions as the (P,N) catalysts.[7]

Because it was unclear why the bidentate **(P,N)Cr** catalysts are highly active, but the tridentate **(P,N,N)Cr** catalyst is inactive, we executed a density functional theory (DFT) analysis to examine 1-hexene catalyst reactivity. Based on a high-spin $Cr^{I/III}$ chromacycle mechanism, and consistent with previous experimental kinetic studies,[16] we found that for the **(P,N)Cr**, **1a**, catalyst there are multiple Cr^{I} ethylene coordinated resting states and multiple turnover frequency (TOF) controlling transition states, and the contribution of the turnover controlling transition states depends on ethylene pressure. In contrast, and a rationale for slower reactivity, the **(P,N,N)Cr** catalyst has a stabilized chromacyclopentane resting state. In addition to understanding the unique reactivity of the **(P,N)Cr** catalyst, we also used DFT to calculate and compare the moderate activity of several other 1-hexene tridentate catalysts. Our catalytic energy span calculations were able to qualitatively and semi-quantitatively replicate relative catalyst reactivity.

4.2 Mechanism

As we embarked on modeling **(P,N)Cr** catalyst reactivity with DFT, we were encouraged by our previous use of DFT to define a quantitative transition-state model to predict 1-hexene/1-octene selectivity.[8] This bolstered confidence in the commonly proposed metallacycle mechanism that provides a rationale for selectivity of short-chain LAOs. The general chromacycle mechanism for 1-hexene formation is outlined in Scheme 4-2. It begins with pre-catalyst activation to give a (mono)ethylene low-valent Cr-species **A** followed by ethylene coordination to form the (bis)ethylene-coordinated intermediate **B**. Oxidative C-C bond coupling forms chromacyclopentane **C**. Ethylene coordination gives intermediate **D** and migratory insertion leads to the chromacycloheptane intermediate **E** that can produce 1-hexene via β-hydrogen transfer (βHT).

Scheme 4-2. Generalized mechanism for Cr-catalyzed ethylene trimerization involving chromacycle intermediates.

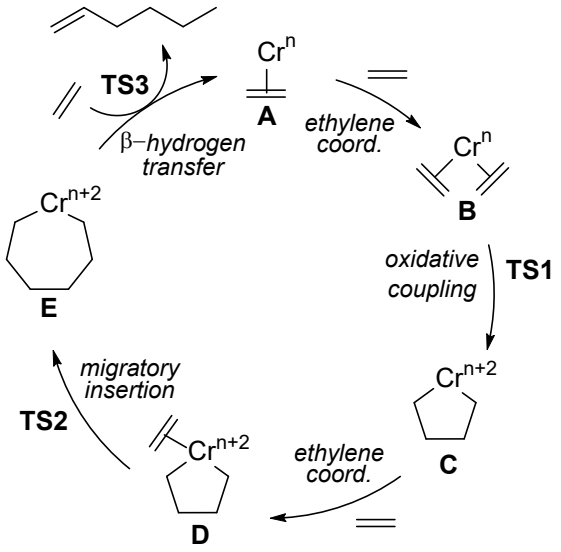

While this chromacycle mechanism was proposed by Manyik more than 40 years ago,[17] and is consistent with the formation of methylcyclopentane and methylenecyclopentane impurities,[18] the most compelling experimental evidence in support of this mechanism was provided by deuterium labeling studies.[19-21] For example, diphosphinoamine-Cr complexes with ortho-methoxy substituted aryl groups, a 1:1 mixture of ethylene and perdeutero ethylene resulted in a 1-hexene isotopologue distribution inconsistent with H/D scrambling. Also, *cis*- and *trans*-ethylene-d_2 showed only terminal deuterium incorporation into 1-hexene, which supports a 3,7-hydrogen shift mechanism without 1-hexene reinsertion. The 1-hexene product distribution using 1,1-dideuterioethylene is consistent with irreversible formation of the chromacycloheptane intermediate.

Because the Cr oxidation state can be significantly influenced by the exact phosphine ligand, several experimental studies have examined the possibility of $Cr^{I/III}$ versus $Cr^{II/IV}$ catalytic cycles. For example, Bercaw isolated and characterized by x-ray a (PNP)(biphenyldiyl)Cr^{III}Br complex,

which produced both 1-hexene and vinylbiphenyl products in the presence of ethylene and upon activation by $NaBAr^F_4$.[19] Wass and Hanton demonstrated for Cr^0 and Cr^I carbonyl complexes with bidentate diphosphinoamine ligands that a Cr^I species with a weakly coordinating anion was necessary to produce an active catalytic system.[22-23] Electron paramagnetic resonance studies identified a **(PNP)Cr^{III}** species that was reduced to Cr^I upon activation with modified-methylaluminumoxane (MMAO).[24] With the addition of ethylene, the signal corresponding to the active species broadened, suggesting a $Cr^{I/III}$ redox cycle during catalysis. Theopold showed that neutral Cr^I dinitrogen complexes catalyze ethylene trimerization as well as the corresponding monomeric Cr^{III} chromacyclopentadiene. However, these neutral complexes are not as active as other cationic Cr catalysts suggesting a more electrophilic cationic chromium metal center is required for high catalytic activity.[25] Consistent with these results, Bercaw showed that a neutral (PNP)Cr catalyst only produced only vinylbiphenyl products and not 1-hexene.[20]

DFT studies have provided direct analysis of the chromacycle mechanism, especially for bidentate and tridentate-ligated Cr catalysts. For example, in 2009 Le Floch used PBEPBE calculations to examine the 3,7-hydrogen shift chromacycle reaction step for $(R'N(CH_2PR_2)_2)Cr$ complexes.[26] In 2011, Liu used B3LYP calculations to examine the chromacycle mechanism for a **(S,N,S)Cr** catalyst (where R = Me).[27] While B3LYP generally does not provide reliable spin-state energies,[28] Liu did examine several spin-states for neutral, cationic, and dicationic Cr metallacycle mechanisms, revealing that spin crossover likely occurs prior to the chromacyclopentane intermediate.[29] More importantly, the lowest energy pathway identified involves a $Cr^{I/III}$ cycle with a protonated monocationic **(S,N,S)Cr** catalyst.[27] The reported ~30 kcal/mol catalytic barriers are likely overestimated with the B3LYP functional. Also, for molecular Cr-based catalysts, these

calculations presented a one-step 3,7-βHT transition-state structure for conversion of chromacycloheptane **E** to 1-hexene, which was previously reported for Ta and other metals.[30-35]

For cationic bidentate **(PNP)Cr** catalysts, Britovsek and McGuinness showed that a $Cr^{I/III}$ cycle with spin crossover (sextet to quartet) is kinetically and thermodynamically more viable than a $Cr^{II/IV}$ cycle using the M06-L density functional.[36-37] The DFT calculations showed that a low energy pathway to 1-hexene involves chromacyclopentane **C** and chromacycloheptane **E** followed by one-step βHT. However, this pathway is only 4 kcal/mol lower in energy than a β-hydride elimination/reductive elimination route from **E** to 1-hexene. β-hydride elimination followed by C-H reductive coupling or one-step βHT from **C** to form 1-butene is 10-20 kcal/mol higher in energy than the 1-hexene pathway. The lowest energy pathway leading to methylcyclopentane was estimated to be ~6 kcal/mol higher in energy than βHT.

Based on the M06-L calculated **(PNP)Cr** chromacycle energy landscape, Britovsek and McGuinness suggested that it is inconclusive, at least for a model ligand, which reaction step controls the rate of 1-hexene formation.[36] They found that the energy from the bis(ethylene) Cr^{I} species to the chromacyclopentane C-C bond forming transition state (**TS1**) is identical to the energy from the chromacycloheptane to the βHT transition state (**TS3**) forming 1-hexene. It was suggested that because the formation of 1-hexene is first order in ethylene concentration, the chromacyclopentane is most likely the turnover limiting step, whereas the βHT reaction step is independent of ethylene concentration. However, this conclusion did not take into account numerical consideration of all possible resting states and turnover-limiting transition states. Britovsek and McGuinness also examined $Ph_2PN(Me)PPh_2$[36-37] and (o-$MeC_6H_4)_2PN(Me)P(o$-$MeC_6H_4)_2$[38] while Jiang investigated $Ph_2PN(R)Si(CH_3)_2CH_2PPh_2$ Cr ligands for reactivity and selectivity based on this chromacycle mechanism.[39]

4.3 Computational Details, Model, and Experimental Reactivity Values

The unrestricted M06-L[40] functional was used with a 6-31G**[LANL2DZ for Cr][41] for geometry optimizations in Gaussian 09.[42] Stationary points were verified as either minima or transition-state structures by calculation and visualization of vibrational frequencies. Intrinsic reaction coordinate (IRC) calculations verified connection between transition states and intermediates on each spin-state surface. For all ground-state and transition-state structures we calculated all reasonable conformations, and lowest energy conformations are reported (see Supporting Information (SI)). Reported free energies at 1 atm and room temperature with an ultrafine integration grid correspond to (U)M06-L/def2-TZVP//(U)M06-L/6-31G**[LANL2DZ for Cr] with the SMD cyclohexane, toluene, or methylcyclohexane solvent models unless otherwise noted for pressure or temperature corrections. Our use of the M06-L density functional here, as well as in our previous study,[8] was motivated from the work of McGuinness and Britovsek who showed that M06-L gave similar spin-state energies and reaction energies compared with the generally accurate G4(MP2,rel) and CCSD(T)/CBS wavefunction methods.[43]

While the complete ligands were used to examine catalyst reactivity, we did not use an explicit counterion for the monocationic Cr catalysts. The neglect of a counterion was motivated because our previous quantitative study calculating relative 1-hexene/1-octene selectivity did not require a counterion. The exact counterion remains unknown, and calculations by Rensburg with trimethylaluminum (TMA) and TMA- methylaluminumoxane (MAO) complexes suggests that a tight Cr-counterion pair is likely in equilibrium with ethylene coordination and potentially off catalytic cycles.[44] Consistent with these findings, de Bruin has also shown that a counterion is not required for modeling Ti-catalyzed ethylene oligomerization reaction profiles.[45]

Scheme 4-3 gives the experimentally reported productivity values for the Cr ligands we examined. These productivity values were scaled to provide an estimate for 1-hexene (labeled as: g 1-C_6/g Cr·h), which could then be directly compared with calculated 1-hexene catalytic cycle turnover frequencies (TOFs). The experimental reaction conditions vary slightly among this set of ligands. See the SI for details. For example, MAO or MMAO are the typical co-catalysts for activating the $CrCl_3$(THF) pre-catalysts and vary between 100-800 molar equivalents relative to Cr. It is known that the co-activator can drastically affect catalyst activity and selectivity.[46] These catalyst activities were measured in either toluene, cyclohexane, or methylcyclohexane, and typically, the best catalytic performance was achieved at temperatures between 60-110°C.

Scheme 4-3. Comparison of experimentally reported ethylene trimerization Cr ligand productivities in g 1-C_6/g Cr·h. The mass percentage of 1-hexene out of all productivity mass is given in parentheses.

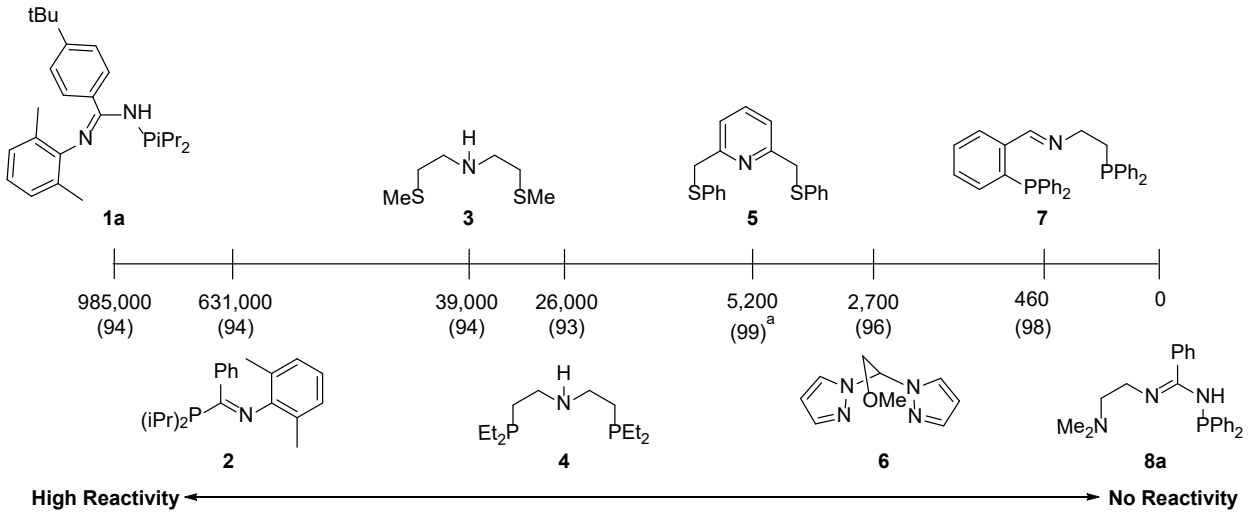

4.4 (P,N)Cr and (P,N,N)Cr Reactivity Comparison

Similar to the previous works by Liu, Britovsek, and McGuinness, we examined the major chromacycle mechanistic features of the very active **(P,N)Cr** catalyst **1a**. As expected, the spin

crossover from sextet to quartet with a $Cr^{I/III}$ cycle was lower in energy than non-spin crossover or a $Cr^{II/IV}$ cycle (see Scheme 4-4 and SI). **1a** is similar to **3**, **(S,N,S)Cr**, and **4**, **(P,N,P)Cr** catalysts where a N-H group can potentially be deprotonated. Therefore, we considered MMAO induced deprotonation of the N-H proton as well as a N($AlMe_2$) type catalyst model. While the N-H protonated ligand catalytic cycles showed the smallest energy difference between the resting states and turnover controlling transition states, the deprotonated and N($AlMe_2$) catalyst models did not have a significantly larger energy difference and can also provide a reactivity model (see SI). We also examined mechanistic variations where additional ethylene is coordinated to the Cr center in the oxidative coupling, migratory insertion, and 1-hexene production reaction steps (see SI). For example, we calculated the *β*HT transition state with an additional ethylene and found that it was ~2 kcal/mol higher in enthalpy and ~13 kcal/mol higher in Gibbs free energy compared with the non-coordinated transition state (see SI). We also examined the traditional multistep *β*-hydride elimination, reductive elimination for formation of 1-hexene. For catalyst **1a**, our calculations showed that *β*-hydride elimination and reductive elimination are 3.7 kcal/mol and 11.4 higher in free energy than the *β*HT transition state, respectively, which is consistent with this higher energy pathway leading to cyclic impurities and potentially polyethylene impurity (see SI).

The simplified chromacycle M06-L Gibbs free energy landscape for ethylene trimerization by **(P,N)Cr** catalyst **1a** is shown in Scheme 4-4. Starting at the sextet spin (P,N)$Cr^{I}(C_2H_4)$, **A**, a second ethylene coordinates to generate the diethylene coordinated (P,N)$Cr^{I}(C_2H_4)_2$, **B**. Spin crossover to the quartet surface facilitates oxidative C-C coupling **TS1** (Figure 4-1) with a $\Delta G^{‡}$ value of 14.9 kcal/mol. This endergonic ethylene coordination indicates that ethylene-coordinated chromacyclopentane intermediate **D** is unlikely to be a catalytic resting state. The barrier for migratory insertion by **TS2** to give the chromacycloheptane is small. It requires only 1.8 kcal/mol

relative to the ethylene-coordinated chromacyclopentane and 16.0 kcal/mol relative to the bis(ethylene) complex **B**. The resulting chromacycloheptane is exergonic by 9.5 kcal/mol relative to **B**. To achieve the βHT transition state **TS3**, a barrier of 12.8 kcal/mol is required from the chromacycloheptane. The energy of **TS3** relative to **B** is 3.3 kcal/mol, and the formation of 1-hexene is 18.6 kcal/mol exergonic.

Scheme 4-4. a) Abbreviated Gibbs free energy landscape for ethylene trimerization with **(P,N)Cr 1a** and **(P,N,P)Cr 8a** catalysts. The ligands are omitted from each structure for clarity. Intermediate **A** and **B** for catalyst **1a** are sextet spin denoted in parentheses. All other intermediates and transition states are quartet spin. b) Gibbs free energy values of the catalytic cycle with ligand complexes **2-7**. (kcal/mol)

a)

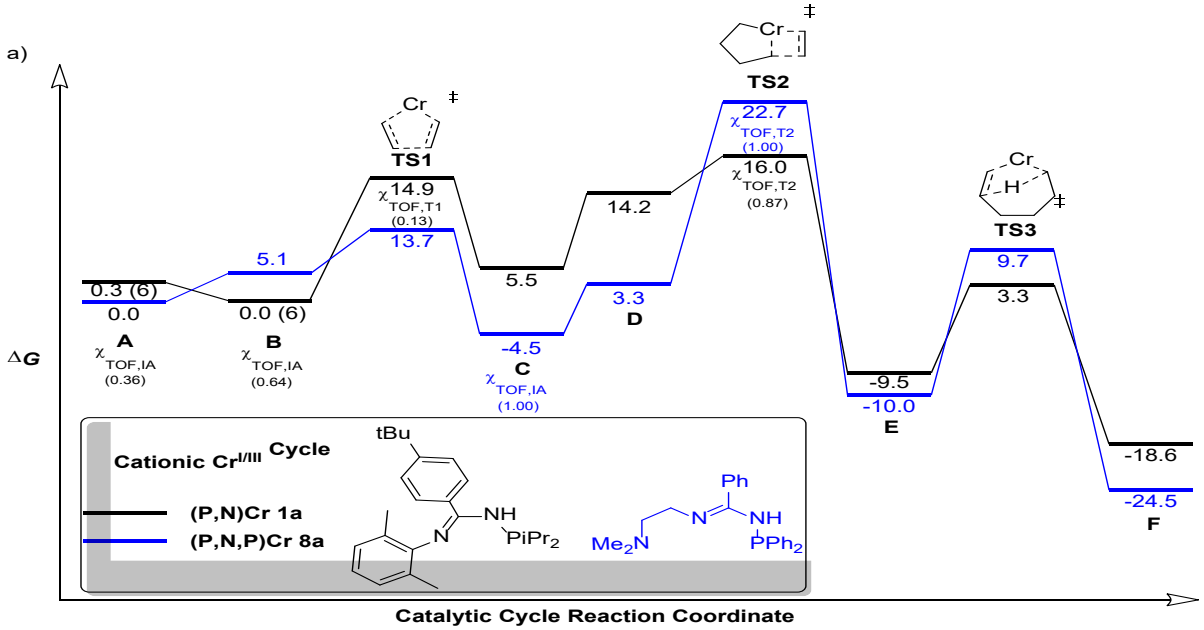

b)

Ligand	A	B	TS1	C	D	TS2	E	TS3	F
2	0.0	3.7	13.3	6.7	12.2	17.8	-11.4	3.4	-18.3
3	1.6	0.0	13.8	-5.3	-2.8	17.9	-16.5	6.1	-22.3
4	4.2	0.0	13.3	-5.7	-1.0	18.3	-16.9	5.6	-21.0
5	0.0	6.8	14.4	3.8	0.9	24.1	-11.6	2.1	-19.5
6	0.0	4.2	17.3	-0.5	6.6	14.2	-17.2	10.3	-17.1
7	0.0	4.2	18.4	-4.4	0.4	24.4	-10.5	7.2	-24.4

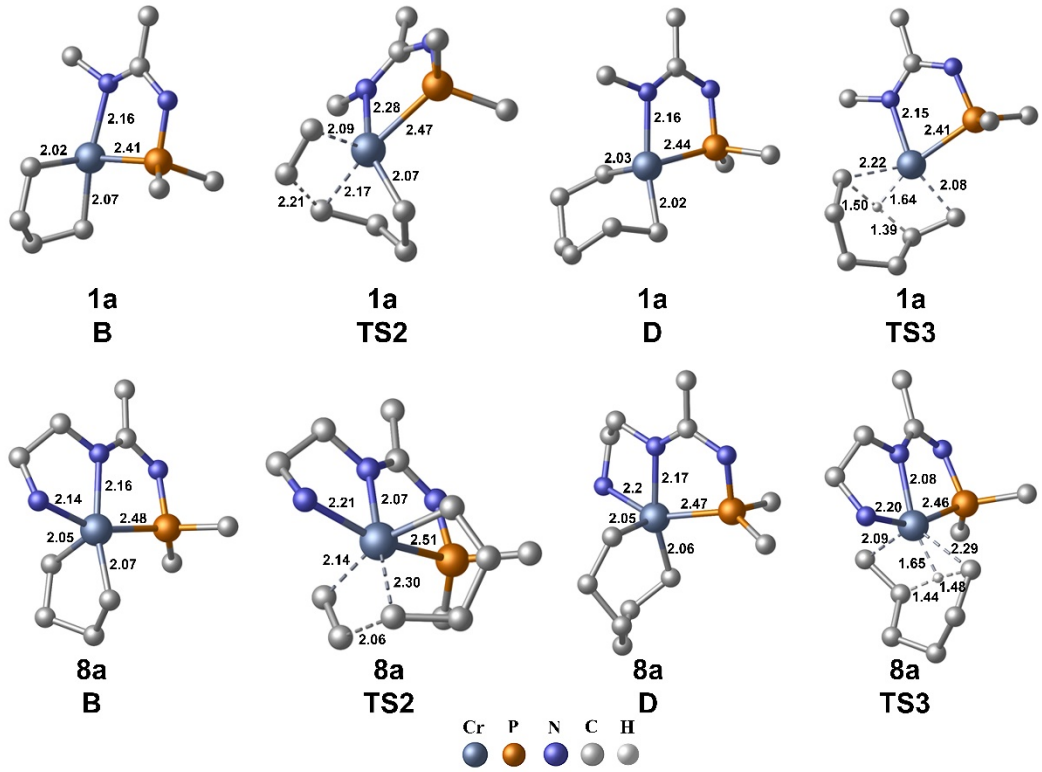

Figure 4-1. 3D representations of key intermediates and transition states for catalysts **1a** and **8a**. Some atoms are removed for clarity.

Because the energies of **A**, **B**, **TS1**, and **TS2** are very close, and the chromacycloheptane that is after these transition states is exergonic, to identify the resting state(s) and rate-limiting transition state(s) we utilized Kozuch and Shaik's definition of energetic span for catalytic reactions,[47] which is related to Campbell's definition.[48-49] In this energetic-span model, calculated Gibbs free energies for each intermediate and transition state are translated to a relative contribution/degree of control to the overall TOF, which is referred to as χ_{TOF}. The TOF described in eq 1 includes the Boltzmann constant, k_b, temperature, T, Planck's constant, h, gas constant, R, number of steps in the catalytic

cycle, N, free energy of the overall catalytic reaction, ΔG_r, free energy of the transition state, T_i, free energy of the intermediate I_j, and $\delta G'_{ij}$, which is described by eq 2.

$$TOF = \frac{k_b T}{h} \frac{e^{\frac{-\Delta G_r}{RT}} - 1}{\sum_{i=1,j=1}^{N} e^{(T_i - I_j - \delta G'_{ij})/RT}} \quad \text{(eq 1)}$$

$$\delta G'_{ij} = \begin{cases} \Delta G_r \quad if\ T_i\ follows\ I_j\ (a) \\ 0 \quad if\ T_i\ precedes\ I_j\ (b) \end{cases} \quad \text{(eq 2)}$$

$$\chi_{TOF,I_K} = \frac{\sum_i e^{(T_i - I_k - \delta G'_{ik})/RT}}{\sum_{ij} e^{(T_i - I_j - \delta G'_{ij})/RT}} \quad \text{(eq 3)}$$

$$\chi_{TOF,T_K} = \frac{\sum_j e^{(T_k - I_j - \delta G'_{kj})/RT}}{\sum_{ij} e^{(T_i - I_j - \delta G'_{ij})/RT}} \quad \text{(eq 4)}$$

Analysis of the energy span[50] and TOF based on the Gibbs free energy landscape for **(P,N)Cr** catalyst **1a** shown in Scheme 4-4a suggests a mixed resting state between (P,N)$Cr^{I}(C_2H_4)$ **A** (36%) and (P,N)$Cr^{I}(C_2H_4)_2$ **B** (64%). This mixed resting state is consistent with Sydora and Abu-Omar's high pressure NMR kinetic studies of ethylene oligomerization with catalyst **1a** that indicated that at least one of the first two ethylene coordination steps in the chromacycle mechanism must be reversible.[16] With the small energy difference between **TS1** and **TS2**, it is not surprising that they both contribute to controlling the overall turnover rate, with χ_{TOF} values of 0.13 and 0.87, respectively. Because of the mixed resting state and **TS2** controlling the majority of the TOF, this would lead to an approximate ethylene rate order of 1.2 (see SI for details). This is consistent with the experimentally measured ethylene reaction order that was observed to be between 1 and 2.[16] The estimated TOF for the Boltzmann weighted energy span is 6.5 mol 1-$C_6 \cdot s^{-1}$, which would result in ~23,400 turnovers·h^{-1} and a total productivity mass of ~2.0 x 10^6 g·h^{-1}, which is consistent with the 9.9 x 10^5 g 1-C_6/g Cr·h reported by Sydora.[7]

Scheme 4-4a also compares the Gibbs free energy landscape of **1a** with the energy landscape for the tridentate **(P,N,N)Cr** catalyst with ligand **8a**. Different from **1a**, the lowest energy catalytic cycle does not require spin crossover because the ground state mono(ethylene) and bis(ethylene) complexes **A** and **B** with ligand **8a** are quartet spin. Also, the mono(ethylene) complex **A** is slightly more stabilized (~5 kcal/mol) than the bis(ethylene) complex **B**. **TS1** requires $\Delta G^{\ddagger}$ value of 13.7 kcal/mol, and this slightly lower barrier compared to ligand **1a** is perhaps not surprising given the Cr^{I} to Cr^{III} oxidation. Importantly, this Cr^{III} oxidation state stabilization is also manifested in the -4.5 kcal/mol ΔG value for formation of the chromacyclopentane relative to **A**. While anticipated from the experimental lack of reactivity, continuation to the chromacycloheptane intermediate **E** by **TS2** requires a Gibbs free energy change of 27.1 kcal/mol relative to **C**. The $\Delta G^{\ddagger}$ value relative to **A** is 22.7 kcal/mol, which is ~7 kcal/mol higher than this **TS2** compared to **A** for catalyst **1a**. Similar to catalyst **1a**, the chromacycloheptane is exergonic and the barrier for conversion to 1-hexene is 24.5 kcal/mol relative to intermediate **F**. The energy span analysis of the **(P,N,N)Cr** catalyst **8a** landscape shows that resting state is entirely the chromacyclopentane **C** and the turnover limiting transition state is exclusively **TS2**. This gives a calculated TOF of 8.0×10^{-8} s^{-1}, which translates to only ~0.02 g of 1-$C_6 \cdot hr^{-1}$, consistent with no product observation.

The kinetic studies by Sydora and Abu-Omar with catalyst **1a** were performed at high ethylene pressure.[16] Therefore, we constructed an ethylene pressure corrected Gibbs free energy surface at 50 bar (Scheme 4-5, also see the SI for a discussion evaluating an entropy-scaled Gibbs free energy surface). Inclusion of ethylene pressure results in several kcal/mol lowering of the **TS2** barrier, and the surrounding landscape. Interestingly, with ωB97X-D/def2-TZVP//M06-L/6-31G**[LANL2DZ for Cr] (Scheme 4-5) the Gibbs free energy surface shows a similar profile to the M06-L surface without correction for ethylene pressure (see SI for ωB97X-D values with

ethylene pressure correction). Except for lowering of the landscape in the vicinity of **TS2**, the M06-L pressure corrected surface, and the ωB97X-D surface, in their shape are qualitatively similar to the M06-L Gibbs free energy surface presented in Scheme 4-4a. However, on the ωB97X-D surface, (P,N)$Cr^{I}(C_2H_4)$ **A** is 2.2 kcal/mol lower in energy than (P,N)$Cr^{I}(C_2H_4)_2$ **B**, which results in the resting state dominated by **A** with a little contribution from chromaheptacycle **E**. The energy difference between **A** and **B** is still consistent with the experimentally observed reversible coordination of an ethylene because **TS1** has a relatively large barrier. Because the ethylene pressure correction lowers **TS2** relative to **TS1**, on this surface **TS1** now dominates controlling the TOF, but there remains a small, but significant contribution from **TS2**. Because the resting state is dominated by **A** and **TS1** and **TS2** both influence the TOF, the predicted rate order for ethylene remains >1 (see SI). The calculated TOFs for the pressure-corrected and ωB97X-D energy landscapes are 67 and 33 mol 1-$C_6 \cdot s^{-1}$, which gives predicted total productivity masses of 2.0 x 10^7 $g \cdot h^{-1}$ and 1.0 x 10^7 $g \cdot h^{-1}$ that overestimates but is consistent with the experimental productivity values. Examination of the pressure corrected surface also provides a possible rationale for experimentally observed irreversible coordination of ethylene to the chromacyclopentane intermediate **C**. The barrier from **D** to **TS2** is 1.9 kcal/mol on the M06-L and only 0.3 kcal/mol on the ωB97X-D surface. These barriers are likely lower than the reverse barrier for ethylene dissociation back to **C**.

Scheme 4-5. Solid surface is the abbreviated Gibbs free energy surface for ethylene trimerization with catalyst **1a** at an ethylene pressure of 50 bar with M06-L. The dotted surface is the ωB97X-D Gibbs free energy landscape. (kcal/mol)

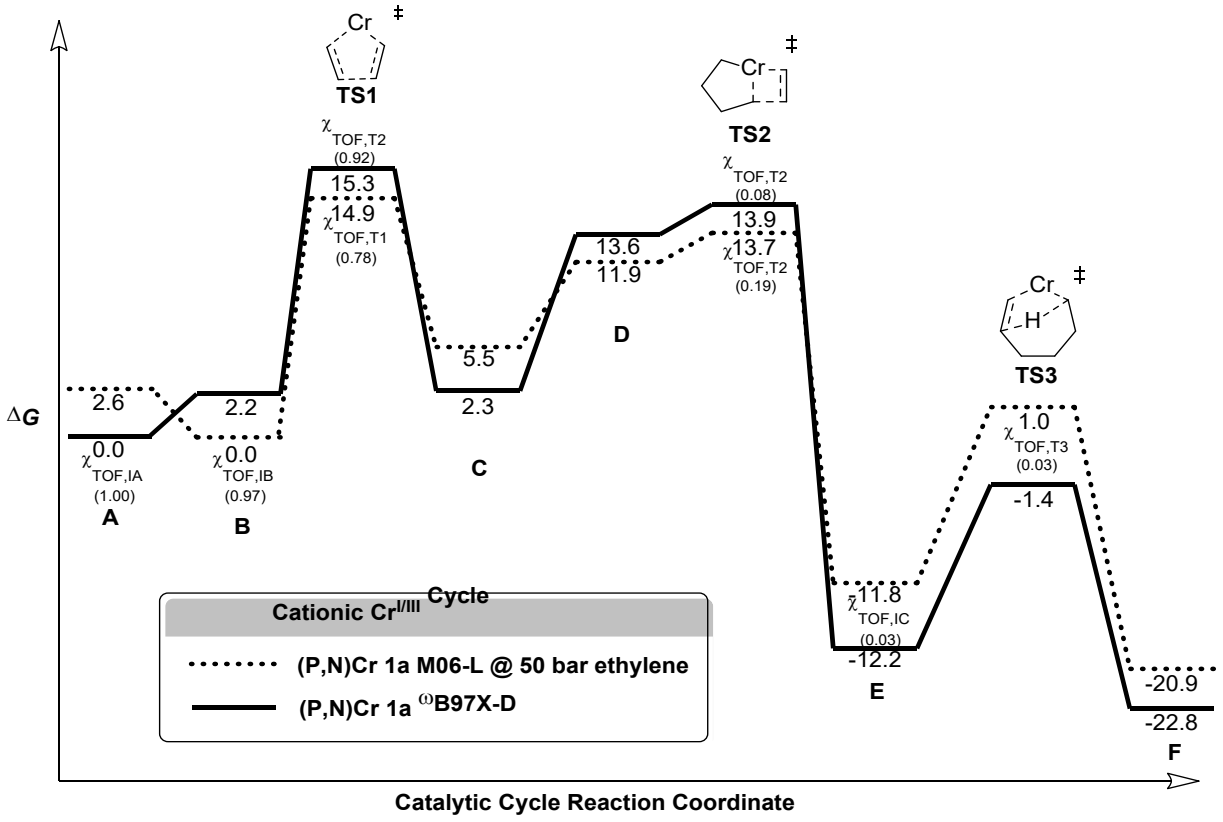

To further investigate the massively decreased TOF for the **(P,N,N)Cr** catalyst, we examined potential steric and electronic effects, as well as ring strain energies. To determine the influence of steric effects, we altered ligands **1a** and **8a** to change aryl and isopropyl groups to methyl groups. Somewhat surprisingly, for truncated ligands **1b** and **8b**, the free energy landscapes are very similar to those presented in Scheme 4-4a, which indicates the ligand size is not responsible for the decreased activity (see Scheme 4-6 and SI). We then examined the impact of third amino donor group on the stability of the chromapentacycle ring. We computed the Cr-C bond homolysis

energies to estimate chromapentacycle ring strains for intermediate **C** with catalysts **(P,N)Cr**, **1a** and **(P,N,N)Cr**, **8a** catalysts. Unexpectedly, the Cr-C bond energies for both these intermediates were similar in energy and calculated to be ~25 kcal/mol, indicating ring strain does not significantly impact reactivity (see SI).

Scheme 4-6. a) Model ligands **1b** and **8b** to examine the impact of steric influence on ethylene trimerization reactivity. Gibbs free energy spans in kcal/mol. b) Dissociation of an amine arm to mimic a bidentate ligand framework.

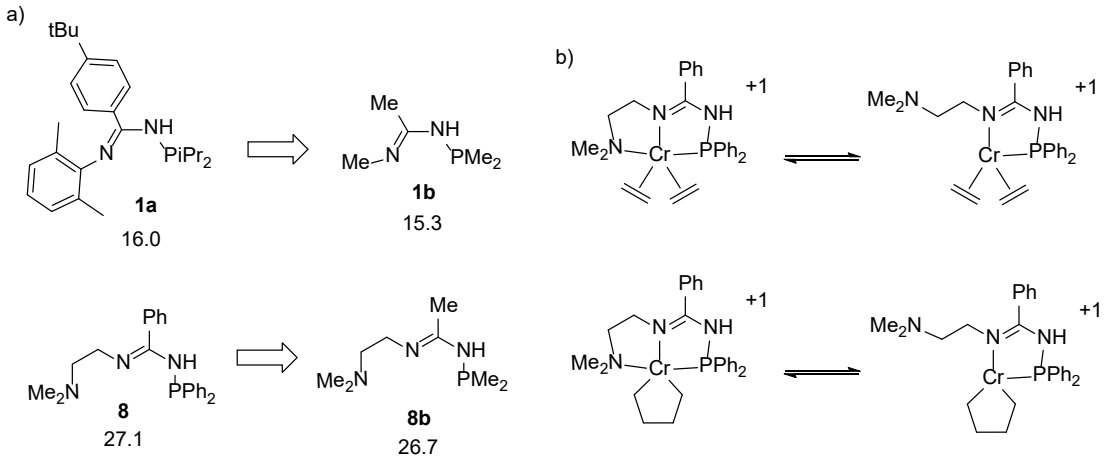

Because the bidentate **(P,N)Cr** catalysts are significantly more reactive than the tridentate catalysts shown in Scheme 4-2, this could signal that for the tridentate catalysts to be reactive, they require one of the ligand arms to dissociate in a hemilabile mechanism (Scheme 4-5). For the bis(ethylene) **(P,N,N)Cr** intermediate **B**, -NMe_2 arm dissociation requires 14.3 kcal/mol. For the predicted resting state, intermediate **C**, -NMe_2 arm dissociation requires 29.5 kcal/mol. All other intermediates and transition states were also calculated with -NMe_2 arm dissociation (see SI). Without -NMe_2 coordination, the resting state becomes intermediate **B** and the turnover limiting transition state has an energy span of 15.4 kcal/mol, which is very similar to the **(P,N)Cr** catalyst

1a. Overall, this indicates that for this type of Cr ligand the third amine coordination overstabilizes the Cr^{III} intermediate and prevents further expansion of the chromacycle.

4.5 Reactivity Comparison of Catalysts 2-7

For **2**, similar to **1a**, the mono(ethylene) and bis(ethylene) complexes are sextet spin states; however, intermediate **A** is 3.7 kcal/mol lower in energy than **B** (see SI for energy surface). The following oxidative C-C coupling barrier is 13.3 kcal/mol relative to **A** and 1.6 kcal/mol lower in energy than **1a**. The formation of the chromacyclopentane and ethylene coordinated chromacycle intermediates are endergonic, analogous to **1a**. The subsequent migratory insertion barrier is 17.8 kcal/mol, which then forms an exergonic chromacycloheptane intermediate. The β-hydrogen transfer transition state to form **F** is 14.8 kcal/mol relative to **E**. The overall energy span of **2** is 1.8 kcal/mol higher than **1a** and slightly underestimates the productivity (Table 4-1) but is consistent with the experimentally observed catalytic activities.

Tridentate **(S,N,S)Cr** (**3**) and **(P,N,P)Cr** (**4**) complexes were modeled as the NH protonated monocationic $Cr^{I/III}$ based on Liu's[27] work and our results and previous work.[8] Our calculations are qualitatively consistent with the previous B3LYP calculations using ligand **3** with one notable exception. We predicted the same sextet to quartet spin crossing during oxidative coupling, but this energy difference is only ~23 kcal/mol compared to the >30 kcal/mol previously reported. Because our model for the inactivity of the tridentate **8a** involves the stability of the chromacyclopentane intermediate **B**, Scheme 4-4 gives the energies of this intermediate for the **(S,N,S)Cr** and **(P,N,P)Cr** catalysts. For **(S,N,S)Cr**, the migratory insertion barrier **TS2** is 17.9 and 23.1 kcal/mol relative to **B** and **C**, respectively. For this catalytic cycle, the Boltzmann weighted energy span of 23.1 kcal/mol results in a predicted TOF of 4.2×10^{-5} mol 1-C_6/s^{-1} and productivity

of 12.7 g 1-C_6/hr^{-1}. While this predicted productivity underestimates the 1-hexene product compared to experiment, it does capture the moderate reactivity between **1a** and **8a**.

Consistent with **(S,N,S)Cr**, the chromacyclopentane intermediate regarding the **(P,N,P)Cr** complex is stabilized relative to **A** (ΔG = -5.7 kcal/mol). The overall Boltzmann weighted energy span that includes the proceeding migratory insertion barrier is 23.8 kcal/mol and translates to a TOF of 1.6 x 10^{-5} mol 1-C_6/s^{-1} and productivity of 4.8 g 1-C_6/h^{-1}. Importantly, the nearly equivalent energy spans of the **(S,N,S)Cr** and **(P,N,P)Cr** catalysts capture the similar experimental productivity values (Scheme 4-4). Furthermore, the energy spans demonstrate that the S,N,S and P,N,P type ligands provide similar effects in stabilizing the chromacyclopentane intermediate resulting in a relatively high migratory insertion barrier. Ligand complexes featuring S,N,S[51] (**5**), N,O,N[52] (**6**), and P,N,P[53] (**7**) tridentate coordination spheres, mirror the S,N,S (**3**) and P,N,P (**4**) complexes with increasing migratory insertion or enhanced stability of the chromacycloheptane intermediate leading to larger energy spans (see table in Scheme 4-4, Table 4-1, and SI). Conversely, the **(P,N)Cr** catalyst provides a balance of moderate to low stability of the chromacyclopentane intermediate and stabilizes the migratory insertion barrier with the phosphine ligand arm resulting in a relatively low migratory insertion barrier.

4.6 Comparison of Calculated and Experimental Productivity

To begin building a general reactivity model that could be useful across several ligand types, we approximated the TOF energy spans including temperature and pressure corrections that reasonably model experimental conditions for the ligands shown in Scheme 4-3 (see SI for full experimental details and reaction condition corrected Gibbs free energy surfaces). Because there was a switch in resting state and turnover limiting transition states for **1a** versus **8a**, this analysis

required calculation of all intermediates and transition states for each ligand. Generally, for meridional coordination complexes, **TS2** dominates rate control and for facial complexes **TS3** dominates rate control. Table 4-1 provides an overview of the calculated Boltzmann weighted energy span $\Delta G^{\ddagger}$, TOF, calculated productivity and reported experimental productivity values.

Complex	Pressure[a]	Temperature[b]	$\Delta G^{\ddagger}$[d]	TOF[e]	Productivity[f]	Exp. Productivity[g]
1a	60	70	17.1	1.4	4.2×10^{5}	9.9×10^{5}
2	40	60	17.6	7.2×10^{-1}	2.2×10^{5}	6.3×10^{5}
3	40	80	23.9	1.2×10^{-5}	3.6	3.9×10^{4}
4	40	80	25.0	2.4×10^{-6}	7.2×10^{-1}	2.6×10^{4}
5	35	50	23.1	3.4×10^{-5}	10.3	5.2×10^{3}
6	25	80	27.4	4.6×10^{-8}	1.4×10^{-2}	2.7×10^{3}
7	30	24	27.1	8.3×10^{-8}	2.5×10^{-2}	4.6×10^{2}
8	30	55	26.7	1.7×10^{-7}	5.1×10^{-2}	0

Table 4-1. [a]Experimental ethylene pressure (bar). [b]Experimental temperature (°C). [c]TOF determining transition state contributions. [d]Boltzmann weighted Gibbs free energy span in kcal/mol. [e]Calculated TOF in mol of 1-$C_6 \cdot s^{-1}$. [f]Calculated productivities of 1-C_6 in $g \cdot hr^{-1}$. [g]Experimental productivities of 1-hexene in g 1-C_6/g Cr·h.

Figure 4-2 provides a quantitative assessment of the natural log of experimental productivity values versus the natural log of pressure and temperature corrected calculated productivity values for the Boltzmann averaged energy spans that dominate rate control. The natural log transformations were necessary to compare the very high activities of catalyst **1a** and **2** to slow or inactive catalyst **6**, **7**, and **8**. While there is clearly a linear correlation, unfortunately, this regression curve is not highly quantitative with an R^2 value of 0.59. However, the moderate correlation results from our predicted productivity for the non-reactive ligand **8a**, which is overestimated relative to the other complexes. A similar moderate correlation was also found using the ωB97X-D functional (see SI), which indicates multiple functionals are able to replicate

experimental productivity. This graph does showcase high, moderate, and low reactivity groupings of ligands. For example, highly active ligand complexes **1a** and **2** are grouped together in a similar region (green in Figure 4-2), while the moderate tridentate complexes **3**, **4**, **5** which yield moderate productivities are grouped in yellow. Low or no productivity complexes **6**, **7**, and **8a** are grouped together in red.

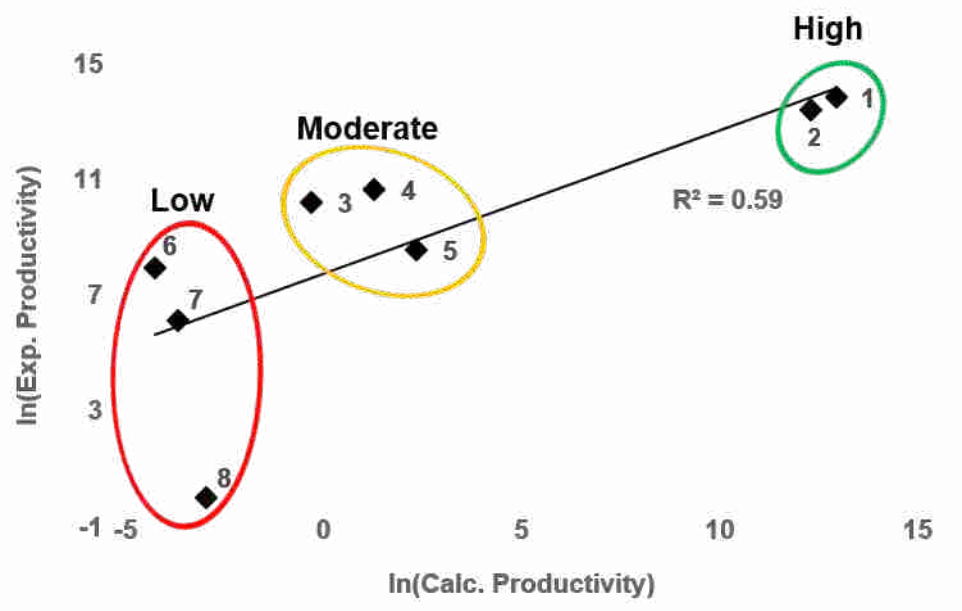

Figure 4-2. Plot of natural log of experimental productivity values corrected for 1-hexene only (g 1-C_6/g Cr·h) versus the natural log calculated 1-C_6 productivity values. **8a** productivity was evaluated as the natural log of 1.

4.7 Conclusions

DFT calculations and an energy-span type analysis were used to examine the difference between the highly reactive **(P,N)Cr** and unreactive **(P,N,P)Cr** catalysts for ethylene trimerization. Our calculations, similar to previous computational studies, suggest a low energy $Cr^{I/III}$ chromacycle catalytic mechanism. For **(P,N)Cr 1a**, our analysis revealed there are multiple Cr^{I} ethylene coordinated resting states and multiple turnover-controlling transition states, which can

account for a partial rate order in ethylene. The calculated productivity mass of 3.0 x 10^6 $g \cdot h^{-1}$ is within one order of magnitude of the experimental value. In contrast to this highly reactive catalyst, for the **(P,N,N)Cr** catalyst, we calculated a much larger energy span which is due to a stabilized chromacyclopentane intermediate along with a higher barrier for the subsequent migratory insertion reaction step. The energy spans of the intermediate activity tridentate catalysts are smaller than **(P,N,N)Cr** but larger than **(P,N)Cr**. These catalysts have moderate activity for different reasons. For example, the thiol ether (**3**) and alkyl phosphine ligands (**4**) do not overstabilize the chromacyclopentane and provide a relatively low barrier for migratory insertion. While there is clearly a linear correlation between experimental productivity values and our calculated energy spans, the correlation is only modest, but potentially useful to qualitatively segregate poor versus highly active Cr catalysts.

4.8 References

1. Green, M. M.; Wittcoff, H. A., *Organic Chemistry Principles and Industrial Practice*, Wiley-VCH Verlag GmbH & Co. 2003.

2. Weissermel, K.; Arpe, H.-J., *Industrial Organic Chemistry*. Chapter 3, 5th ed; Wiley-VCH Verlag GmbH & Co. 2010.

3. Dixon, J. T.; Green, M. J.; Hess, F. M.; Morgan, D. H. Advances in selective ethylene trimerisation – a critical overview. *J. Organomet. Chem.* **2004,** *689*, 3641-3668.

4. McGuinness, D. S. Olefin Oligomerization via Metallacycles: Dimerization, Trimerization, Tetramerization, and Beyond. *Chem. Rev.* **2011,** *111*, 2321-2341.

5. Agapie, T. Selective ethylene oligomerization: Recent advances in chromium catalysis and mechanistic investigations. *Coord. Chem. Rev.* **2011,** *255*, 861-880.

6. Alferov, K. A.; Belov, G. P.; Meng, Y. Chromium catalysts for selective ethylene oligomerization to 1-hexene and 1-octene: Recent results. *Appl. Catal., A* **2017,** *542*, 71-124.

7. Sydora, O. L.; Jones, T. C.; Small, B. L.; Nett, A. J.; Fischer, A. A.; Carney, M. J. Selective Ethylene Tri-/Tetramerization Catalysts. *ACS Catal.* **2012,** *2*, 2452-2455.

8. Kwon, D.-H.; Fuller, J. T.; Kilgore, U. J.; Sydora, O. L.; Bischof, S. M.; Ess, D. H. Computational Transition-State Design Provides Experimentally Verified Cr(P,N) Catalysts for Control of Ethylene Trimerization and Tetramerization. *ACS Catal.* **2018,** *8*, 1138-1142.

9. Carter, A.; Cohen, S. A.; Cooley, N. A.; Murphy, A.; Scutt, J.; Wass, D. F. High activity ethylene trimerisation catalysts based on diphosphine ligands. *ChemComm* **2002**, 858-859.

10. Bollmann, A.; Blann, K.; Dixon, J. T.; Hess, F. M.; Killian, E.; Maumela, H.; McGuinness, D. S.; Morgan, D. H.; Neveling, A.; Otto, S.; Overett, M.; Slawin, A. M. Z.; Wasserscheid, P.;

Kuhlmann, S. Ethylene Tetramerization: A New Route to Produce 1-Octene in Exceptionally High Selectivities. *J. Am. Chem. Soc.* **2004,** *126*, 14712-14713.

11. Sydora, O. L. Selective Ethylene Oligomerization. *Organometallics* **2019,** *38*, 997-1010.

12. van Leeuwen, P. W. N. M.; Clément, N. D.; Tschan, M. J. L. New processes for the selective production of 1-octene. *Coord. Chem. Rev.* **2011,** *255*, 1499-1517.

13. Peitz, S.; Peulecke, N.; Müller, B. H.; Spannenberg, A.; Drexler, H.-J.; Rosenthal, U.; Al-Hazmi, M. H.; Al-Eidan, K. E.; Wöhl, A.; Müller, W. Heterobimetallic Al−Cl−Cr Intermediates with Relevance to the Selective Catalytic Ethene Trimerization Systems Consisting of CrCl3(THF)3, the Aminophosphorus Ligands Ph2PN(R)P(Ph)N(R)H, and Triethylaluminum. *Organometallics* **2011,** *30*, 2364-2370.

14. McGuinness, D. S.; Wasserscheid, P.; Keim, W.; Morgan, D.; Dixon, J. T.; Bollmann, A.; Maumela, H.; Hess, F.; Englert, U. First Cr(III)−SNS Complexes and Their Use as Highly Efficient Catalysts for the Trimerization of Ethylene to 1-Hexene. *J. Am. Chem. Soc.* **2003,** *125*, 5272-5273.

15. McGuinness, D. S.; Wasserscheid, P.; Morgan, D. H.; Dixon, J. T. Ethylene Trimerization with Mixed-Donor Ligand (N,P,S) Chromium Complexes: Effect of Ligand Structure on Activity and Selectivity. *Organometallics* **2005,** *24*, 552-556.

16. Gunasekara, T.; Kim, J.; Preston, A.; Steelman, D. K.; Medvedev, G. A.; Delgass, W. N.; Sydora, O. L.; Caruthers, J. M.; Abu-Omar, M. M. Mechanistic Insights into Chromium-Catalyzed Ethylene Trimerization. *ACS Catal.* **2018,** *8*, 6810-6819.

17. Manyik, R. M.; Walker, W. E.; Wilson, T. P. A soluble chromium-based catalyst for ethylene trimerization and polymerization. *J. Catal.* **1977,** *47*, 197-209.

18. Emrich, R.; Heinemann, O.; Jolly, P. W.; Krüger, C.; Verhovnik, G. P. J. The Role of Metallacycles in the Chromium-Catalyzed Trimerization of Ethylene. *Organometallics* **1997,** *16*, 1511-1513.

19. Agapie, T.; Schofer, S. J.; Labinger, J. A.; Bercaw, J. E. Mechanistic Studies of the Ethylene Trimerization Reaction with Chromium−Diphosphine Catalysts: Experimental Evidence for a Mechanism Involving Metallacyclic Intermediates. *J. Am. Chem. Soc.* **2004,** *126*, 1304-1305.

20. Agapie, T.; Labinger, J. A.; Bercaw, J. E. Mechanistic Studies of Olefin and Alkyne Trimerization with Chromium Catalysts: Deuterium Labeling and Studies of Regiochemistry Using a Model Chromacyclopentane Complex. *J. Am. Chem. Soc.* **2007,** *129*, 14281-14295.

21. Hirscher, N. A.; Labinger, J. A.; Agapie, T. Isotopic labelling in ethylene oligomerization: addressing the issue of 1-octene vs. 1-hexene selectivity. *Dalton Trans.* **2019,** *48*, 40-44.

22. Bowen, L. E.; Haddow, M. F.; Orpen, A. G.; Wass, D. F. One electron oxidation of chromium N,N-bis(diarylphosphino)amine and bis(diarylphosphino)methane complexes relevant to ethene trimerisation and tetramerisation. *Dalton Trans.* **2007**, 1160-1168.

23. Rucklidge, A. J.; McGuinness, D. S.; Tooze, R. P.; Slawin, A. M. Z.; Pelletier, J. D. A.; Hanton, M. J.; Webb, P. B. Ethylene Tetramerization with Cationic Chromium(I) Complexes. *Organometallics* **2007,** *26*, 2782-2787.

24. Brückner, A.; Jabor, J. K.; McConnell, A. E. C.; Webb, P. B. Monitoring Structure and Valence State of Chromium Sites during Catalyst Formation and Ethylene Oligomerization by in Situ EPR Spectroscopy. *Organometallics* **2008,** *27*, 3849-3856.

25. Monillas, W. H.; Young, J. F.; Yap, G. P. A.; Theopold, K. H. A well-defined model system for the chromium-catalyzed selective oligomerization of ethylene. *Dalton Trans.* **2013,** *42*, 9198-9210.

26. Klemps, C.; Payet, E.; Magna, L.; Saussine, L.; Le Goff, X. F.; Le Floch, P. PCNCP Ligands in the Chromium-Catalyzed Oligomerization of Ethylene: Tri- versus Tetramerization. *Chem. Eur. J.* **2009,** *15*, 8259-8268.

27. Yang, Y.; Liu, Z.; Zhong, L.; Qiu, P.; Dong, Q.; Cheng, R.; Vanderbilt, J.; Liu, B. Spin Surface Crossing between Chromium(I)/Sextet and Chromium(III)/Quartet without Deprotonation in SNS-Cr Mediated Ethylene Trimerization. *Organometallics* **2011,** *30*, 5297-5302.

28. Reiher, M.; Salomon, O.; Artur Hess, B. Reparameterization of hybrid functionals based on energy differences of states of different multiplicity. *Theor. Chem. Acc.* **2001,** *107*, 48-55.

29. Hossain, M. D.; Kim, H. S.; Houk, K. N.; Cheong, M. *Bull. Korean Chem. Soc.* **2014,** *35*, 2835.

30. Yu, Z.-X.; Houk, K. N. Why Trimerization? Computational Elucidation of the Origin of Selective Trimerization of Ethene Catalyzed by [TaCl3(CH3)2] and An Agostic-Assisted Hydride Transfer Mechanism. *Angew. Chem. Int. Ed.* **2003,** *42*, 808-811.

31. Blok, A. N. J.; Budzelaar, P. H. M.; Gal, A. W. Mechanism of Ethene Trimerization at an ansa-(Arene)(cyclopentadienyl) Titanium Fragment. *Organometallics* **2003,** *22*, 2564-2570.

32. de Bruin, T. J. M.; Magna, L.; Raybaud, P.; Toulhoat, H. Hemilabile Ligand Induced Selectivity: a DFT Study on Ethylene Trimerization Catalyzed by Titanium Complexes. *Organometallics* **2003,** *22*, 3404-3413.

33. Deckers, P. J. W.; Hessen, B.; Teuben, J. H. Catalytic Trimerization of Ethene with Highly Active Cyclopentadienyl−Arene Titanium Catalysts. *Organometallics* **2002,** *21*, 5122-5135.

34. Tobisch, S.; Ziegler, T. Catalytic Linear Oligomerization of Ethylene to Higher α-Olefins: Insight into the Origin of the Selective Generation of 1-Hexene Promoted by a Cationic Cyclopentadienyl-Arene Titanium Active Catalyst. *Organometallics* **2003,** *22*, 5392-5405.

35. Robinson, R; McGuinness, D. S.; Yates, B. F. The Mechanism of Ethylene Dimerization with the $Ti(OR')_4/AlR_3$ Catalytic System: DFT Studies Comparing Metallacycle and Cosse Proposals. *ACS Catal.* **2013**, *3*, 3006-3016.

36. Britovsek, G. J. P.; McGuinness, D. S.; Wierenga, T. S.; Young, C. T. Single- and Double-Coordination Mechanism in Ethylene Tri- and Tetramerization with Cr/PNP Catalysts. *ACS Catal.* **2015,** *5*, 4152-4166.

37. Britovsek, G. J. P.; McGuinness, D. S. A DFT Mechanistic Study on Ethylene Tri- and Tetramerization with Cr/PNP Catalysts: Single versus Double Insertion Pathways. *Chem. Eur. J.* **2016,** *22*, 16891-16896.

38. Britovsek, G. J. P.; McGuinness, D. S.; Tomov, A. K. Mechanistic study of ethylene tri- and tetramerisation with Cr/PNP catalysts: effects of additional donors. *Catal. Sci. Technol.* **2016,** *6*, 8234-8241.

39. Zhang, L.; Meng, X.; Chen, Y.; Cao, C.; Jiang, T. Chromium-Based Ethylene Tetramerization Catalysts Supported by Silicon-Bridged Diphosphine Ligands: Further Combination of High Activity and Selectivity. *ChemCatChem* **2017,** *9*, 76-79.

40. Zhao, Y.; Truhlar, D. The M06 suite of density functionals for main group thermochemistry, thermochemical kinetics, noncovalent interactions, excited states, and transition elements: two new functionals and systematic testing of four M06-class functionals and 12 other functionals. *Theor. Chem. Acc.* **2008,** *120*, 215-241.

41. Hay, P. J.; Wadt, W. R. Ab initio effective core potentials for molecular calculations. Potentials for the transition metal atoms Sc to Hg. *J. Chem. Phys.* **1985,** *82*, 270-283.

42. Frisch, M.; Trucks, G.; Schlegel, H.; Scuseria, G.; Robb, M.; Cheeseman, J.; Scalmani, G.; Barone, V.; Mennucci, B.; Petersson, G. Gaussian 09, revision B. 01. *Gaussian, Inc., Wallingford, CT* **2010**.

43. McGuinness, D. S.; Chan, B.; Britovsek, G. J. P.; Yates, B. F. Ethylene Trimerisation with Cr-PNP Catalysts: A Theoretical Benchmarking Study and Assessment of Catalyst Oxidation State. *Aust. J. Chem.* **2014,** *67*, 1481-1490.

44. Janse van Rensburg, W.; van den Berg, J.-A.; Steynberg, P. J. Role of MAO in Chromium-Catalyzed Ethylene Tri- and Tetramerization: A DFT Study. *Organometallics* **2007,** *26*, 1000-1013.

45. Pasha, F. A.; Basset, J.-M.; Toulhoat, H.; de Bruin, T. DFT Study on the Impact of the Methylaluminoxane Cocatalyst in Ethylene Oligomerization Using a Titanium-Based Catalyst. *Organometallics* **2015,** *34*, 426-431.

46. McGuinness, D. S.; Rucklidge, A. J.; Tooze, R. P.; Slawin, A. M. Z. Cocatalyst Influence in Selective Oligomerization: Effect on Activity, Catalyst Stability, and 1-Hexene/1-Octene Selectivity in the Ethylene Trimerization and Tetramerization Reaction. *Organometallics* **2007,** *26*, 2561-2569.

47. Kozuch, S.; Shaik, S. How to Conceptualize Catalytic Cycles? The Energetic Span Model. *Acc. Chem. Res.* **2011,** *44*, 101-110.

48. Campbell, C. T. Future Directions and Industrial Perspectives Micro- and macro-kinetics: Their relationship in heterogeneous catalysis. *Top Catal.* **1994,** *1*, 353-366.

49. Campbell, C. T. The Degree of Rate Control: A Powerful Tool for Catalysis Research. *ACS Catal.* **2017,** *7*, 2770-2779.

50. Uhe, A.; Kozuch, S.; Shaik, S. Automatic analysis of computed catalytic cycles. *J. Comput. Chem.* **2011,** *32*, 978-985.

51. Temple, C. N.; Gambarotta, S.; Korobkov, I.; Duchateau, R. New Insight into the Role of the Metal Oxidation State in Controlling the Selectivity of the Cr-(SNS) Ethylene Trimerization Catalyst. *Organometallics* **2007,** *26*, 4598-4603.

52. Zhang, J.; Braunstein, P.; Hor, T. S. A. Highly Selective Chromium(III) Ethylene Trimerization Catalysts with [NON] and [NSN] Heteroscorpionate Ligands. *Organometallics* **2008,** *27*, 4277-4279.

53. Bluhm, M. E.; Walter, O.; Döring, M. Chromium imine and amine complexes as homogeneous catalysts for the trimerisation and polymerisation of ethylene. *J. Organomet. Chem.* **2005,** *690*, 713-721.

5 THE CHALLENGE OF USING PRACTICAL DFT TO MODEL FE PENDANT DONOR DIIMINE CATALYZED ETHYLENE OLIGOMERIZATION

5.1 Introduction

Linear α-olefins (LAOs, 1-alkenes) are important co-monomers used to produce linear low-density polyethylene, plasticizers, lubricants, surfactants, and waxes.[1,2] A variety of transition metal ethylene oligomerization catalysts are utilized commercially to achieve a full range of LAO carbon lengths (e.g. C_4-C_{30}). Select examples include Ni catalysts employed in the Shell higher olefin process (SHOP)[3-6] and Zr based metallocene catalysts developed by Idemitsu[7,8] and SABIC-Linde.[9] Because of the significant demand for specific shorter length LAOs, often between C_4 and C_{18}, there remains significant interest in developing and understanding molecular catalysts for ethylene oligomerization that yield these desirable lighter distributions.

A prominent example of molecular catalysis for LAO production was reported in 1998 by Small and Brookhart where modified-methylaluminoxanes (MMAO) activated Fe tridentate pyridine bisimine (PBI) complexes catalyze ethylene oligomerization with a general distribution range of C_4-C_{20} (Scheme 5-1a).[10,11] While Bennett, Brookhart, and Gibson showed that the bis-ortho aryl substituted complexes catalyze ethylene polymerization,[12-14] mono-ortho aryl substituted (PBI)$FeCl_2$ complexes catalyze oligomerization with turnover frequencies up to 10^8/hour following activation.[10,15] The oligomerization LAO distribution follows a Schulz-Flory pattern with a so-called K value (propagation/(propagation + termination)) typically between 0.7 and 0.8, and chain growth and chain transfer were determined to be first order in ethylene.[10] While (PBI)Fe complexes provide fast catalysis with a useful distribution of LAOs, there is often a significant percentage percent of isomeric oligomers produced.[10] Analysis of the

C_{10} oligomers indicated that isomers are generated from branching and are not internal olefins or oligomers with vinylidene end groups.[10]

Scheme 5-1. a) Examples of Fe diimine catalysts for ethylene oligomerization. b) Overview of molecular catalysis for ethylene oligomerization to LAOs.

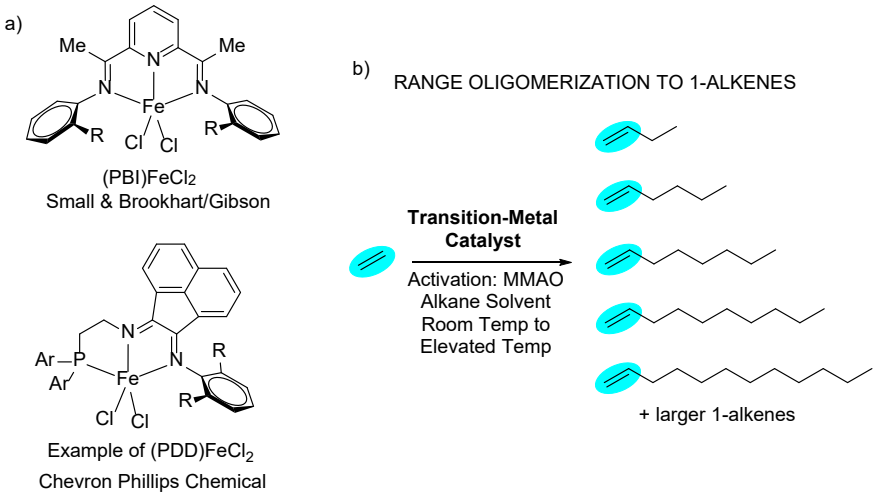

Since the original reports of the (PBI)Fe ethylene oligomerization catalyst system, several groups, including Chevron Phillips Chemical Co. LP, have made ligand and metal modifications to tune lifetime, reactivity, and selectivity.[16-22] One important improvement has been catalysts that decrease olefin oligomer branching. For example, Small and co-workers at Chevron Phillips Chemical identified pendant donor diimine (PDD)Fe complexes (phosphine example shown in Scheme 5-1a), where essentially no branched olefin oligomers are formed during ethylene oligomerization resulting in high olefin purities >98 wt% 1-ene,[23-28] albeit the (PDD)Fe catalysts exhibit reduced rates compared to the (PBI)Fe catalysts.

The goal of this work was to test a practical density functional theory (DFT) protocol to qualitatively and quantitatively model ethylene oligomerization branching, propagation/termination, and K values for (PDD)Fe catalysts, which could later be used for evaluation of potential new catalyst targets. As a launching point for our DFT modeling, we first experimentally evaluated the olefin oligomer purity (i.e. lack of branching) and measured K values of LAO fractions for a Chevron Phillips Chemical (PDD)Fe catalyst, which showed the expected very high purity (>99% for 1-alkenes) and progressively larger K values as a function of carbon chain length. Using DFT calculations, we were able to model the

higher olefin oligomerization purity for (PDD)Fe compared to (PBI)Fe, which showed enhanced regioselectivity for migratory insertion between Fe-H intermediates and LAOs. Despite some previous literature success of modeling (PBI)Fe catalysis,[29-34] we found modeling (PDD)Fe propagation/termination and K values significantly challenging, and caution should be used for quantitative assessment of these catalysis values.

5.2 Experimental Section

General Considerations: All manipulations were carried out using a nitrogen filled drybox and standard Schlenk techniques using oven dried glassware (>1 h at 110 °C under vacuum, -30 mm Hg). Dichloromethane (DCM) was anhydrous grade from Fisher, utilized in the drybox, and stored over molecular sieves. Heptane and *n*-nonane were anhydrous grade from Aldrich, utilized in the drybox, and stored over molecular sieves. Other reagents were obtained commercially from Aldrich Chemical Company, Acros Organics, or Digital Specialty Chemicals and used as received. Cyclohexane was purchased from Aldrich or acquired from internal company resources, degassed, and pumped repeatedly in a circular loop over a molecular sieve bed. MMAO-3A (Al 7% by wt) in heptane was purchased from Akzo Nobel. Liquid phase organic products were analyzed with an Agilent 6890 equipped with a 50 m DB-5 cross-linked methyl silicone gum capillary column and were confirmed by retention time to authentic standards. Data was prepared utilizing an MS Excel program. General synthetic procedures and characterization for PDD complexes was previously reported by Small et al.[23]

5.2.1 Ethylene Oligomerization/Polymerization

A 500 mL Zipperclave reactor from Autoclave Engineers was used for the oligomerization reactions. The catalyst (2.94 umol) was dissolved in a small amount of dichloromethane (~1 mL) in an NMR tube, which was then sealed and bound to the stirrer shaft of the clean, dry reactor. Also in the drybox, a glass charger was prepared with cyclohexane (typically ~200 mL) and MMAO (350:1, mol Al:mol Fe). With the reactor under vacuum, the solution was then charged directly to the reactor. The

desired pressure of ethylene was introduced (~1000 psig), and the reactor stirrer was started, resulting in breakage of the NMR tube and catalyst activation. Ethylene was fed "on demand" using a TESCOM regulator, and the reactor temperature was maintained by an internal cooling coil with chilled water. Reactions were run for 30 mins before being terminated by slowly venting the reactor over a few minutes and placing the system under full cooling until atmospheric pressure and room temperature were obtained. Liquid products were sampled and analyzed by GC-FID utilizing added n-nonane as an internal standard.

5.2.2 Experimental Results

(PDD)Fe Experiments. With 3,5-xylyl phosphine and 2,6-xylyl aniline substitution, pre-catalyst **1a** was synthesized using standard reaction conditions initially reported by Small et al. (Scheme 5-2).[23,35-37] **1a** was readily activated with excess MMAO-3A to generate an active ethylene oligomerization catalyst. Catalyst performance results from 500 mL batch reactions are summarized in Table 5-1. At 50 °C, under 1000 psig of ethylene and 2.94 μmol of **1a**, production of 77 g of LAO product with a productivity of 26,200 g LAO/mmol of **1a** was observed. Activated **1a**, compared to previously reported (PDD)Fe catalysts, produced a relatively light weight distribution where 80-90% of the LAO products are in the C_4-C_{10} range. Interestingly, the K values (measured as $C_{n+2}/(C_{n+2}+C_n)$) for each carbon fraction between C_4-C_{20} increased from 0.44 for C_6/C_4 to 0.56 for C_{20}/C_{18} (Figure 5-1).

Scheme 5-2. General (PDD)Fe synthesis route previously reported by Small et al.

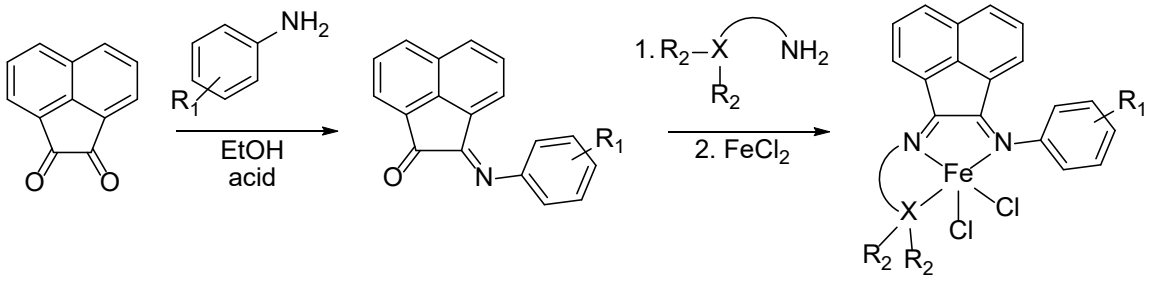

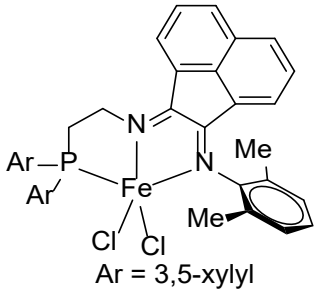

1a

CATALYST PERFORMANCE

Condition	Value/Result
Temp (°C)	50
Al:Fe (mol:mol)	350:1
Pressure (psig)	1000
Time (min)	30
Yield (g)	77.2
Productivity (g LAO/mmol Cat.)	26,200
K (C_{12}/C_{10})	0.469
C_6 Purity (wt% 1-ene)	99.47%
C_8 Purity (wt% 1-ene)	99.28%
C_{10} Purity (wt% 1-ene)	99.66%

Table 5-1. Performance results for pre-catalyst **1a**.

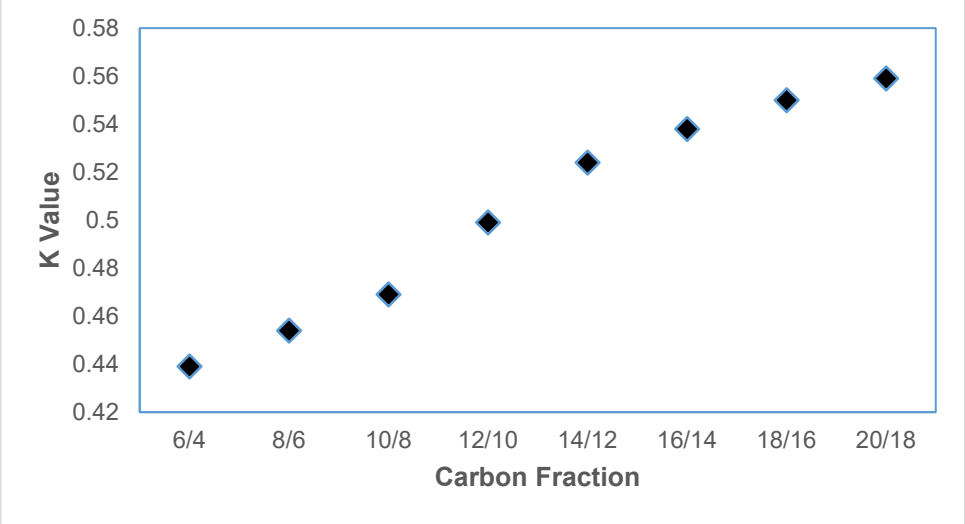

Figure 5-1. Plotted experimental K values for C_4-C_{20} ethylene oligomerization by activated pre-catalyst **1a**.

5.3 Computational Details

All DFT calculations were performed in Gaussian 09.[38] Geometry optimizations were carried out with unrestricted UM06-L/6-31G**(LANL2DZ for Fe).[39-43] Vibrational frequencies confirmed stationary points as either minima or transition-state structures. Intrinsic reaction coordinate (IRC) calculations verified connection between transition-state structures and minima on each spin-state surface. Final electronic energies were calculated using UM06-L/def2-TZVP.[44] All calculations were carried out using the SMD continuum model of cyclohexane to include the standard-state solvation free energy change

(ΔG_{solv}).[45] Reported enthalpies correspond to the sum of $E_{(SCF,large)} + \Delta E_{ZPE(small)} + \Delta U_{(small)} + nRT + \Delta G_{solv(large)}$ (Large = UM06-L/def2-TZVP; Small = UM06-L/6-31G**(LANL2DZ for Fe)). Reported Gibbs free energies also include $-T\Delta S_{(small)}$. $S_{(small)}$ values are comprised from translational, rotational, and vibrational component terms and were not scaled. B3LYP,[46] ωB97X-D,[47] and M06 functionals with the def2-TZVP basis set were also used for comparison to M06-L. It is important to note that predicting relative spin-state energies is not trivial.[48-55] Our choice to emphasize the M06-L functional is based on our previous experience and several other studies that show this is one of a few functionals that generally predict accurate spin-state energies for first-row transition metal complexes.[56-58] Nearly all previous computational examinations of (PBI)Fe complex characterization and ethylene oligomerization catalysis used the B3LYP functional. Therefore, a major challenge tackled here is determining if using the currently most accessible and most accurate functional for first-row transition metals, M06-L, with typical approximations, such as no spin-orbit coupling, it is possible to qualitatively and quantitatively model key features of ethylene oligomerization catalysis. However, Minaev and Sun in a recent review provided new calculations and suggested an important role of spin orbit coupling for (PBI)Fe^{II} catalyzed polymerization, but with the B3LYP functional.[59]

5.4 Catalyst Models

Scheme 5-1b indicates that for ethylene oligomerization by (PDD)$FeCl_2$ and (PBI)$FeCl_2$ pre-catalysts an MMAO activator is typically required. Presumably, MMAO activates these pre-catalysts by chloride abstraction followed by alkylation to form cationic Fe-CH_3 structures,[60-62] which are subsequently transformed to Fe-H or Fe-Et reactive structures, based on the observation that odd olefin oligomers are a very minor fraction of product from catalysis. While the exact nature of MAO and MMAO remains somewhat unclear, previous computational work showed that explicit inclusion of a MAO model did not significantly alter energies and structures for modeling ethylene oligomerization.[63]

Scheme 5-3 shows the (PDD)Fe and (PBI)Fe models used in this work. The structure **1b** provides a highly pruned PDD ligand structure where all ancillary portions of the ligand have been substituted with methyl groups, while structures **1c** and **1d** truncate the ligand at either the phosphine or imine aryl (Scheme 5-3a). One of the Brookhart/Gibson (PBI)$FeCl_2$ ethylene oligomerization pre-catalysts is shown as **2a** containing ortho substituted aryl groups (Scheme 5-3b). Structure **2b** provides a highly truncated model structure analogous to **1b**. Structure **2c** is a (PBI)Fe ethylene polymerization pre-catalyst that yields high molecular weight polyethylene.[10]

Scheme 5-3. a) (PDD)$FeCl_2$ pre-catalyst (1a) and truncated ligand models (1b-1d) for ethylene oligomerization. b) (PBI)$FeCl_2$ pre-catalyst (2a) and truncated ligand model (2b) for ethylene oligomerization, and (PBI)$FeCl_2$ pre-catalyst (2c) for ethylene polymerization.

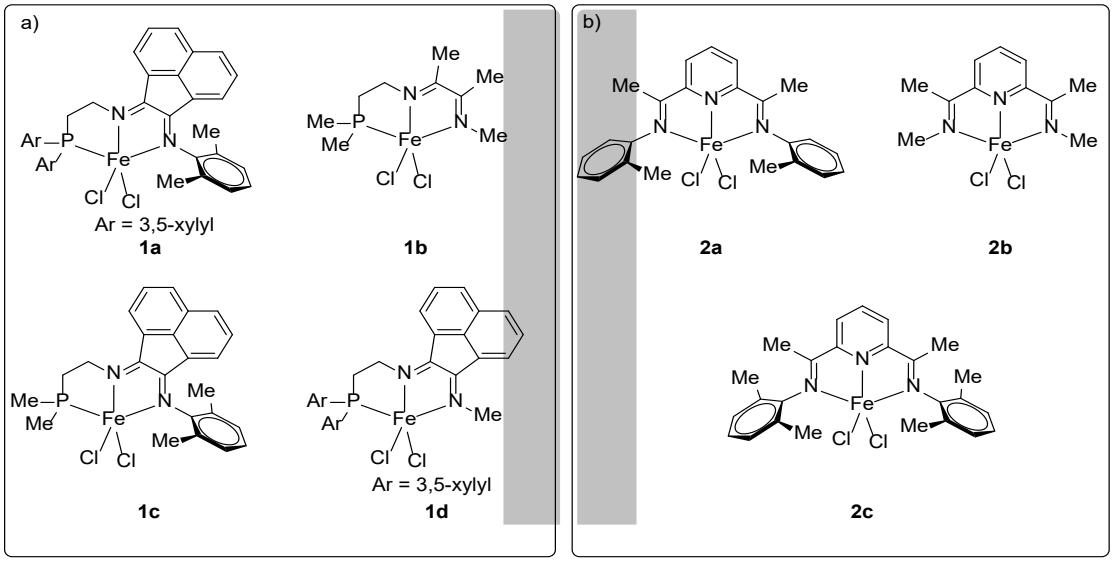

While the pre-catalysts shown in Scheme 5-3 have Fe^{II} formal oxidation state assignments, there is ambiguity whether under the complex activation conditions catalysis occurs with Fe^{II} or Fe^{III}.[64-68] In separate studies, Ziegler[29] as well as Musaev and Morokuma[32] used a computational Fe^{II} model for (PBI)Fe polymerization catalysis. Bryliakov et al.[66,67] and Scott et al.[19] also performed calculations with an Fe^{II} model. In contrast to these Fe^{II} models, de Bruin and Toro-Labbe emphasized an Fe^{III} computational model.[69,70] Experimentally, early studies supported active cationic Fe^{II}-alkyl and Fe^{II}-

hydride species,[64-66] and later EPR and NMR studies also suggested Fe^{II},[67] but there are Mössbauer and EPR measurements suggesting active Fe^{III} species.[68] Importantly, Chirik showed by synthesis of a cationic (PBI)Fe^{II}-alkyl species, and catalysis without MMAO activation, that Fe^{II} is competent for ethylene polymerization.[20] However, this does not rule out Fe^{III} intermediates or the possibility of both Fe^{II} and Fe^{III} active species under activated catalytic conditions. Therefore, in our efforts to explore a practical and useful DFT model, we examined both Fe^{II} and Fe^{III} structures, and all possible spin states, as computational models for polymerization branching, propagation/termination, and K values.

5.5 Catalytic Cycle and Summary of Previous Computational Studies

Quickly after the reports of Brookhart[10] and Gibson,[12,14] Ziegler reported DFT calculations that examined the bis-ortho aryl substituted $[(PBI)Fe^{II}(C_3H_7)]^+$ complex relevant to ethylene polymerization catalysis.[29] Ziegler used BP86 theory for a model ligand with aryl and methyl groups replaced with hydrogens, and BP86/Amber (QM/MM) for the complete ligand model. Metal-alkyl and ethylene π coordination structures were reported, along with transition states for ethylene migratory insertion, β-hydrogen transfer (βHT), and β-hydrogen elimination (βHE). Scheme 5-4 shows the most plausible oligomerization/polymerization catalytic cycle that emerged from this and subsequent DFT studies where βHT and βHE transition states result in LAO olefin formation. However, it is known that for the (PBI)Fe catalyst that the rate of termination, similar to propagation, is dependent on ethylene pressure, which may suggest which may suggest βHT is more viable than βHE.[10] Only the low-spin singlet energy surface was reported because the BP86 functional disfavored the quintet spin state by more than 15 kcal/mol. Based on this singlet-spin energy surface, a triplet-spin transition state for alkene coordination was reported where the dominant ethylene polymerization termination pathway was proposed to be by βHT not βHE. Also, it was proposed that the rates of chain propagation and chain transfer result from alkene coordination with the Fe-alkyl structure, and not ethylene migratory insertion.

Scheme 5-4. Catalytic cycle for tridentate diimine Fe catalyzed ethylene oligomerization.

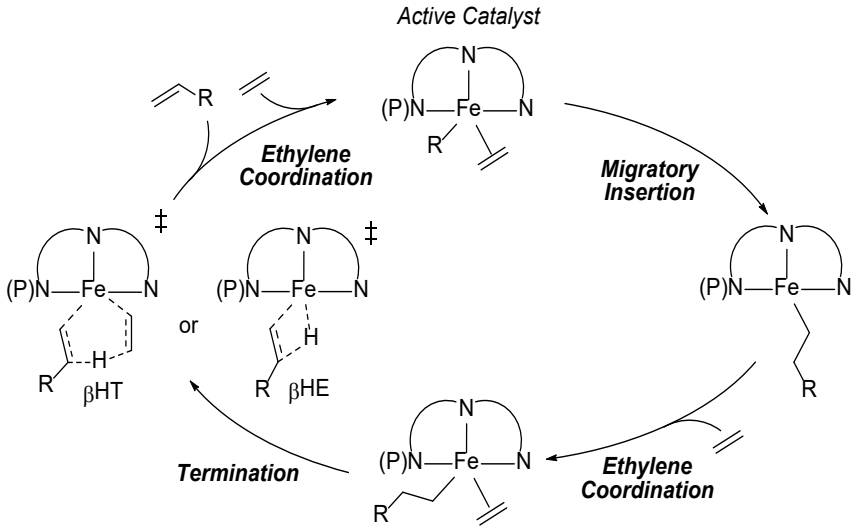

Two years after the report by Ziegler, Musaev reported calculated chain propagation and termination pathways with B3LYP DFT for a truncated ligand and B3LYP/MM3 (QM/MM) for the complete bis-ortho aryl substituted $[(PBI)Fe^{II}(C_3H_7)]^+$ structure.[32] Calculated structures for mono-ortho aryl substituted LAO catalysts were not reported. For the complete ligand system, it was reported that the ligand significantly destabilizes the entire singlet spin-state energy surface while triplet and quintet spin-state structures are less destabilized. The most stable $[(PBI)Fe^{II}(C_3H_7)]^+$ and $[(PBI)Fe^{II}(C_3H_7)(C_2H_4)]^+$ structures were identified to be on the quintet spin-state surface. The lowest energy transition states for chain propagation and termination via ethylene migratory insertion and βHT were located on the triplet spin-state energy surface with βHT more than 17 kcal/mol higher in energy than migratory insertion. Comparison of the complete ligand and truncated model calculations indicated that without ligand aryl groups, the free energies for ethylene migratory insertion and βHT transition state are highly competitive.

In 2009, de Bruin used B3LYP DFT to calculate mono-ortho aryl substituted $[(PBI)Fe^{II}(CH_3)]^+$ and $[(PBI)Fe^{III}(CH_3)]^{2+}$ structures and their ethylene coordination structures.[69] It was suggested that the Fe^{III}-dialkyl structures are unlikely to be catalytically viable. For $[(PBI)Fe^{II}(CH_3)]^+$, ethylene migratory insertion is proposed to occur on the quintet energy surface. For $[(PBI)Fe^{III}(CH_3)]^{+2}$, ethylene migratory insertion was lowest in energy for the quartet energy surface. However, the lowest energy βHT pathways

were identified on the low-spin energy surfaces (singlet and doublet). It was reported that for $[(PBI)Fe^{II}(CH_3)]^+$ the termination via the βHT transition state has a ~10 kcal/mol lower activation enthalpy than ethylene migratory insertion, and this was proposed as evidence against this oxidation state for oligomerization. In contrast, for $[(PBI)Fe^{III}(CH_3)]^{+2}$ there was a much lower migratory insertion barrier, and βHT has a 2.1 kcal/mol higher activation enthalpy than termination. However, it was not explored if $[(PBI)Fe^{III}(CH_3)]^{+2}$ is a kinetically viable intermediate arising from activation of the $(PBI)Fe^{II}Cl_2$ pre-catalyst. Later, de Bruin also used B3LYP to calculate structures for 1-butene oligomerization catalyzed by (PBI)Fe.[69] de Bruin has also calculated $(PBI)FeCl_2$ pre-catalyst structures using B3LYP, BHandHLYP, X3LYP, and other functionals.[71]

In a more recent computational analysis of the (PBI)Fe system, Cruz reverted to the BP86 functional to examine high-spin ethylene insertion and βHT transition states for $[(PBI)Fe^{II}(propyl)]^+$ and $[(PBI)Fe^{III}(propyl)]^{2+}$ structures,[70] despite Ziegler previously reporting that BP86 predicts significantly lower energy low-spin structures.[29] Interestingly, with this functional, Cruz showed that Fe^{II} and Fe^{III} transition states have a 4.3 and 2.8 kcal/mol difference between propagation and termination, which is consistent with reported polymer molecular weights, and therefore, the possibility that both Fe oxidation states are catalytically active was proposed.

5.5.1 (PDD)Fe-H and (PDD)Fe-Et Catalytic Intermediates

The two likely catalytic intermediates generated through activation of the $FeCl_2$ pre-catalyst are Fe-H or Fe-Et structures.[72-75] Figure 5-2a and 5-2b displays the singlet-spin M06-L molecular orbitals for $[(PDD)Fe^{II}\text{-}H]^+$ and $[(PBI)Fe^{II}\text{-}H]^+$. Overall, the orbitals for these Fe-H structures are qualitatively very similar. For both structures, the occupied orbitals are mostly metal centered while the unoccupied orbitals are ligand centered. The $[(PDD)Fe^{II}\text{-}H]^+$ has a slightly smaller HOMO-LUMO gap of 1.2 eV while the $[(PBI)Fe^{II}\text{-}H]^+$ has a gap of 1.3 eV. These small HOMO-LUMO gaps indicate a high-spin ground state. Similar to the dichloride pre-catalyst structure **1a** (see SI), the $[(PDD)Fe^{II}\text{-}H]^+$ structure has a quintet ground spin state, but it is only lower in energy than the triplet state by 0.6 kcal/mol. The quintet is 14.8

kcal/mol lower in energy than the singlet spin state. Consistent with the slightly larger HOMO-LUMO gap, $[(PBI)Fe^{II}\text{-}H]^{+}$ has a quintet structure that is 4.1 kcal/mol lower in energy than the triplet spin state and 14.0 kcal/mol lower in energy than the singlet spin state.[69]

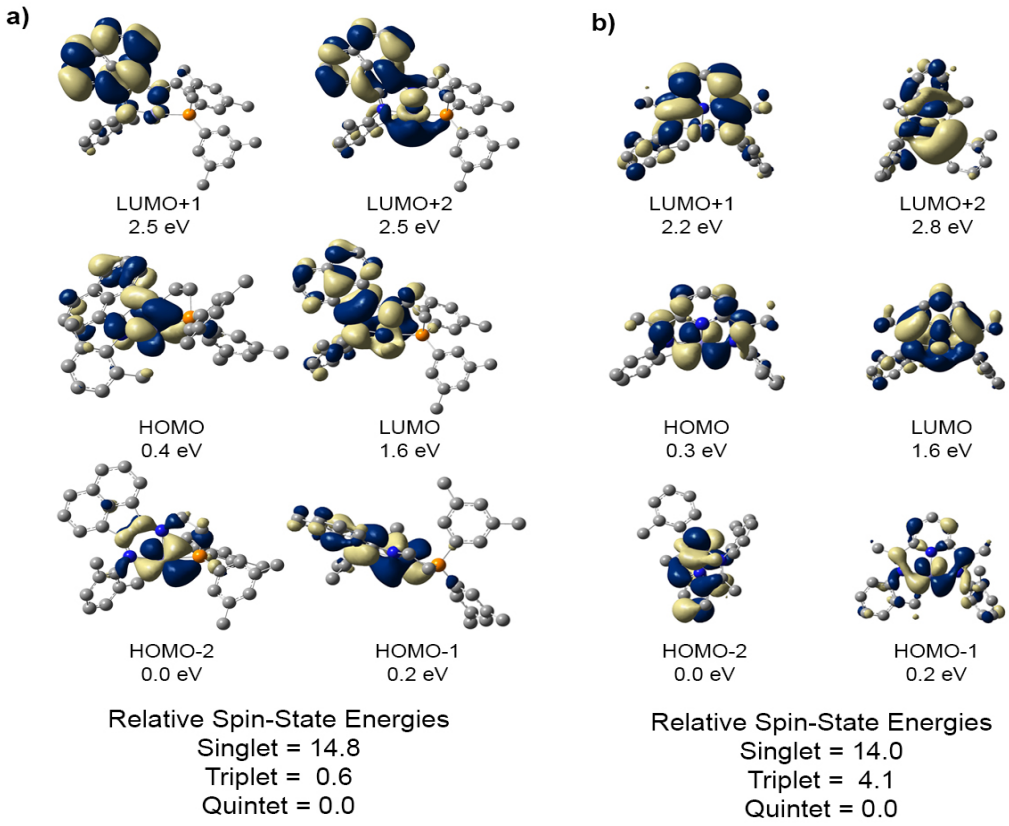

Figure 5-2. M06-L singlet molecular orbitals and spin state energies (S = singlet, T= triplet, Q = quintet) for a) (PDD)FeII-H and b) (PBI)FeII-H. Hydrogen atoms are omitted for clarity. Relative spin-state energies reported in kcal/mol.

Fe alkyl intermediates, $[(PDD)Fe^{II}\text{-}Et]^{+}$ that is generated after migratory insertion between the Fe-H and ethylene (see below), has a triplet ground state which is close in energy with the quintet. The $[(PDD)Fe^{II}\text{-}Et]^{+}$ quintet and singlet spin states are 3.0 and 18.5 kcal/mol higher in energy. The $[(PBI)Fe^{II}\text{-}Et]^{+}$ intermediate has a quintet ground state where the triplet and singlet spin states are 0.6 and 9.7 kcal/mol higher in energy. For $[(PDD)Fe^{III}\text{-}Et]^{+2}$, the ground state is a quartet spin state where the doublet and sextet are 14.1 and 7.5 kcal/mol higher in energy respectively. Similarly, the $[(PBI)Fe^{III}\text{-}Et]^{+2}$ is also a

quartet ground state where the doublet and sextet are 7.0 and 3.3 kcal/mol higher in energy. The prediction of high-spin ground states for these Fe-Et structures is consistent with the characterization of a paramagnetic (PBI)$Fe^{II}(CH_2SiMe_3)$ complex.[76]

5.5.2 Branching

As discussed in the introduction, one advantage of (PDD)Fe catalysts versus (PBI)Fe catalysts is the decreased amount of branched oligomers. There are several possible reasons for decreased LAO branching for (PDD)Fe catalysis. One reason could be decreased Fe-alkyl group chain walking to convert Fe(*n*-alkyl) structures to Fe(*iso*-alkyl) structures. However, we dismissed this reason because βHE barriers for (PDD)Fe(Bu) and (PBI)Fe(Bu) are very similar for both Fe^{II} and Fe^{III} (see SI). There is also a similar thermodynamic preference (0.2 kcal/mol) for linear Fe-alkyl groups over internal branched Fe-alkyl groups for both the (PDD)Fe(Bu) and (PBI)Fe(Bu) complexes. Instead, we propose that branching results from competitive regioselective migratory insertion of Fe-H structures with LAOs, such as 1-butene. In this scenario, an Fe(H)(C_2H_4) structure is in equilibrium with a Fe(H)(1-butene) structure, which can then react by either **TS(1,2)** or **TS(2,1)** (Scheme 5-5). **TS(1,2)** provides migratory insertion with a (1,2)-addition orientation where the Fe adds to the terminal end of 1-butene and leads to an Fe(*n*-butyl) structure that can continue oligomerization to generate a linear olefin (Scheme 5-5b). **TS(2,1)** provides migratory insertion with (2,1)-addition orientation where an Fe(*iso*-butyl) structure is generated (Scheme 5-5c). Further ethylene insertion with this structure generates a branched LAO.

Scheme 5-5. Potential pathways for reaction of Fe-H structures with a) ethylene, b) (1,2)-insertion with a LAO leading to a longer LAO, and c) (2,1)-insertion with a LAO leading to a branched α-olefin (AO).

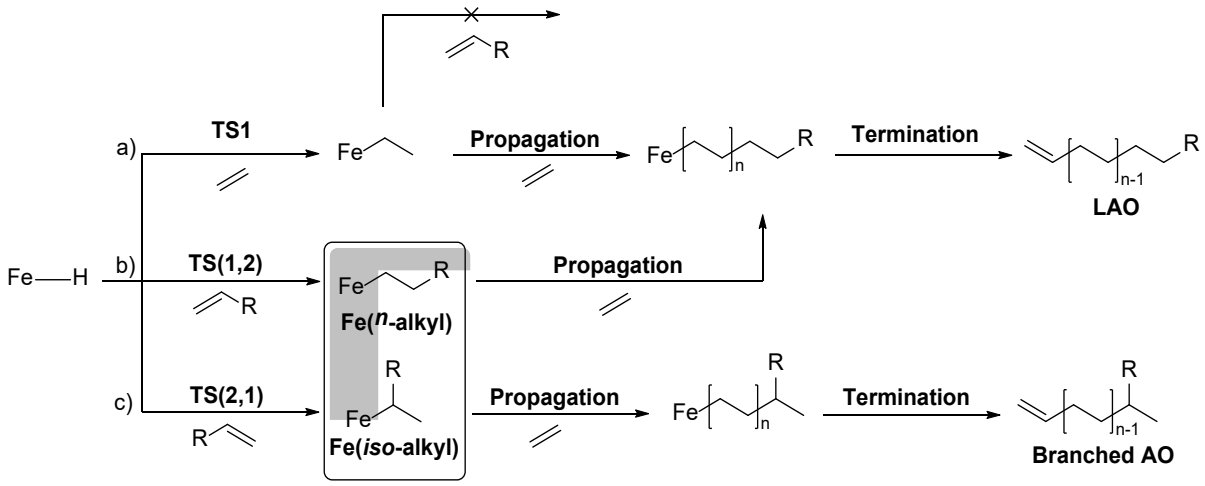

3D representations of **TS(1,2)** and **TS(2,1)** structures for $[(PDD)Fe^{II}(H)(1\text{-butene})]^{+}$ are shown in Figure 5-3, which show that in the **TS(2,1)** the ethyl group of 1-butene resides close to the diimine section of the PDD ligand. Table 5-2 reports and plots the calculated $\Delta\Delta H^{\ddagger}_{(\mathbf{TS(2,1)\text{-}TS(1,2)})}$ and $\Delta\Delta G^{\ddagger}_{(\mathbf{TS(2,1)\text{-}TS(1,2)})}$ values for $[(PDD)Fe^{II}(H)(1\text{-butene})]^{+}$, $[(PDD)Fe^{III}(H)(1\text{-butene})]^{+2}$, $[(PBI)Fe^{II}(H)(1\text{-butene})]^{+}$, $[(PBI)Fe^{III}(H)(1\text{-butene})]^{+2}$ with the complete and model ligands shown in Scheme 5-2. For the most highly truncated (PDD)Fe model **1b**, the negative $\Delta\Delta H^{\ddagger}$ and $\Delta\Delta G^{\ddagger}$ values for Fe^{II} and Fe^{III} complexes indicates a preference for (2,1)-addition leading to the Fe(*iso*-butyl) structure. Model ligand **1c** truncates only the phosphine ligand motif and **1d** truncates only the imine aryl ligand motif. For Fe^{II} and Fe^{III} **1c** and **1d** complexes, **TS(2,1)** is 1-2 kcal/mol lower than **TS4** (except for the Fe^{II} $\Delta\Delta H^{\ddagger}$ value of **1c**), which predicts preferred branching. Perhaps not unexpectedly, it is the interplay between both the phosphine and imine ligand motifs for **1a** that results in preference for forming the Fe(*n*-butyl) structures. Unexpectedly, the predicted linear/branching selectivity was very similar for both Fe^{II} and Fe^{III} models. The Fe^{II} and Fe^{III} $\Delta\Delta H^{\ddagger}$ values are 1.4 and 1.8 kcal/mol, and the $\Delta\Delta G^{\ddagger}$ values are 2.6 and 2.7 kcal/mol. These $\Delta\Delta G^{\ddagger}$ values translate to LAO selectivity of ~97% at 60 °C using transition-state theory, and only slightly underestimates the 99% selectivity reported in Scheme 5-2.

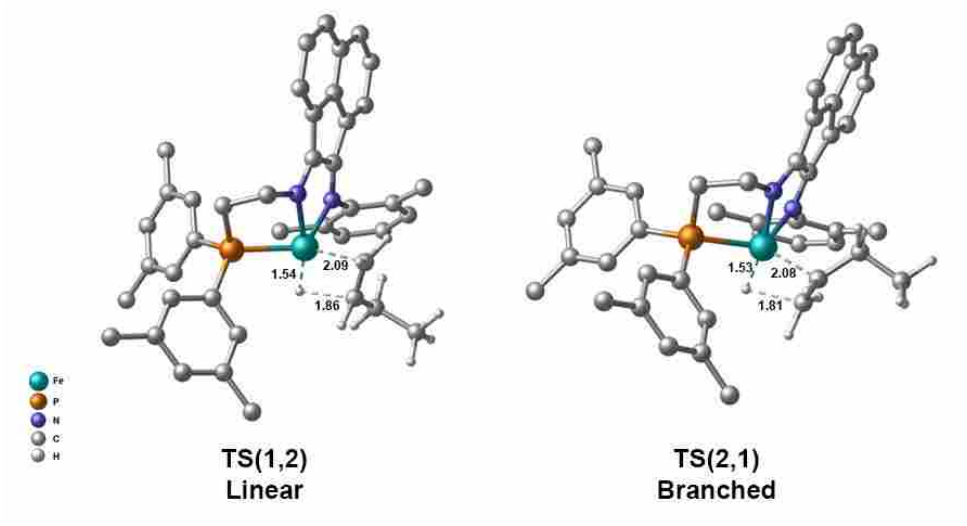

Figure 5-3. 3D representation of migratory insertion transition states that result in linear or branched LAO. Bond lengths reported in Å.

Pre-catalyst Model	Fe^{II} (spin state)	Fe^{III} (spin state)	Fe^{II} (spin state)	Fe^{III} (spin state)
	$\Delta\Delta H^{\ddagger}_{(TS(2,1)-TS(1,2))}$	$\Delta\Delta H^{\ddagger}_{(TS(2,1)-TS(1,2))}$	$\Delta\Delta G^{\ddagger}_{(TS(2,1)-TS(1,2))}$	$\Delta\Delta G^{\ddagger}_{(TS(2,1)-TS(1,2))}$
1a	1.2 (triplet)	1.8 (quartet)	2.6 (triplet)	2.7 (quartet)
1b	-1.7 (triplet)	-1.0 (quartet)	-0.8 (triplet)	-0.9 (quartet)
1c	0.4 (triplet)	-0.5 (quartet)	-1.3 (triplet)	-1.4 (quartet)
1d	-0.3 (triplet)	-1.1 (quartet)	-1.8 (triplet)	-2.7 (quartet)
2a	1.1 (quintet)	1.7 (quartet)	0.9 (quintet)	1.8 (quartet)
2b	0.9 (triplet)	0.4 (quartet)	-0.2 (triplet)	0.3 (quartet)

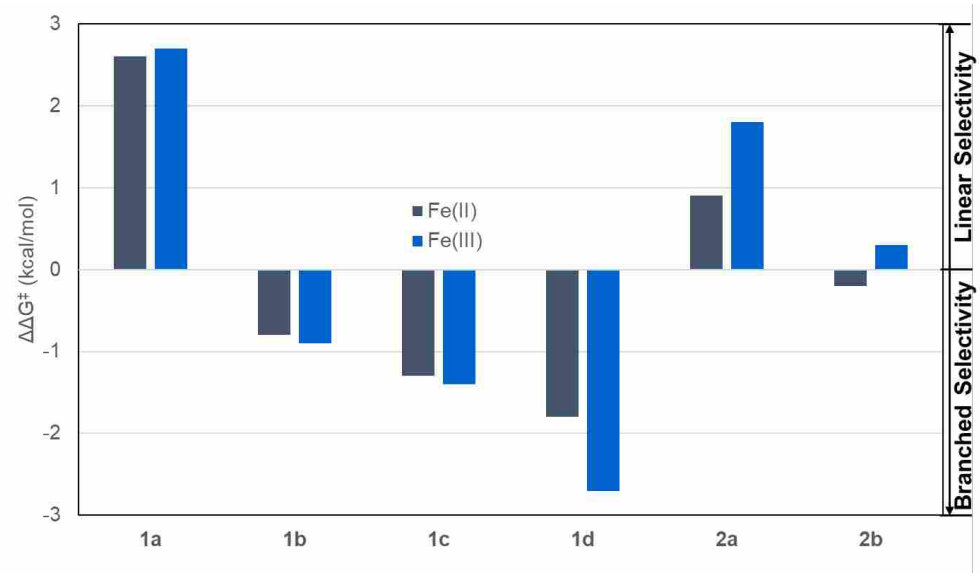

Table 5-2. Relative enthalpies and free energies for Fe(H)(1-butene) migratory insertion leading to linear and branched Fe-alkyl structures. (kcal/mol)

In comparison, for (PBI)Fe **2a**, our DFT calculations qualitatively replicate the reduced selectivity. The $\Delta\Delta H^{\ddagger}$ values for (PBI)Fe-H transition states derived from pre-catalyst **2a** are 0.1 kcal/mol lower, and again, the results are insensitive to using Fe^{II} or Fe^{III} as the model. The $\Delta\Delta G^{\ddagger}$ values at 0.9 and 1.8 kcal/mol are ~1-2 kcal/mol smaller than the (PDD)Fe values. Overall, both enthalpy and free energies are consistent with the decreased branching that occurs during (PDD)Fe catalysis compared with (PBI)Fe catalysis, and suggests that future designed (PDD)Fe catalysts can be evaluated for their linear/branching selectivity using this DFT protocol.

5.5.3 Fe-H and Fe-Et Coordination and Migratory Insertion with Ethylene

Because of the very close spin state energies for Fe-H and Fe-Et structures, we examined ethylene oligomerization transition states and intermediates for all possible spin states to identify the lowest energy pathways, which involve spin-state crossover.[77-80] As generally outlined in the Scheme 5-4 catalytic cycle, beginning with an Fe(H)(C_2H_4) coordination intermediate **A**, ethylene undergoes migratory insertion via **TS1** and results in an Fe-Et intermediate that can coordinate ethylene forming **B** (Scheme 5-6). For Fe(Et)(C_2H_4), a second migratory insertion for an oligomerization propagation step via **TS2** and ethylene coordination gives the Fe(Bu)(C_2H_4) intermediate **C**. Continued chain elongation can occur by **TS3**. Several prior computational studies discussed in a previous section indicate that Fe-catalyzed ethylene polymerization involves termination by one of two possible transition states. For example, from the Fe(Bu)(C_2H_4) intermediate, loss of ethylene followed by βHE via **TS4**, which is identical to **TS(1,2)**, reforms an Fe-H intermediate and a LAO, in this case 1-butene. Alternatively, there is the possibility of βHT by **TS5**, which is a transition state that merges βHE and migratory insertion to provide a one-step pathway to directly give an Fe-Et intermediate and a LAO.

Scheme 5-6. Outline of ethylene oligomerization mechanism illustrating general propagation and termination pathways.

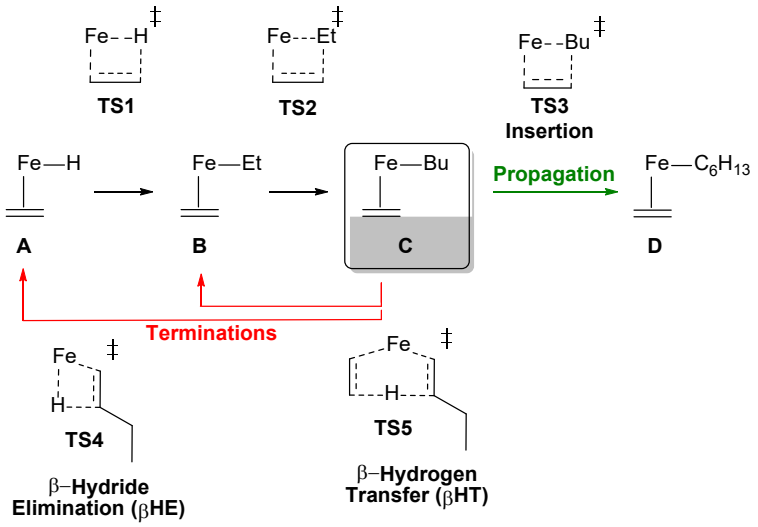

Schemes 5-7a and 5-7b show the enthalpy landscapes for $[(PDD)Fe^{II}\text{-}H]^+$ and $[(PDD)Fe^{III}\text{-}H]^{+2}$ coordination and migratory insertion with ethylene to give the $[(PDD)Fe(Bu)(C_2H_4)]$ structures, and then diverging pathways for propagation and termination. Schemes 5-8a and 5-8b show the Gibbs free energy landscapes for the same catalytic steps. On the enthalpy surface, while the $[(PDD)Fe^{II}\text{-}H]^+$ structure has a high-spin quintet ground state, the corresponding ethylene coordination structure ($[(PDD)Fe^{II}(H)(C_2H_4)]^+$) and **TS1** structures are lowest on the singlet surface. The triplet surface is very close in energy compared to the singlet surface, and on the free energy surface triplet $[(PDD)Fe^{II}(H)(C_2H_4)]^+$ and **TS1** are the lowest energy pathway to $[(PDD)Fe^{II}(Et)]^+$. **TS1** for ethylene insertion with the $[(PDD)Fe^{II}(H)(C_2H_4)]^+$ structure has a $\Delta H^{\ddagger}$ of only 1.7 kcal/mol relative to this ethylene complex, and subsequent spin crossover leads to the triplet $[(PDD)Fe^{II}\text{-}Et]^+$ structure, which is exothermic by 17.8 kcal/mol. The low barrier for Fe-H ethylene migratory insertion is similar to the previously reported BP86 barrier for $[(PBI)Fe^{II}(H)(C_2H_4)]^+$. A second ethylene coordination to give $[(PDD)Fe^{II}(Et)(C_2H_4)]^+$ leads to a high-spin migratory insertion **TS2** with a larger $\Delta H^{\ddagger}$ value of 13.4 kcal/mol, relative to $[(PDD)Fe^{II}(Et)(C_2H_4)]^+$.[81] Again, the spin-state surfaces are very close in energy, and the singlet **TS2** is ~1 kcal/mol higher in energy. The conversion of this second ethylene π-bond to a σ-

bond results in $[(PDD)Fe^{II}(Bu)]^+$ and $[(PDD)Fe^{II}(Bu)(C_2H_4)]^+$ that are 41.2 and 49.9 kcal/mol exothermic relative to $[(PDD)Fe^{II}(H)(C_2H_4)]^+$.

Scheme 5-7. Ethylene oligomerization enthalpy (ΔH) landscapes for the lowest energy spin state pathways for a) $(PDD)Fe^{II}$ and b) $(PDD)Fe^{III}$. (kcal/mol)

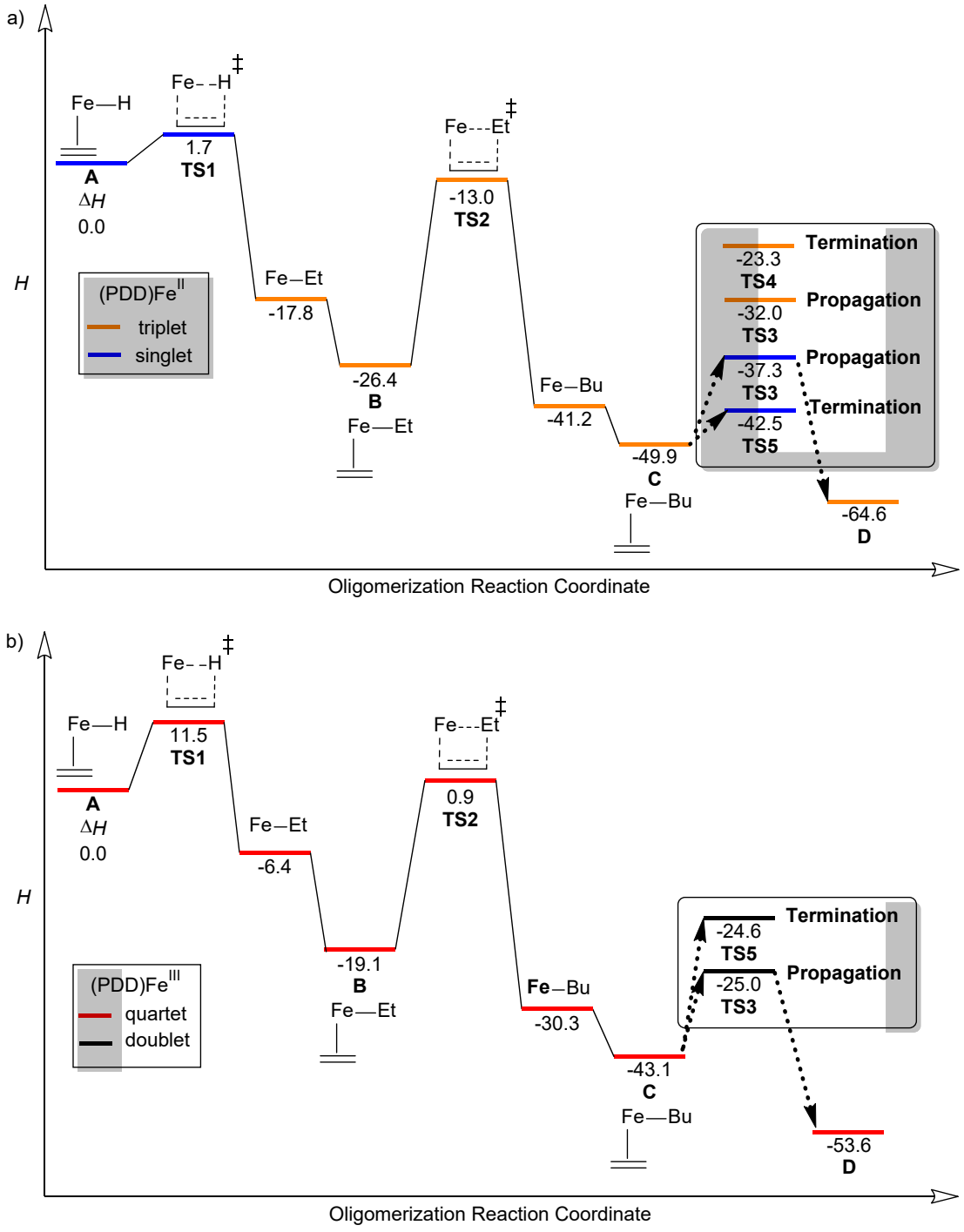

Scheme 5-8. Ethylene oligomerization Gibbs free energy (ΔG) landscapes for the lowest energy spin state pathways for a) (PDD)Fe^{II} and b) (PDD)Fe^{III}. (kcal/mol)

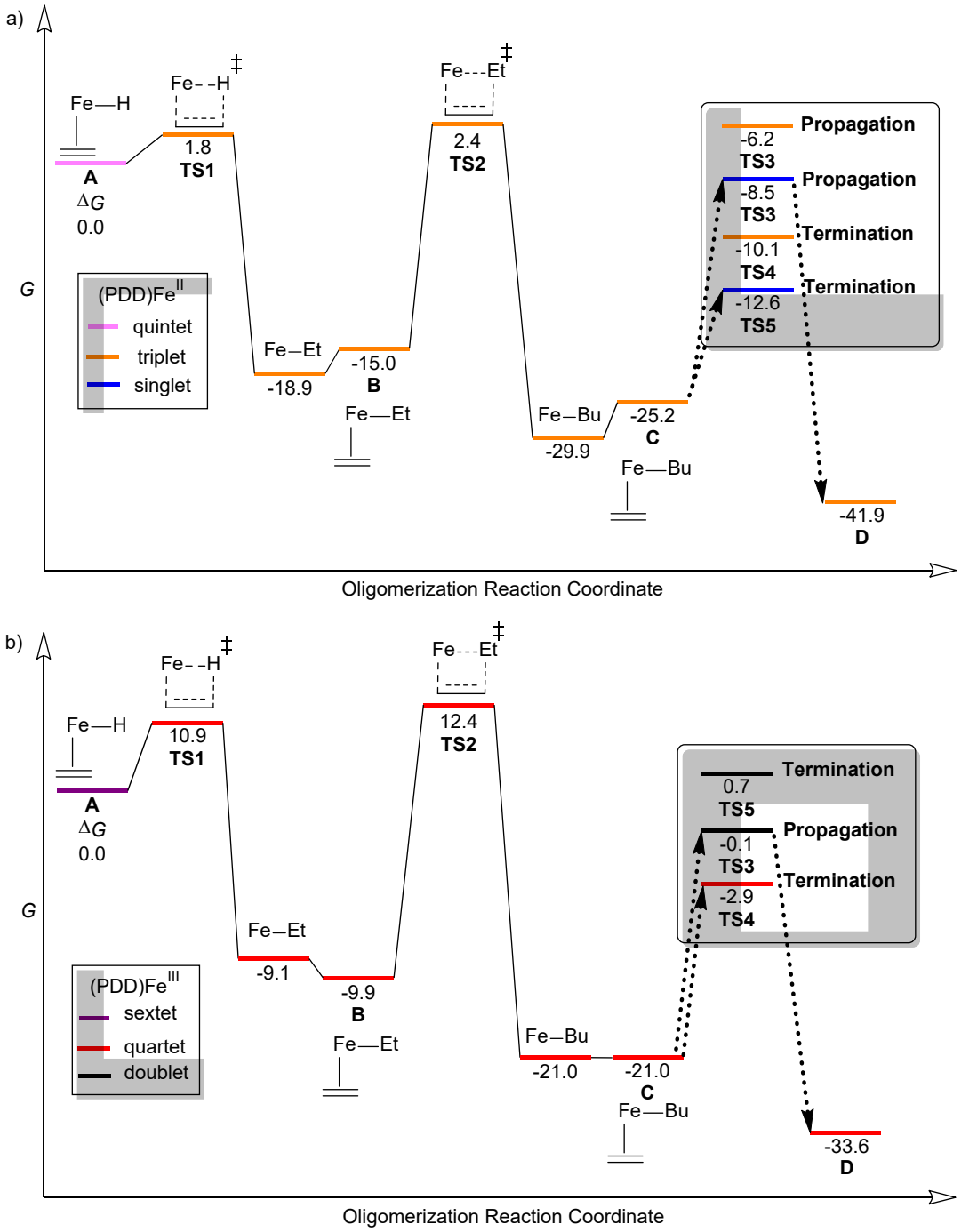

On the enthalpy surface for [(PDD)Fe^{III}-H]$^{+2}$, the lowest energy route to [(PDD)Fe^{III}(Bu)(C_2H_4)]$^{+2}$ is on the high-spin quartet surface with no spin crossover. **TS1** that leads to [(PDD)Fe^{III}(Et)]$^{+2}$ has a $\Delta H^{\ddagger}$ of 11.5 kcal/mol relative to [(PDD)Fe^{III}(H)(C_2H_4)]$^{+2}$. Related high-spin state diketiminate Fe-H alkene

migratory insertion transition states have been reported by Cundari and Holland.[73] This ~10 kcal/mol larger Fe^{III} **TS1** compared to Fe^{II} results from a more stabilized Fe^{III} ethylene complex. Because of the more stabilized ethylene coordination to $[(PDD)Fe^{III}\text{-}H]^{+2}$, after **TS1** $[(PDD)Fe^{III}\text{-}Et]^{+2}$ and $[(PDD)Fe^{III}\text{-}Et]^{+2}$ structures are ~10 kcal/mol less exothermic compared to the similar Fe^{II} structures. Migratory insertion **TS2** has $\Delta H^{\ddagger}$ of 18.2 kcal/mol relative to $[(PDD)Fe^{III}(Et)(C_2H_4)]^{+2}$. We were surprised that the Fe^{II} complex has an ~5 kcal/mol lower barrier than the Fe^{III} complex because previously calculated B3LYP barriers showed Fe^{II} alkyl structures to have ~10 kcal/mol higher activation enthalpies than Fe^{III} alkyl structures.[33,69] On the free energy surfaces, the **TS2** $\Delta G^{\ddagger}$ barriers for Fe^{II} and Fe^{III} are 17.4 and 22.3 kcal/mol.

5.5.4 Propagation and Termination Steps

Figure 5-1 reported the oligomerization C_6/C_4 K value of 0.44, and showed that it increased to 0.56 at C_{20}/C_{18}. The K values are measured as ratios using eq. 1, and can be approximated by the kinetic ratio of propagation versus the sum of propagation and termination (eq. 2) from an Fe-alkyl intermediate. This concentration independent approximate equation can be used since both propagation and termination are known to both dependent on ethylene pressure.[10] Assuming the rates of k_{C6} and k_{C4} are dominated by one propagation and one termination transition state, this corresponds to $\Delta\Delta G^{\ddagger}_{(C6\text{-}C4)}$ of 0.49 kcal/mol, which can be calculated by setting $\Delta G^{\ddagger}_{prop}$ to zero and reduce eq. 3 to the selectivity equation eq. 4. The larger K value for longer oligomer lengths corresponds to a larger $\Delta\Delta G^{\ddagger}_{(C20\text{-}C18)}$ of 0.75 kcal/mol. The K values reported for the (PBI)Fe **3a** between 0.7 and 0.8 correspond to a $\Delta\Delta G^{\ddagger}$ value, usually measured for C_{12}/C_{10}, of ~1.3 kcal/mol.

$$\mathrm{K} = \frac{C_nH_{2n}}{C_nH_{2n} + C_{n-2}H_{2n-4}} \quad (eq\ 5-1.)$$

$$\mathrm{K} = \frac{k_{prop}}{k_{prop} + k_{term}} \quad (eq. 5-2)$$

$$\mathrm{K} = \frac{\exp\left(\frac{-\Delta G^{\ddagger}_{prop}}{RT}\right)}{\exp\left(\frac{-\Delta G^{\ddagger}_{prop}}{RT}\right) + \exp\left(\frac{-\Delta G^{\ddagger}_{term}}{RT}\right)} \quad (eq\ 5-3.)$$

$$\mathrm{K} = \frac{\exp\left(\frac{-\Delta G^{\ddagger}_{prop-term}}{RT}\right) - 1}{\exp\left(\frac{-\Delta G^{\ddagger}_{prop-term}}{RT}\right) + 1} \quad (eq\ 5-4.)$$

The previous computational studies examining (PBI)Fe catalysis using older popular density functionals, such as BP86 and B3LYP, either analyzed a single, potentially non-ground spin state (based on DFT) and likely fortuitously found a small energy difference between propagation and termination transition states or reported very large $\Delta\Delta G^{\ddagger}$ values. For example, de Bruin used B3LYP to estimate the $\Delta\Delta G^{\ddagger}$ between migratory insertion and βHT transition states for seven aryl-substituted (PBI)Fe catalysts.[33] The energy difference was only calculated for transition states with (PBI)Fe(Et)(C_2H_4) despite the experimental K values measured for C_{12}/C_{14} oligomer fractions. For the catalyst derived from pre-catalyst **2a**, the $\Delta\Delta G^{\ddagger}$ was reported to be 10.8 kcal/mol favoring migratory insertion. Presumably, because this and the other $\Delta\Delta G^{\ddagger}$ values are too large, de Bruin used linear correlation with the natural log of experimental K values. Therefore, we wondered whether it was possible for DFT, specifically M06-L with the typical approximations, to qualitatively and quantitatively predict the relative rates of propagation versus termination for (PDD)Fe.

Schemes 5-7 and 5-8 outlined the (PDD)Fe^{II} and (PDD)Fe^{III} energy landscapes for propagation to the Fe-(*n*-hexyl) structure. At the Fe-Bu intermediate **C** there is the possibility for competition between continued oligomer elongation by **TS3** and termination by βHE/**TS4** or βHT/**TS5** (see Scheme 5-6). Different than modeling oligomer branching selectivity, and unfortunately, quantitative and even qualitative evaluation of propagation/termination selectivity is dependent on the Fe oxidation state, spin state, and choice of enthalpy or free energy. This means that significant caution should be taken in interpreting and using a standard DFT model.

We initially assumed that analysis of (PDD)Fe^{II} energy surfaces would be the most straightforward to model propagation/termination selectivity. However, inspection of the enthalpy surface for $[(PDD)Fe^{II}(Bu)(C_2H_4)]^+$ revealed that the lowest energy propagation and termination transition states are on the singlet spin state surface and the βHT termination transition state **TS5** is more than 5 kcal/mol lower in enthalpy than the propagation migratory insertion transition state **TS3**, which is inconsistent with a K value between 0 and 1. Realizing that the M06-L Fe^{II} singlet spin transition-state enthalpies did not model propagation/termination, we also examined ωB97X-D, M06, and B3LYP functionals, which similarly showed too low of enthalpy for the singlet termination transition state (see SI). We then explored if inclusion of entropy on the free energy surface would model competitive propagation and termination transition states. But again, inspection of Scheme 5-8a shows that on the Gibbs free energy surface termination by both **TS4** and **TS5** are lower in energy than **TS3**. This indicates that using the low-spin Fe^{II} transition states does not provide a model for propagation/termination selectivity.

Interestingly, consideration of the higher energy route by the triplet-spin enthalpy surface without spin crossover for $[(PDD)Fe^{II}(Bu)(C_2H_4)]^+$ shows that propagation **TS3** is lower in enthalpy than termination **TS4**. However, with a difference of ~9 kcal/mol this would not be quantitatively consistent with the K value. Also, termination with **TS4** is inconsistent with the known ethylene pressure dependency for (PBI)Fe catalysts.[10] This could suggest that M06-L, and the broadly applicable functionals ωB97X-D and M06 over stabilize the singlet transition states.

With no satisfactory (PDD)Fe^{II} model for propagation and termination, we then examined the enthalpy surface for $[(PDD)Fe^{III}(Bu)(C_2H_4)]^{+2}$ (Scheme 5-7b). This surface predicts **TS3** to be lower in enthalpy than **TS4** and **TS5**. The $\Delta\Delta H^{\ddagger}_{(\mathbf{TS5}\text{-}\mathbf{TS3})}$ is 0.4 kcal/mol, which provides a K value of 0.33 that is relatively close to the experimental value of 0.44. We also calculated the transition-state enthalpies at 60 °C, but this changed the predicted values by less than 0.1 kcal/mol. This positive correlation with experiment should be interpreted cautiously because there is a lack of definitive experimental and computational evidence for (or against) an active Fe^{III} oxidation state. However, this oxidation state may

computationally be providing a more useful model than Fe^{II} because of the different orbital electron occupation (see Figure 5-2). More caution should also be taken about using the Fe^{III} oxidation state because similar to the Fe^{II} free energy surface, the lowest energy Fe^{III} propagation and termination transition states on the free energy surface incorrectly suggest termination is favored by ~3 kcal/mol (quartet **TS4** and doublet **TS3**).

With the (PDD)Fe^{III} enthalpy surface providing the only potentially reasonable estimate of the K value for C_6/C_4, we explored if this model could be useful predicting K values with larger Fe-alkyl groups. Therefore, we calculated $\Delta\Delta H^{\ddagger}_{(\mathbf{TS5\text{-}TS3})}$ for $[(PDD)Fe^{III}(C_8H_{17})(C_2H_4)]^{+2}$ and $[(PDD)Fe^{III}(C_{10}H_{21})(C_2H_4)]^{+2}$. The calculated K values for C_{10}/C_8 and C_{12}/C_{10} are 0.77, which is an overestimate, but is consistent with the increase as the LAO carbon length increases. However, caution is warranted since the C_8/C_6 value for $[(PDD)Fe^{III}(C_6H_{13})(C_2H_4)]^{+2}$ does not fit the experimental trend with a calculated value of 0.14. As expected, the use of $\Delta\Delta G^{\ddagger}$ values to estimate the change in K values is problematic (see SI).

We also examined propagation and termination transition states for $[(PBI)Fe^{II}(Bu)(C_2H_4)]^{+}$ and $[(PBI)Fe^{III}(Bu)(C_2H_4)]^{+2}$ (see energy landscapes in the SI). For $[(PBI)Fe^{II}(Bu)(C_2H_4)]^{+}$, similar to $[(PDD)Fe^{II}(Bu)(C_2H_4)]^{+}$, on the enthalpy surface **TS5** is ~5 kcal/mol lower in energy than **TS3**. For $[(PBI)Fe^{III}(Bu)(C_2H_4)]^{+2}$, M06-L predicts competitive propagation and termination transition states with a difference of -1.6 kcal/mol and predicts **TS5** to be lower than **TS3**. On the free energy surface, **TS3** is lower than **TS5** with a $\Delta\Delta G^{\ddagger}_{(\mathbf{TS5\text{-}TS3})}$ value of 0.2 kcal/mol. Previously, de Bruin reported a $\Delta\Delta H^{\ddagger}_{(\mathbf{TS5\text{-}TS3})}$ of 2.1 kcal/mol for $[(PBI)Fe^{III}(Me)(C_2H_4)]^{+2}$ using the B3LYP functional. For $(PBI)Fe^{III}$, neither the $\Delta\Delta H^{\ddagger}_{(\mathbf{TS5\text{-}TS3})}$ or $\Delta\Delta G^{\ddagger}_{(\mathbf{TS5\text{-}TS3})}$ values predict the generally expected increase in K value for larger oligomer lengths (see SI).

For the $(PBI)FeCl_2$ pre-catalyst **2c**, the bis-ortho aryl substituted complexes produce polyethylene while mono-ortho aryl substituted complexes produce LAOs. Despite the multiple previous computational studies on the polymerization catalysts, there has been no DFT comparison of relative transition-state energies for elongation versus termination comparing catalytic structures of **2a** versus **2c**. Therefore, we

calculated **TS3**, **TS4**, and **TS5** for the bis-ortho aryl substituted complexes $[(PBI)Fe^{II}(Bu)(C_2H_4)]^+$ and $[(PBI)Fe^{III}(Bu)(C_2H_4)]^{+2}$ (see SI). For Fe^{II}, on both the enthalpy and free energy surfaces termination is favored over propagation. In contrast, for Fe^{III}, the $\Delta\Delta H^{\ddagger}_{(\mathbf{TS5}\text{-}\mathbf{TS3})}$ value is 6.5 kcal/mol, which is an 8.1 kcal/mol shift in transition state energies, and clearly shows a K value approaching 0.9 consistent with polyethylene formation.

5.6 Conclusions

We first showed that ethylene oligomerization catalysis by the activated (PDD)Fe pre-catalyst **1a** provides very high olefin oligomer purity without branching and K values of LAO fractions that increase with progressively longer chain lengths. Extrapolation gave a C_6/C_4 K value of 0.44 and at C_{20}/C_{18} a value of 0.56. We then showed that M06-L DFT calculations can be used to successfully model the very high oligomerization purity resulting from competitive 1,2-addition versus 2,1-addition. Despite several previous computational reports on propagation versus termination for (PBI)Fe catalysis, we found modeling propagation/termination and K values for (PDD)Fe catalysis significantly more challenging. In contrast to modeling oligomer branching selectivity, and unfortunately, quantitative and even qualitative evaluation of propagation/termination selectivity was dependent on the Fe oxidation state, spin state, and choice of enthalpy or free energy, and therefore caution is advised. The only potentially useful model was identified by using Fe^{III} propagation and termination transition-state enthalpies. However, caution is warranted since there has been no synthesis of a dicationic Fe^{III}-alkyl or hydride, with either PDD or PBI ligands, demonstrating ethylene oligomerization catalysis.

5.7 References

1. Green, M. M.; Wittcoff, H. A. *Organic Chemistry Principles and Industrial Practice,* Wiley-VCH Verlag GmbH & Co., 2003.

2. Weissermel, K.; Arpe, H.-J. *Industrial Organic Chemistry,* Chapter 3, 5th ed. Wiley-VCH Verlag GmbH & Co., 2010.

3. Keim, W.; Kowaldt, F. H.; Goddard, R.; Krüger, C. Novel Coordination of (Benzoylmethylene)triphenylphosphorane in a Nickel Oligomerization Catalyst. *Angew. Chem. Int. Ed.* **1978**, *17*, 466-467.

4. Peuckert, M.; Keim, W. A New Nickel Complex for the Oligomerization of Ethylene. *Organometallics* **1983**, *2*, 594-597.

5. Keim, W. Nickel: An Element with Wide Application in Industrial Homogeneous Catalysis. *Angew. Chem. Int. Ed.* **1990**, *29*, 235-244.

6. Keim, W. Oligomerization of Ethylene to α-Olefins: Discovery and Development of the Shell Higher Olefin Process (SHOP). *Angew. Chem. Int. Ed.* **2013**, *52*, 12492-12496.

7. Shiraki, Y.; Tamura, T. Production of Linear Alpha-Olefins. US Patent 4886933, 1989.

8. Tanaka, S.; Shiraki, Y.; Tamura, T.; Kuramoto, M.; Sato, H.; Watanabe, M. Catalysts for α-Olefin Production and Processes for Producing α-Olefin. US Patent 6555633, 2003.

9. Aliyev, V.; Mosa, F.; Al-Hazmi, M. Catalyst Composition for Oligomerization of Ethylene Oligomerization Process and Method for its Preparation. US Patent 8481444, 2013.

10. Small, B. L.; Brookhart, M. Iron-Based Catalysts with Exceptionally High Activities and Selectivities for Oligomerization of Ethylene to Linear α-Olefins. *J. Am. Chem. Soc.* **1998**, *120*, 7143-7144.

11. For polyethylene catalysis see: Small, B. L.; Brookhart, M.; Bennett, A. M. A. Highly Active Iron and Cobalt Catalysts for the Polymerization of Ethylene. *J. Am. Chem. Soc.* **1998**, *120*, 4049-4050.

12. Britovsek, G. P.; Gibson, V.; McTavish, S.; Solan, G.; White, A. P.; Williams, D.; Kimberley, B.; Maddox, P. Novel Olefin Polymerization Catalysts Based on Iron and Cobalt. *Chem. Commun.* **1998**, 849-850.

13. Small, B. L.; Brookhart, M. Polymerization of Propylene by a New Generation of Iron Catalysts: Mechanisms of Chain Initiation, Propagation, and Termination. *Macromolecules* **1999**, *32*, 2120-2130.

14.Britovsek, G. J. P.; Bruce, M.; Gibson, V. C.; Kimberley, B. S.; Maddox, P. J.; Mastroianni, S.; McTavish, S. J.; Redshaw, C.; Solan, G. A.; Strömberg, S.; White, A. J. P.; Williams, D. J. Iron and Cobalt Ethylene Polymerization Catalysts Bearing 2,6-Bis(Imino)Pyridyl Ligands: Synthesis, Structures, and Polymerization Studies. *J. Am. Chem. Soc.* **1999**, *121*, 8728-8740.

15. Sun, W.-H.; Hao, P.; Zhang, S.; Shi, Q.; Zuo, W.; Tang, X.; Lu, X. Iron(II) and Cobalt(II) 2-(Benzimidazolyl)-6-(1-(arylimino)ethyl)pyridyl Complexes as Catalysts for Ethylene Oligomerization and Polymerization. *Organometallics* **2007**, *26*, 2720-2734.

16. Small, B. L.; Marcucci, A. J. Iron Catalysts for the Head-to-Head Dimerization of α-Olefins and Mechanistic Implications for the Production of Linear α-Olefins. *Organometallics* **2001**, *20*, 5738-5744.

17. Gibson, V. C.; Spitzmesser, S. K. Advances in Non-Metallocene Olefin Polymerization Catalysis. *Chem. Rev.* **2003**, *103*, 283-316.

18. Small, B. L.; Schmidt, R. Comparative Dimerization of 1-Butene with a Variety of Metal Catalysts, and the Investigation of a New Catalyst for C-H Bond Activation. *Chem. Eur. J.* **2004**, *10*, 1014-1020.

19. Scott, J.; Gambarotta, S.; Korobkov, I.; Budzelaar, P. H. M. Metal versus Ligand Alkylation in the Reactivity of the (Bis-iminopyridinato)Fe Catalyst. *J. Am. Chem. Soc.* **2005**, *127*, 13019-13029.

20. Bouwkamp, M. W.; Lobkovsky, E.; Chirik, P. J. Bis(imino)pyridine Iron(II) Alkyl Cations for Olefin Polymerization. *J. Am. Chem. Soc.* **2005**, *127*, 9660-9661.

21. Bianchini, C.; Giambastiani, G.; Rios, I. G.; Mantovani, G.; Meli, A.; Segarra, A. M. Ethylene Oligomerization, Homopolymerization and Copolymerization by Iron and Cobalt Catalysts with 2,6-(bis-organylimino)pyridyl Ligands. *Coord. Chem. Rev.* **2006**, *250*, 1391-1418.

22. Gibson, V. C.; Redshaw, C.; Solan, G. A. Bis(imino)pyridines: Surprisingly Reactive Ligands and a Gateway to New Families of Catalysts. *Chem. Rev.* **2007**, *107*, 1745-1776.

23. Small, B. L.; Rios, R.; Fernandez, E. R.; Carney, M. J. Oligomerization of Ethylene Using New Iron Catalysts Bearing Pendant Donor Modified α-Diimine Ligands. *Organometallics* **2007**, *26*, 1744-1749.

24. Small, B. L.; Rios, R.; Fernandez, E. R.; Gerlach, D. L.; Halfen, J. A.; Carney, M. J. Oligomerization of Ethylene Using New Tridentate Iron Catalysts Bearing α-Diimine Ligands with Pendant S and P Donors. *Organometallics* **2010**, *29*, 6723-6731.

25. Bianchini, C.; Giambastiani, G.; Luconi, L.; Meli, A. Olefin Oligomerization, Homopolymerization and Copolymerization by Late Transition Metals Supported by (imino)pyridine Ligands. *Coord. Chem. Rev.* **2010**, *254*, 431-455.

26. Zhang, W.; Sun, W.-H.; Redshaw, C. Tailoring Iron Complexes for Ethylene Oligomerization and/or Polymerization. *Dalton Trans.* **2013,** *42*, 8988-8997.

27. Small, B. L. Discovery and Development of Pyridine-bis(imine) and Related Catalysts for Olefin Polymerization and Oligomerization. *Acc. Chem. Res* **2015**, *48*, 2599-2611.

28. Schaefer, B. A.; Margulieux, G. W.; Tiedemann, M. a.; Small, B. L.; Chirik, P. J. Synthesis and Electronic Structure of Iron Borate Betaine Complexes as a Route to Single-Component Iron Ethylene Oligomerization and Polymerization Catalysts. *Organometallics* **2015**, *34*, 5615-5623.

29. Deng, L.; Margl, P.; Ziegler, T. Mechanistic Aspects of Ethylene Polymerization by Iron(II)−Bisimine Pyridine Catalysts: A Combined Density Functional Theory and Molecular Mechanics Study. *J. Am. Chem. Soc.* **1999**, *121*, 6479-6487.

30. Griffiths, E. A. H.; Britovsek, G. J. P.; Gibson, V. C.; Gould, I. R. Highly active ethylene polymerisation catalysts based on iron: an ab initio study. *Chem. Commun.* **1999**, *14*, 1333-1334.

31. Rappe, A. K.; Skiff, W. M.; Casewit, C. J. Modeling Metal-Catalyzed Olefin Polymerization. *Chem. Rev.* **2000**, *100*, 1435-1456.

32. Khoroshun, D. V.; Musaev, D. G.; Vreven, T.; Morokuma, K. Theoretical Study on Bis(imino)pyridyl−Fe(II) Olefin Poly- and Oligomerization Catalysts. Dominance of Different Spin States in Propagation and β-Hydride Transfer Pathways. *Organometallics* **2001**, *20*, 2007-2026.

33. Raucoules, R.; de Bruin, T.; Raybaud, P.; Adamo, C. Evidence for the Iron(III) Oxidation State in Bis(imino)pyridine Catalysts. A Density Functional Theory Study. *Organometallics* **2008**, *27*, 3368-3377.

34. Cruz, V. L.; Ramos, J.; Martínez-Salazar, J.; Gutiérrez-Oliva, S.; Toro-Labbé, A. Theoretical Study on a Multicenter Model Based on Different Metal Oxidation States for the Bis(imino)pyridine Iron Catalysts in Ethylene Polymerization. *Organometallics* **2009**, *28*, 5889-5895.

35. Small, B. L.; Carney, M. Diimine Metal Complexes, Methods of Synthesis, and Methods of Using in Oligomerization and Polymerization. US Patent 7129304, 2006.

36. Small, B. L.; Carney, M. Diimine Metal Complexes, Methods of Synthesis, and Methods of Using in Oligomerization and Polymerization. US 7,727,926, 2010.

37. Small, B. L.; Carney, M. Diimine Metal Complexes, Methods of Synthesis, and Methods of Using in Oligomerization and Polymerization. US 7,977,269, 2011.

38. Frisch, M. J.; Trucks, G. W.; Schlegel, H. B.; Scuseria, G. E.; Robb, M. A.; Cheeseman, J. R.; Scalmani, G.; Barone, V.; Mennucci, B.; Petersson, G. A.; et al. Gaussian 09, Revision B.01. Wallingford CT, 2009.

39. Zhao, Y.; Truhlar, D. G. A New Local Density Functional for Main-group Thermochemistry, Transition Metal Bonding, Thermochemical Kinetics, and Noncovalent Interactions. *J. Chem. Phys* **2006**, *125*, 194101-194101-18.

40. Zhao, Y.; Truhlar, D. G. Density Functionals with Broad Applicability in Chemistry. *Acc. Chem. Res* **2008**, *41*, 157-167.

41. Zhao, Y.; Truhlar, D. The M06 Suite of Density Functionals for Main Group Thermochemistry, Thermochemical Kinetics, Noncovalent Interactions, Excited States, and Transition Elements: Two New Functionals and Systematic Testing of Four M06-class Functionals and 12 Other Functionals. *Theor Chem Acc* **2008**, *120*, 215-421.

42. Jacquemin, D.; Perpète, E. A.; Ciofini, I.; Adamo, C.; Valero, R.; Zhao, Y.; Truhlar, D. G. On the Performances of the M06 Family of Density Functionals for Electronic Excitation Energies. *J. Chem. Theory Comput.* **2010**, *6*, 2071-2085.

43. Hay, P. J.; Wadt, W. R. Ab Initio Effective Core Potentials for Molecular Calculations. Potentials for the Transition Metal Atoms Sc to Hg. *J. Chem. Phys.* **1985**, *82*, 270-283.

44. Weigend, F.; Ahlrichs, R. Balanced Basis Sets of Split Valence, Triple Zeta Valence and Quadruple Zeta Valence Quality for H to Rn: Design and Assessment of Accuracy. *Phys. Chem. Chem. Phys.* **2005**, *7*, 3297-3305.

45. Marenich, A. V.; Cramer, C. J.; Truhlar, D. G. Universal Solvation Model Based on Solute Electron Density and on a Continuum Model of the Solvent Defined by the Bulk Dielectric Constant and Atomic Surface Tensions. *J. Phys. Chem. B* **2009**, *113*, 6378-6396.

46. Lee, C.; Yang, W.; Parr, R. G. Density Functional Thermochemistry. III. The Role of Exact Exchange. *Phys. Rev. B* **1993**, *98*, 5648-5652.

47. Chai, J.-D.; Head-Gordon, M. Long-range Corrected Hybrid Density Functionals With Damped Atom-atom Dispersion Corrections. *Phys. Chem. Chem. Phys.* **2008**, *10*, 6615-6620.

48. Swart, M.; Groenhof, A. R.; Ehlers, A. W.; Lammertsma, K. Validation of Exchange−Correlation Functionals for Spin States of Iron Complexes. *J. Phys. Chem. A* **2004**, *108*, 5479-5483.

49. Conradie, J.; Ghosh, A. DFT Calculations on the Spin-Crossover Complex Fe(salen)(NO): A Quest for the Best Functional. *J. Phys. Chem. B Lett.* **2007**, *111*, 12621-12624.

50. Swart, M. Accurate Spin-State Energies for Iron Complexes. *J. Chem. Theory Comput.* **2008**, *4*, 2057-2066.

51. Jensen, K.; Cirera, J. Accurate Computed Enthalpies of Spin Crossover in Iron and Cobalt Complexes. *J. Phys. Chem. A* **2009**, *113*, 10033-10039.

52. Hughes, T. F.; Friesner, R. A. Correcting Systematic Errors in DFT Spin-Splitting Energetics for Transition Metal Complexes. *J. Chem. Theory Comput.* **2011**, *7*, 19-32.

53. Kepp, K. P. Consistent Descriptions of Metal–ligand Bonds and Spin-crossover in Inorganic Chemistry. *Coord. Chem. Rev.* **2013**, *257*, 196-209.

54. Mortensen, S. R.; Kepp, K. P. Spin Propensities of Octahedral Complexes from Density Functional Theory. *J. Phys. Chem. A* **2015**, *119*, 4041-4050.

55. Ashley, D. C.; Jakubikova, E. Ironing Out the Photochemical and Spin-crossover Behavior of Fe(II) Coordination Compounds with Computational Chemistry. *Coord. Chem. Rev.* **2017**, *337*, 97-111.

56. Coskun, D.; Jerome, S. V.; Friesner, R. A. Evaluation of the Performance of the B3LYP, PBE0, and M06 DFT Functionals, and DBLOC-Corrected Versions, in the Calculation of Redox Potentials and Spin Splittings for Transition Metal Containing Systems. *J. Chem. Theory Comput.* **2016**, *12*, 1121-1128.

57. Wilbraham, L.; Adamo, C.; Ciofini, I. Communication: Evaluating Non-empirical Double Hybrid Functionals for Spin-state Energetics in Transition-metal Complexes. *J. Chem. Phys.* **2018**, *148*, 041103-1-041103-5.

58. Radón, M.; Gąssowska, K.; Szklarzewicz, J.; Broclawik, E. Spin-State Energetics of Fe(III) and Ru(III) Aqua Complexes: Accurate ab Initio Calculations and Evidence for Huge Solvation Effects. *J. Chem. Theory Comput.* **2016**, *12*, 1592-1605.

59. Minaev, B.; Baryshnikova, A.; Sun, W-H. Spin-dependent Effects in Ethylene Polymerization with Bis(imino)pyridine Iron(II) Complexes. *J. Organom. Chem.* **2016**, *811*, 48-65.

60. Chen, E. Y.-X.; Marks, T. J. Cocatalysts for Metal-Catalyzed Olefin Polymerization: Activators, Activation Processes, and Structure−Activity Relationships. *Chem. Rev.* **2000**, *100*, 1391-1434.

61. Castro, P. M.; Lahtinen, P.; Axenov, K.; Viidanoja, J.; Kotiaho, T.; Leskela, M.; Repo, T. Activation of 2,6-Bis(imino)pyridine Iron(II) Chloride Complexes by Methylaluminoxane: An Electrospray Ionization Tandem Mass Spectrometry Investigation. *Organometallics* **2005**, *24*, 3664-3670.

62. Boudene, Z.; Boudier, A.; Breuil, P.-A. R.; Olivier-Bourbigou, H.; Raybaud, P.; Toulhoat, H.; de Bruin, T. Understanding the Role of Aluminum-based Activators in Single Site Iron Catalysts for Ethylene Oligomerization. *J. Catal.* **2014**, *317*, 153-157.

63. Pasha, F. A.; Basset, J.-M.; Toulhoat, H.; de Bruin, T. DFT Study on the Impact of the Methylaluminoxane Cocatalyst in Ethylene Oligomerization Using a Titanium-Based Catalyst. *Organometallics* **2015**, *34*, 426-431.

64. Babik, S. T.; Fink, G. Propylene Polymerization with a Bisiminepyridine Iron Complex: Activation with $Ph_3C[B(C_6F_5)_4]$ and AlR_3; Iron Hydride Species in the Catalytic Cycle. *J. Mol. Catal. A: Chem.* **2002**, *188*, 245-253.

65. Britovsek, G. J.; Gibson, V. C.; Spitzmesser, S. K.; Tellmann, K. P.; White, A. J.; Williams, D. J. Cationic 2,6-bis(imino)pyridine Iron and Cobalt Complexes: Synthesis, Structures, Ethylene Polymerisation and Ethylene/polar Monomer Co-polymerisation Studies. *J. Chem. Soc., Dalton Trans.* **2002**, 1159-1171.

66. Bryliakov, K. P.; Semikolenova, N. V.; Zakharov, V. A.; Talsi, E. P. Active Intermediates of Ethylene Polymerization over 2,6-Bis(imino)pyridyl Iron Complex Activated with Aluminum Trialkyls and Methylaluminoxane. *Organometallics* **2004**, *23*, 5375-5378.

67. Bryliakov, K. P.; Semikolenova, N. V.; Zudin, V. N.; Zakharov, V. A.; Talsi, E. P. Ferrous Rather Than Ferric Species are the Active Sites in bis(imino)pyridine Iron Ethylene Polymerization Catalysts. *Catal. Commun.* **2004**, *5*, 45-48.

68. Britovsek, G. J. P.; Clentsmith, G. K. B.; Gibson, V. C.; Goodgame, D. M. L.; McTavish, S. J.; Pankhurst, Q. A. The Nature of the Active Site in bis(imino)pyridine Iron Ethylene Polymerisation Catalysts. *Catal. Commun.* **2002**, *3*, 207-211.

69. Raucoules, R.; de Bruin, T.; Raybaud, P.; Adamo, C. Theoretical Unraveling of Selective 1-Butene Oligomerization Catalyzed by Iron−Bis(arylimino)pyridine. *Organometallics* **2009**, *28*, 5358-5367.

70. Martínez, J.; Cruz, V.; Ramos, J.; Gutiérrez-Oliva, S.; Martínez-Salazar, J.; Toro-Labbé, A. On the Nature of the Active Site in bis(imino)Pyridyl Iron, a Catalyst for Olefin Polymerization. *J. Phys. Chem. C* **2008**, *112*, 5023-5028.

71. Fayet, G.; Raybaud, P.; Toulhoat, H.; de Bruin, T. Iron bis(arylimino)pyridine Precursors Activated to Catalyze Ethylene Oligomerization as Studied by DFT and QSAR Approaches. *Comput. Theor. Chem.* **2009**, *903*, 100-107.

72. Zakharov, I. I.; Zakharov, V. A. A DFT Quantum-Chemical Study of the Structure of Precursors and Active Sites of Catalyst Based on 2,6-Bis(imino)pyridyl Fe(II) Complexes. *Macromolecular Theory and Simulations* **2004**, *13*, 583-591.

73. a) Vela, J.; Vaddadi, S.; Cundari, T. R.; Smith, J. M.; Gregory, E. A.; Lachicotte, R. J.; Flaschenriem, C. J.; Holland, P. L. Reversible Beta-Hydrogen Elimination of Three-Coordinate Iron(II) Alkyl Complexes: Mechanistic and Thermodynamic Studies. *Organometallics* **2004**, *23*, 5226-5239.

74. Trovitch, R. J.; Lobkovsky, E.; Chirik, P. J. Bis(imino)pyridine Iron Alkyls Containing β-Hydrogens: Synthesis, Evaluation of Kinetic Stability, and Decomposition Pathways Involving Chelate Participation. *J. Am. Chem. Soc.* **2008**, *130*, 11631-11640.

75. Gridley, B. M.; Blake, A. J.; Davis, A. L.; Lewis, W.; Moxey, G. J.; Kays, D. L. Low-coordinate Cobalt(II) Terphenyl Complexes: Precursors to Sterically Encumbered Ketones. *Chem. Commun.* **2012**, *48*, 8910-8912.

76. Sauer D. C.; Kruck, M.; Wadepohl, H.; Enders, M.; Gade, L. H. Spin Density Distribution in Iron(II) and Cobalt(II) Alkyl Complexes Containing 1,3-Bis(2-pyridylimino)isoindolate Ligands. *Organometallics*, **2013**, *32*, 885-892.

77. Harvey, J. N.; Poli, R.; Smith, K. M. Understanding the Reactivity of Transition Metal Complexes Involving Multiple Spin States. *Coord. Chem. Rev.* **2003**, *238*, 347-361.

78. Carreón-Macedo, J-L.; Harvey, J. N. Do Spin State Changes Matter in Organometallic Chemistry? A Computational Study. *J. Am. Chem. Soc.* **2004**, *126*, 5789-5797.

79. Poli, R. Harvey, J. N. Spin Forbidden Chemical Reactions of Transition Metal Compounds. New Ideas and New Computational Challenges. *Chem. Soc. Rev.* **2003**, *32*, 1-8.

80. Harvey, J. N. Understanding the Kinetics of Spin-forbidden Chemical Reactions. *Phys. Chem. Chem. Phys.* **2007**, *9*, 331-343.

81G. Ramos, J.; Cruz, V.; Muñoz-Escalona, A.; Martínez-Salazar, J. A Computational Study of Iron-based Gibson–Brookhart Catalysts for the Copolymerisation of Ethylene and 1-hexene. *Polymer* **2002**, *43*, 3635-3645.